AN APPROXIMATE METHOD TO CALCULATE THE STIFFNESS OF SHALLOW FOUNDATIONS SUBJECTED TO ECCENTRIC LOADS

A THESIS SUBMITTED TO
THE GRADUATE SCHOOL OF NATURAL AND APPLIED SCIENCES
OF
MIDDLE EAST TECHNICAL UNIVERSITY

BY

AYŞE RUŞEN DURUCAN

IN PARTIAL FULFILLMENT OF THE REQUIREMENTS
FOR
THE DEGREE OF DOCTOR OF PHILOSOPHY
IN
ENGINEERING SCIENCES

DECEMBER 2016

Approval of the thesis:

AN APPROXIMATE METHOD TO CALCULATE THE STIFFNESS OF SHALLOW FOUNDATIONS SUBJECTED TO ECCENTRIC LOADS

submitted by **AYŞE RUŞEN DURUCAN** in partial fulfillment of the requirements for the degree of **Doctor of Philosophy in Engineering Sciences Department, Middle East Technical University** by,

Prof. Dr. Gülbin Dural Ünver
Dean, Graduate School of **Natural and Applied Sciences** _____

Prof. Dr. Murat Dicleli
Head of Department, **Engineering Sciences** _____

Assoc. Prof. Dr. Mustafa Tolga Yılmaz
Supervisor, **Engineering Sciences Dept., METU** _____

Examining Committee Members:

Prof. Dr. Turgut Tokdemir
Engineering Sciences Dept., METU _____

Assoc. Prof. Dr. Mustafa Tolga Yılmaz
Engineering Sciences Dept., METU _____

Prof. Dr. Özgür Anıl
Civil Engineering Dept., Gazi University _____

Assoc. Prof. Dr. Tolga Akış
Civil Engineering Dept., Atılım University _____

Prof. Dr. Murat Altuğ Erberik
Civil Engineering Dept., METU _____

Date: 06.12.2016

I hereby declare that all information in this document has been obtained and presented in accordance with academic rules and ethical conduct. I also declare that, as required by these rules and conduct, I have fully cited and referenced all material and results that are not original to this work.

Name, Last name : Ayşe Ruşen Durucan

Signature :

ABSTRACT

AN APPROXIMATE METHOD TO CALCULATE THE STIFFNESS OF SHALLOW FOUNDATIONS SUBJECTED TO ECCENTRIC LOADS

Durucan, Ayşe Ruşen

Ph.D., Department of Engineering Sciences

Supervisor: Assoc. Prof. Dr. Mustafa Tolga Yılmaz

December 2016, 147 pages

A computationally simple method to calculate the static response of arbitrarily shaped shallow foundations subjected to eccentric loading is proposed. A theoretical relationship to estimate the area beneath the foundation that is contact with the load bearing support is developed. This relationship yielded an equation to calculate rocking angle of an arbitrarily shaped foundation under any load eccentricity. Consequently, a simple theoretical model capable of simulating the effects of material and geometrical nonlinearities on the response of arbitrarily shaped shallow foundations subjected to monotonically increasing eccentric and inclined load is developed. The theoretical results are justified by using the results of three available sets of experiments from the literature. Then the parametric analyses of shallow foundations subjected to eccentric loading are performed. It is observed that the proposed theoretical method yields reasonably accurate results in terms of moment-rotation response of shallow foundations.

Keywords: Foundation uplift, soil nonlinearity, shallow footing, monotonic loading

ÖZ

EKSANTRİK YÜKLER ALTINDAKİ SIĞ TEMELLERİN RİJİTLİK HESABI İÇİN YAKLAŞIK BİR YÖNTEM

Durucan, Ayşe Ruşen
Doktora, Mühendislik Bilimleri Bölümü
Tez Yöneticisi: Doç. Dr. Mustafa Tolga Yılmaz

Aralık 2016, 147 sayfa

Değişken şekillere sahip olan temellerin statik eksantrik statik yüklere karşı tepkisinin hesaplanması için sayısal hesabı basit bir yöntem önerilmiştir. Çalışmada, değişken şekilli temeller üzerinde etkiyen devrilme momenti ile temas yüzeyi genişliği arasında teorik bir ilişki kurulmuştur. Daha sonra, herhangi bir şekle sahip olan sığ temellerde uygulanabilir şekilde, devrilme momenti ve devrilme açısı arasındaki ilişkinin hesaplanması için bir yöntem geliştirilmiştir. Geometrik açıdan doğrusal olmayan probleme, malzeme özelliklerinden kaynaklanan doğrusal olmayan davranış da dahil edilmiştir. Ortaya çıkan hesap yöntemi literatürden alınan üç deney setine ait sonuçlar kullanılarak doğrulanmıştır. Daha sonra eksantrik yükleme altındaki sığ temeller için parametrik analizleri yapılmıştır. Önerilen yöntemin sığ temellerin moment – devrilme açışı ilişkilerini isabetli olarak hesaplayabildiği görülmüştür.

Anahtar Kelimeler: Temel kalkması, doğrusal olmayan zemin davranışı, sığ temel, monotonik yükleme

To My Family

ACKNOWLEDGEMENTS

I would like to express my sincere thanks to my advisor Assoc. Prof. Dr. Mustafa Tolga Yılmaz for his inspiring supervision, continuous encouragement, precious help and patience during this thesis.

I would like to give my deepest thanks to my husband Cengizhan Durucan for his understanding and support during my thesis.

I wish to express special thanks to my family for their emotional support and encouragement during my thesis.

TABLE OF CONTENTS

ABSTRACT v

ÖZ vi

ACKNOWLEDGEMENTS viii

TABLE OF CONTENTS ix

LIST OF TABLES xiii

LIST OF FIGURES xiv

NOMENCLATURE xx

CHAPTERS

1. INTRODUCTION 1

1.1. Introduction 1

1.2. Objective 5

1.3. Literature Review 5

1.4. Scope of the Study 9

2. THE STATIC IMPEDANCE COEFFICIENTS OF SHALLOW FOUNDATION RESTING ON IDEALLY ELASTIC MEDIA 11

2.1. Introduction 11

2.2. The Static Impedance Coefficients for a Shallow Foundation on an Elastic Half-space 13

2.3. The Static Impedance Coefficients for Rectangular Foundation on Elastic Layer 16

2.4. The Static Impedance Coefficients for a Strip Foundation resting on Deep Inhomogeneous Deposits 18

2.5. The Static Impedance Coefficients for Shallow Foundation on Winkler Springs 18

3. A SIMPLE MODEL ON FOUNDATION UPLIFT 21

3.1. Introduction 21

3.2. Basic equations of equilibrium 21

3.3. Theory for calculation of impedance for a foundation during uplift 23

3.4. The relationship between M, v and θ during uplift 29

4. JUSTIFICATIONS AND APPLICATIONS 37

4.1. Normalization 37

4.2. Verifications 38

4.3. Applications 44

4.3.1. A Comparison of Rocking Impedances for Rectangular Foundations Resting on Different Types of Elastic Supports 44

4.3.2. A Circular Foundation Resting on Elastic Half-space 48

4.3.3. A Strip Foundation Resting on Deep Inhomogeneous Deposits and Elastic Half-space 49

4.3.4. A Square Foundation Subjected to 2 Way Eccentric Loading Resting on Elastic Half-space 51

5. EFFECT OF SOIL NONLINEARITY ON BEARING CAPACITIES OF SHALLOW FOUNDATIONS 55

5.1 Introduction 55

5.2. Methodology 59

5.2.1 The Hyperbolic Model 60

5.2.2 Exponential Model 62

5.2.3 Estimation of V_{ult} 62

5.3. Model Validations 68

5.3.1. Foundation model of PWRI 68

5.3.2. Simulation of TRISEE tests 84

5.3.3. Simulation of the tests conducted by Kokkali et al. (2015) 88

6. APPLICATIONS 93

6.1. Introduction 93

6.1.1. The Effect of h_s on the variation of $M/M_\infty - \theta_N$ and $v/v_\infty - \theta_N$ relationships 93

6.1.2. Effect of ϕ on the $M/M_\infty - \theta_N$ and $v/v_\infty - \theta_N$ relationships 95

6.1.3. Effect of c_S on the variation of $M/M_\infty - \theta_N$ and $v/v_\infty - \theta_N$ relationships 97

6.1.4. The effect of foundation shape and loading direction on the relationship between $M/M_\infty - \theta_N$ and $v/v_\infty - \theta_N$ 98

6.1.5. The effect of foundation dimensions on $M/M_\infty - \theta_N$ and $v/v_\infty - \theta_N$ relationships..... 101

7. SUMMARY AND CONCLUSIONS..... 105

7.1. Summary 105

7.2. Conclusions 106

7.3. Future Studies..... 107

REFERENCES..... 109

APPENDICES

A 123

B 131

C 133

D 135

E..... 137

VITA 147

LIST OF TABLES

TABLES

Table 2.1 The static impedance coefficients of arbitrarily shaped foundation on homogeneous halfspace (Dobry and Gazetas, 1986 and Gazetas, 1991) 14

Table 2.2 The static impedance coefficients of rectangular foundation, circular foundation and strip foundation on homogeneous halfspace (Dobry and Gazetas, 1986 and Gazetas, 1991) 15

Table 3.1 Comparative results for α on the verge of uplift 28

Table 3.2 Options to simulate the soil conditions in the computer program 33

Table 3.3 Options for $\mathrm{param}(5)$ in the computer program 33

Table 5.1 Functional forms in the proposed method 67

Table 5.2 Selected load cases in the experiments of PWRI 69

Table 5.3 Calculated parameters used in the theoretical model for PWRI tests .. 71

Table 5.4 Calculated parameters used in the theoretical model for TRISEE tests 86

Table 5.5 Calculated parameters used in the theoretical model for the tests conducted by Kokkali et al. (2015) 89

LIST OF FIGURES

FIGURES

Figure 1.1 The uplift of shallow foundations under tensile forces.....2

Figure 1.2 The change in typical M-θ relationships due to the uplift of the foundation, and material nonlinearity 4

Figure 2.1 An arbitrarily shaped foundation 12

Figure 2.2 A shallow foundation with no separation 12

Figure 2.3 A shallow foundation resting on elastic halfspace.....13

Figure 2.4 A shallow foundation resting on an elastic layer 16

Figure 2.5 (a) $\beta - D/B$ relationship for a rectangular foundation resting on finite layer, (b) $\gamma - D/B$ relationship for a rectangular foundation resting on finite layer (Sovinc, 1969). 17

Figure 2.6 A rigid foundation resting on tensionless Winkler springs.....20

Figure 3.1 Reduction in effective foundation width due to loss of contact with load bearing medium.....22

Figure 3.2 Actual and assumed contact boundaries during the uplift of foundation28

Figure 3.3 Flow Chart: (a) main program, (b) routine to calculate α……..……31

Figure 4.1 The relationship between M_N and θ_N for a square foundation under static loading on elastic half-space and Winkler springs 39

Figure 4.2 The relationship between v_N and θ_N for a square foundation under static loading on elastic half-space and Winkler springs.....40

Figure 4.3 The relationship between α and θ_N obtained using Equation 3.11 for circular foundations resting on homogeneous half-space. 41

Figure 4.4 The relationship between M_N and θ_N for a circular foundation on homogeneous half-space 42

Figure 4.5 The relationship between v_N and θ_N for a circular foundation on homogeneous half-space 43

Figure 4.6 The relationship between α and θ_N (Equation 3.11) for strip foundations on homogeneous half-space 43

Figure 4.7 The relationship between M_N and θ_N for strip foundations on elastic half-space 44

Figure 4.8 The relationship between α and θ_N for various rectangular foundations resting on homogeneous half-space 45

Figure 4.9 The relationship between M_N and θ_N for rectangular $(B = 5L)$ foundations on homogeneous half-space 46

Figure 4.10 The relationship between M_N and θ_N for a rectangular $(B = 5L)$ foundation under static loading 47

Figure 4.11 The relationship between M_N and θ_N for various rectangular foundations resting on an elastic half-space for cases 47

Figure 4.12 The relationship between v_N and θ_N for various rectangular foundations resting on elastic half-space 48

Figure 4.13 The relationship between M_N and θ_N for circular foundations on homogeneous halfspace 49

Figure 4.14 The relationship between M_N and θ_N for strip foundations on homogeneous half-space 50

Figure 4.15 The relationship between M_N and θ_N for strip foundations on deep inhomogeneous deposits 51

Figure 4.16 The relationship between α and θ_N for square foundations subjected to 2 way eccentric loading resting elastic halfspace 52

Figure 4.17 The relationships between M_N and θ_N for square foundations subjected to 1 way and 2 way eccentric loading resting elastic halfspace 53

Figure 4.18 The relationships between v_N and θ_N for square foundations subjected to 1 way and 2 way eccentric loading resting elastic halfspace 53

Figure 5.1 Normalized shear modulus versus shear strain for Toyoura sand (Kokusho, 1980).....56

Figure 5.2 Variation of secant shear modulus with shear strain 58

Figure 5.3 Comparison of the vertical load – displacement relationships calculated using exponential and hyperbolic law with those calculated using the finite element analyses (Apostolou, 2011) 59

Figure 5.4 Contact pressures for cohesive and granular soils under rigid foundations (Holtz, 1991).....63

Figure 5.5 Flow Chart to calculate G.....66

Figure 5.6 Sketches and photo of the test setup used for cyclic loading experiments (Shirato et al., 2008).....68

Figure 5.7 The experimental model for vertical loading.....70

Figure 5.8 Results of the vertical loading tests (Shirato et al., 2008; $V_m = V_{ult}$) 70

Figure 5.9 Typical V-v relationship of a shallow foundation in exponential form ..71

Figure 5.10 The schematic view of the horizontal loading experiment 72

Figure 5.11 The relationship between M_N and θ_N calculated by considering (a) an exponential function, (b) a hyperbolic function, (c) a linear response, and (d) the experimental data for load Case 3. 74

Figure 5.12 Variation of $K_\theta/K_{\theta 0}$ with θ_N for load Case 3 74

Figure 5.13 The relationship between M_N and θ_N calculated by considering (a) an exponential function, (b) a hyperbolic function, (c) a linear response, and (d) the experimental data for load Case 6 75

Figure 5.14 The relationship between M_N and θ_N calculated by considering (a) an exponential function, (b) a hyperbolic function, (c) a linear response, and (d) the experimental data for load Case 9..... 76

Figure 5.15 Comparison of ratio of experimental to theoretical (exponential function) K_θ for Load Cases 6 and 9 77

Figure 5.16 The relationship between v_N and θ_N calculated by considering (a) an exponential function, (b) a hyperbolic function, (c) a linear response, and (d) the experimental data for load Case 3..... 78

Figure 5.17 The relationship between v_N and θ_N calculated by considering (a) an exponential function, (b) a hyperbolic function, (c) a linear response, and (d) the experimental data for load Case 6..... 79

Figure 5.18 The relationship between v_N and θ_N calculated by considering (a) an exponential function, (b) a hyperbolic function, (c) a linear response, and (d) the experimental data for load Case 9..... 80

Figure 5.19 The relationship between M_N and θ_N calculated by considering (a) an exponential function and by experimental data for (b) Case 3 and (c) Case 5..... 81

Figure 5.20 The relationship between M_N and θ_N calculated by considering (a) an exponential function and by experimental data for (b) Case 6 and (c) Case 8..... 81

Figure 5.21 The relationship between M_N and θ_N calculated by considering (a) an exponential function and by experimental data for (b) Case 9 and (c) Case 11..... 82

Figure 5.22 The relationship between M_N and θ_N in the lower range of θ_N calculated by considering (a) an exponential function and by experimental data for (b) Case 3 and (c) Case 5..... 83

Figure 5.23 The relationship between M_N and θ_N in the lower range of θ_N calculated by considering (a) an exponential function and by experimental data for (b) Case 6 and (c) Case 8……..……..83

Figure 5.24 The relationship between M_N and θ_N in the lower range of θ_N calculated by considering (a) an exponential function, and by experimental data for (b) Case 9 and (c) Case 11.....84

Figure 5.25 The relationship between M and θ for loose sand conditions and loading Type 3.....87

Figure 5.26 The relationship between M and θ for dense sand conditions and loading Type 3.....87

Figure 5.27 Results of the vertical loading tests (Kokkali et al., 2015).....88

Figure 5.28 The relationships between M_N and θ_N according to the results of the monotonic loading tests (Kokkali et al., 2015).....90

Figure 5.29 Comparison of the relationship between M_N and θ_N for loose sand conditions: (a) experimental, (b) theoretical with $\phi = 44.5°$, (c) theoretical with $\phi = 37°$.....91

Figure 5.30 Comparison of the relationship between M_N and θ_N for dense sand conditions: (a) experimental, (b) theoretical with $\phi = 48°$, (c) theoretical with $\phi = 41.5°$.....92

Figure 6.1 Variation of the relationship between M/M_∞ and θ_N by h_s.....94

Figure 6.2 Variation of the relationship between v/v_∞ and θ_N with h_s.....95

Figure 6.3 Variation of the relationship between M/M_∞ and θ_N with ϕ.....96

Figure 6.4 Variation of the relationship between v/v_∞ and θ_N with ϕ.....96

Figure 6.5 Variation of the relationship between M/M_∞ and θ_N as a function of c_s97

Figure 6.6 Variation of the relationship between v/v_∞ and θ_N as a function of c_s.98

Figure 6.7 Variation of the relationship between M/M_∞ and θ_N by the shape of foundation.....99

Figure 6.8 Variation of the relationship between M/M_∞ and θ_N as a function of loading direction.....100

Figure 6.9 Variation of the relationship between v/v_∞ and θ_N by the foundation shape 100

Figure 6.10 Variation of the relationship between v/v_∞ and θ_N by loading direction 101

Figure 6.11 Variation of the relationship between M/M_∞ and θ_N as a function of rectangular foundation dimensions for $FS = 5$ 102

Figure 6.12 Variation of the relationship between v/v_∞ and θ_N as a function rectangular foundation size for $FS = 5$ 103

Figure A.1 Reduction in effective foundation width of the rectangular foundation after initiation of uplift 123

Figure A.2 Reduction in effective foundation width of the circular foundation after initiation of uplift 124

Figure A.3 Applied loading: (a) one way eccentricity, (b) two-way eccentricity .. 125

Figure A.4 Reduction in effective foundation width of the diagonal square foundation after initiation of uplift 125

Figure A.5 The relation between b_N and c_N' for (a) rectangular foundations, (b) circular foundations and (c) diagonal square foundations 127

Figure A.6 The relation between c_N and c_N' for (a) rectangular foundations, (b) circular foundations and (c) diagonal square foundations 127

Figure A.7 The relation between f_N and c_N' for (a) rectangular foundations, (b) circular foundations and (c) diagonal square foundations 128

Figure A.8 The relation between I_N and c_N' for (a) rectangular foundations, (b) circular foundations and (c) diagonal square foundations 128

Figure A.9 The relation between L_N and c_N' for (a) rectangular foundations, (b) circular foundations and (c) diagonal square foundations 129

Figure C.1 Typical behavior of foundation on Winkler springs 133

NOMENCLATURE

A	Transformation matrix
b	Contact width of foundation
b_N	Normalized contact width of foundation
B	Width of foundation
c	Distance between O and O'
c_N	Normalized distance between O and O'
c_s	Unit cohesion
c'	Distance between edge of foundation and O'
c'_N	Normalized distance between edge of foundation and O'
C	Distance between edge of foundation and O
D	Thickness of layer
D_r	Relative density of soil
f	Contact area of foundation
FS	Factor of safety against bearing failure
G_0	Initial shear modulus of soil
G	Shear modulus of soil
h	Horizontal displacement acting on centroidal axis of foundation
h'	Horizontal displacement acting on centroidal axis of contact area

h_s	The length of moment arm
H	Horizontal load acting on centroidal axis of foundation
H'	Horizontal load acting on centroidal axis of contact area
I	Moment of inertia of foundation
I_N	Normalized moment of inertia of foundation
k_h	Horizontal stiffness of Winkler spring
k_v	Vertical stiffness of Winkler spring
K	Static stiffness matrix of foundation
K_h	Static horizontal impedance coefficient of foundation
K_v	Static vertical impedance coefficient of foundation
K_{v0}	Initial static vertical impedance coefficient of foundation
K_θ	Static rotational impedance coefficient of foundation
L	Length of foundation
m, n	Constants of hyperbolic functional form
M	Moment acting on centroidal axis of foundation
M'	Moment acting on centroidal axis of contact area
M_N	Normalized moment acting on centroidal axis of foundation
M_{ult}	Moment capacity of foundation
M_{uplift}	Threshold moment for uplift
N_c, N_q, N_γ	Bearing capacity factors

O	Centroidal axes of foundation
O'	Centroidal axes of contact area
q	Effective overburden pressure at the base level of the foundation
q_u	The bearing capacity of foundation
v	Vertical displacement acting on centroidal axis of foundation
v_N	Normalized vertical displacement acting on centroidal axis of foundation
v'	Vertical displacement acting on centroidal axis of contact area
V	Vertical load acting on centroidal axis of foundation
V'	Vertical load acting on centroidal axis of contact area
V_{ult}	Ultimate vertical load acting on centroidal axis of foundation
α	Parameter for uplift initiation
β, γ	Parameters of the static impedance coefficients for rectangular foundation on elastic layer
β_i	Angle of load inclination
γ_s	Unit weight of soil
ν	Poisson's ratio of soil
θ_N	Normalized rotation of the centroidal axis of foundation
θ'	Rotation of the centroidal axis of contact area
ϕ	Internal angle of friction
$\lambda_{*s}, \lambda_{*d}, \lambda_{*i}$	Shape, depth and inclination factors

CHAPTER 1

INTRODUCTION

1.1. Introduction

An excessive increase in overturning moment (*M*) acting on foundation yields a severe increase in the eccentricity of vertical load (*V*) acting on foundation, and builds a demand for tensile contact stress on the interface between soil and foundation. The lack of tensile strength on this interface yields partial separation of foundation's base from the underlying soil. The rocking motion of buildings during severe earthquakes may cause partial separation of the shallow foundations from underlying soil, and consequently uplift of a side of foundation, because of the lack of tensional strength in load bearing soil. Figure 1.1 illustrates the separation of a shallow foundation from the load-bearing medium (soil) due to excessive *M*. This is particularly important for slender structures, such as towers, chimneys and bridge piers because of the loss in rocking stiffness of foundation (Apostolou et al., 2007; Yim and Chopra, 1984; Celep and Güler, 1991; Psycharis, 1991; Jennings, P.C. and Bielak, J., 1973). Morever, Chopra and Yim (1985) stated that design forces acting on buildings (i.e., hospitals) may be larger than those required to initiate the uplift. The overturning moments acting on the base of typical buildings, such as hospitals, offices and low-rise structures, may exceed the overturning moment resistance provided by the gravity forces (Rutenberg et al., 1982; Hayashi et al., 1999; Kutanis et al., 2002; Zhou et al, 2012). The buildings constructed using a combination of structural frames and shear walls may experience uplift during severe seismic motion. For such structural systems, uplift behavior of shear walls increase the level of lateral load transferred to structural

frames of buildings, and may cause important levels of damage on structural frame (Mori et al, 2008).

Foundation uplift may seriously modify the structural deformations and the seismic response characteristics due to increase in the period of structural vibrations (Chopra and Yim, 1985; Roeder et al., 1996; Xu and Spyrakos, 1996; Mergos and Kavashima, 2005).

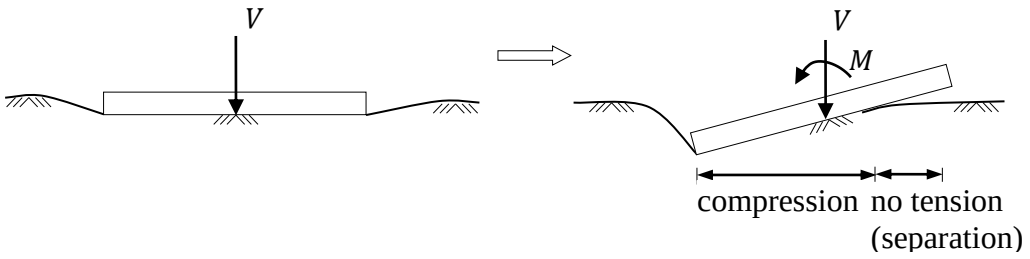

Figure 1.1 The uplift of shallow foundations under tensile forces

Figini et al. (2012) stated that the numerical tools, capable of accurately simulating the effects of foundation uplift on the response of foundations, are still in research stage. Accordingly, computationally expensive finite element modeling techniques and simplified approaches such as modeling the reaction of soil as a bed of independent nonlinear springs (i.e. namely the Winkler foundation), are among the alternatives. However, such simplified approaches cannot accurately simulate the soil-structure interaction if the reaction springs are considered to have uniform properties. For rigid rectangular foundations, the rotational stiffness of a uniform bed of springs is less than that of the same foundation resting on a continuous elastic material. The main reason for this difference is that unlike a rigid foundation resting on uniform springs the actual pressure distribution beneath a rigid foundation on a continuous elastic material is not uniform. The imposed vertical displacement causes large pressure at the edges of the foundation. Moreover, the pressure at a point under the foundations affects the pressure at

other points which is not accounted for in models consisting independent springs (Pender, 2007; Figini et al., 2012). The document FEMA273 (FEMA, 1997) presents an approach to consider the non-uniform pressure distribution by recommending the use of stiffer springs at the ends of the foundation. Moreover, Wotherspoon et al. (2004a,b) and Pender et al. (2006) proposed methods to consider the interaction between discrete springs. Nevertheless, the model still would not be capable of accurately estimating the bending moment and shear force distribution in the foundation (Pender, 2007). Furthermore, calibration of model parameters is not easy (Pender, 2007; Chatzigogos et al., 2011). A more robust method for calculation of stiffness of shallow foundations necessitates a model involving more than a simple bed of discrete springs.

The macro-element modeling technique became more popular among the researchers due to its computational feasibility. All nonlinearities are condensed in a finite domain, namely the macro-element and generalized forces as well as displacements on this domain are used to simulate the behavior of shallow foundations (Grange et al., 2008). Generally, the footing and the underlying soil are considered to be a single element with horizontal, vertical and rotational load deformation responses defined on the center of the footing. The first macro element model was developed by Nova and Montrasio (1991). This model was based on a strain hardening theory and an incremental formulation of plasticity. However, the behavior of uplifting foundation was not considered. The effect of foundation uplift on the response of foundations was first simulated by the macro element model proposed by Cremer et al. (2001, 2002) considering strip foundations.

In the macro-element approaches (Chatzigogos et al., 2011) the uplifting behavior of shallow foundations has been generally simulated through appropriately modifying the static impedances and recalculating the stiffness matrix based on the reduced contact area between soil and foundation due to uplift. For the dynamic

loads, as in the case of the ground motion excitation, the reduction of the contact area between the soil and foundation is transient and the instantaneous stiffness of foundation continuously varies.

Another source of nonlinearity in the behavior of shallow foundations is the nonlinearity of the stress vs. strain response of soils. The yielding of soil is an essential feature of the load deformation response of foundations (Pecker et al, 2012). Therefore many researchers put emphasize on the soil nonlinearity for their macro elements (Nova and Montrasio, 1991; Gottardi et al., 1995; Pecker, 1998; Cremer at al., 2002; Allotey et al., 2003; Chatzigogos et al., 2009; Gajan and Kutter, 2009; Figini, 2010). Typical $M-\theta$ relationships with and without the nonlinearity of the soil are presented in Figure 1.2 to illustrate the effect of soil nonlinearity and uplift on the response of shallow foundations to monotonic loading.

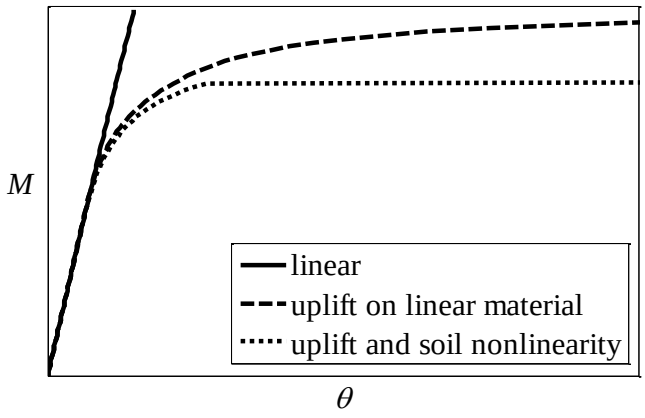

Figure 1.2 The change in typical $M-\theta$ relationships due to the uplift of the foundation, and material nonlinearity

Consequently, robust and yet simple modeling of nonlinear load-displacement response of shallow foundations that partially loose contact with underlying soil due to excessive overturning moment is critically important for more precise estimation of foundation displacements in structural analyses. A reasonably

accurate relationship is also important for calibration and justification of cyclic loading models, such as the macro-elements used for computation of response of shallow foundations to irregular seismic loading. The coupling between vertical displacement and rocking angle of foundation should be accurately modeled for simulation of the relationship between V and M during rocking of foundations (Deng et al., 2012; Kutter et al., 2010).

In this study, an approximate method for computation of vertical displacement and rocking angle of an arbitrarily-shaped ideal rigid shallow foundation under eccentric and inclined load is presented.

1.2. Objective

The objective of this study is to develop a computationally simple yet robust method for calculation of nonlinear load-deformation relationships for shallow foundations that are partially separated from load-bearing soil by excessive overturning moment. The method also aims to estimate the relationship between vertical displacement and rocking angle of an arbitrarily shaped shallow foundation with a feasible computational cost. The applicable range of loading is limited to the ultimate bearing capacity of shallow foundation, such that the continuous plastic flow of soil under sustained foundation load is not possible.

1.3. Literature Review

Several theoretical and experimental models on foundation uplift are presented in literature. The experimental studies (Negro et al., 2000; Gajan et al., 2005; Gajan and Kutter, 2008; Paolucci et al., 2008; Shirato et al., 2008; Tamura et al., 2011; Hung et al., 2011; Deng and Kutter, 2012; Anastasopoulos et al., 2012, 2013, 2015; Deng et al., 2012; Drosos et al., 2012; Massimino and Maugeri, 2013; Kokkali et al., 2014, 2015; Hung et al., 2014; Loli et al., 2014, 2015; Biondi et al.,

2015; Liu et al., 2015) have considerably contributed to the understanding of the rocking response of shallow foundations. The well-known Winkler model, in which several springs that have limited tensional load capacity are located beneath the rigid foundation, is successively used by a number of researchers to model foundation during severe cyclic loading (Wolf and Skrikerud, 1978; Celep and Güler, 1991; Psycharis, 1991, 2008; Chen and Lai, 2003; Houlsby et al., 2005; Allotey and El Naggar, 2003; Raychowdhury and Hutchinson, 2009, 2011). A major limitation of simple Winkler type models is the lack of interaction between individual springs, which react uniformly to the foundation displacements. Although it is possible to adjust the distribution of stiffness among springs to simulate the response of continuum, this adjustment becomes more difficult as the level of material and geometric nonlinearity increases, and as the shape of contact area beneath the foundation becomes non-prismatic (Figini et al. 2012, Pender, 2007, Chatzigogos et al. 2011). Another option to simulate the uplift behavior of shallow foundations is the finite element modeling of elastic continuum, which is a complex, computationally expensive but accurate technique (Wolf, 1976; Ibrahimbegovic and Wilson, 1990; McCallen and Romstad, 1994; Yılmaz and Bakır, 2009).

In the literature, also there are other alternatives to consider the uplift behavior of foundations. The discrete element modeling (DEM) technique is shown to be an alternative technique. The DEM is defined as a powerful tool to analyze the granular materials at small and large strains (Zamani and El Shamy, 2014).

A computationally feasible alternative is the use of conical continuum models instead of springs for computation of the foundation stiffness by estimating the dimensions of contact surface beneath the foundation (Wolf, 1976). The accuracy of this model is similar to that of finite element approach, though it requires fewer computations. However, the determination of the dimensions of the contact surface area requires an optimization algorithm.

The macro-element approaches stand as robust alternatives for finite element techniques. A macro-element is a generalized finite element that is based on a constitutive relationship between generalized nodal displacements and external loads. A macro-element simulating the partial separation of shallow foundations from the load-bearing soil was first proposed by Cremer et al. (2001, 2002). The model is defined through a non-linear constitutive law written in terms of generalized force and displacement parameters. A strip foundation on purely cohesive soil is considered. Figini et al. (2012) developed a macro-element to simulate soil-footing separation and the plastic flow of soil, and implemented a function for stiffness degradation. The uplift of the footing was simulated by a simple non-linear elastic model, which presumes that the load eccentricity (i.e. M/V) necessary for separation is only a function of foundation width (B). The plasticity of the soil is considered by using a bounding surface approach.

Implementation of foundation uplift in dynamic response analyses of structures was another issue to be solved. Analytical solutions for differential equations of motion may be directly employed for simple problems that involve inversed pendulum structures resting on two-spring models (Song and Lee, 1993; Oliveto et al., 2003). Rayleigh-Ritz method or Galerkin's method may also be used to get approximate solutions for geometrically simple problems (Yim and Chopra, 1984; Celep and Güler, 1991). Applications with Newmark's scheme with Winkler and conical models are presented in literature (Wolf and Skrikerud, 1978; Wolf, 1976; Mergos and Kavashima, 2005). The deviation of instantaneous stiffness of foundation must be calculated using an external routine, which initially calculate the dimensions of contact surface, beneath the foundation, due to transient loads induced on the foundation. Runge-Kutta method is an accurate alternative for Newmark's scheme for dynamic foundation uplift problems (Wang and Gould, 1993). Combinations of Newmark's scheme and Runge-Kutta algorithms have been implemented in dynamic response analyses of simple structural models that involve a macro-element modeling foundation behavior (Paolucci, 1997; Mergos

and Kawashima, 2005). These algorithms were useful for understanding the beneficial consequences of nonlinear foundation response to severe seismic loading. One of the beneficial consequences of the nonlinear foundation response is the reduced moment bearing capacity of the foundation causing a "rocking isolation system" by limiting the inertial forces transferred to the super-structure (Mergos and Kawashima, 2005; Anastasopoulos and Kontoroupi, 2014; Paolucci, 1997; Gazetas et al., 2003; Pecker, 2003; Gajan et al., 2005; Pender, 2007; Harden et al., 2006; Gajan and Kutter, 2008; Anastasopoulos et al., 2010; Anastasopoulos, 2010; Gelagoti et al., 2012a, 2012b; Kourkoulis et al., 2012a, 2012b; Paolucci et al., 2013). The combined load resisting systems consisting of shear walls and reinforced concrete frames may be significantly affected by the uplift behavior of the foundations. On the document ATC-40 (Applied Technology Council, 1996), it was stated that the slender shear wall frames, slender bearing shear walls with aspect ratios greater than 2 and narrow frames are very sensitive to the uplift of the foundations. Rotations of the foundations at the base of such shear walls may induce significantly large displacement demands on the connected frame elements. On the other hand, short shear wall frames, short bearing shear walls with aspect ratios smaller than 2 and long frames are relatively less sensitive to the uplift of the foundations. However, tall and narrow frames can also be sensitive to the uplift behavior of the foundation due to the possible large overturning forces during ground motion excitations. A major disadvantage of the rocking isolation is the possible settlement particularly on poor soil layers. In the absence of a reliable estimation method for foundation settlement during seismic loading, the foundation settlement can be limited to relatively small magnitudes if the eccentric load on foundation does not reach to the ultimate bearing capacity, so that plastic flow of foundation material cannot severely accumulate (Deng et al. 2012).

1.4. Scope of the Study

The literature review presents the efforts for the analysis of structures on foundations that partially loose contact width underlying medium due to excessive *M*. The numerical integration schemes are useful for computation of dynamic structural response provided that the nonlinear reactions of foundation are precisely calculated. The first difficulty in calculation of foundation impedance during uplift is the estimation of the dimensions of foundation section that is separated from the load-bearing medium. If these dimensions are accurately estimated, the calculation of the effective impedance of foundation section in contact with soil will be straightforward. Hence, the principal aim of this study is to propose a theoretical relationship between the contact width and overturning (rocking) moment acting on foundation. Then, a robust method for computation of the relationship between overturning moment and rocking angle that is applicable to any arbitrarily shaped shallow foundation will be developed. The proposed method will be mainly based on two assumptions. The first assumption is the static impedance coefficients used in the calculations are accurate. The second assumption is that the boundary between the part of foundation that is in contact with soil and the part that is not supported by soil is linear.

The theoretical study aims to contribute rigorous effort in literature by presenting a simple theoretical model capable of simulating the effects of material and geometrical nonlinearities on the response of an arbitrarily shaped shallow foundation to monotonic loading.

This study is organized as presented by the following paragraphs

The first chapter of the thesis presents introductory information and a review of literature.

In the second chapter, the static impedance coefficients for shallow foundations resting on ideally elastic media are presented.

Third chapter defines the theoretical model used for calculation of foundation impedance during uplift. The computational algorithm and the computer program developed for impedance calculations are explained. The typical relationships between the load and displacement are presented.

In chapter four, the computed responses of a shallow foundation resting on elastic halfspace, elastic layer, uniformly distributed springs, and inhomogeneous medium to eccentric loading are presented. The proposed theoretical model is justified by using the results of available solutions. The effect of foundation dimensions, that of thickness of deformable layer, and that of material nonlinearity on the load - deformation relationships are investigated.

In the fifth chapter, the effect of soil nonlinearity on the response of arbitrarily shaped shallow foundations is investigated. First, a literature review on the modeling techniques of soil nonlinearity for problems involving soil-structure interaction is presented. Then, the method used for calculation of the nonlinear response of shallow foundations resting on soil deposits is presented. Finally, the theoretical relationship between load and deformation is compared with those of former experimental studies.

Chapter six presents the results of parametric analyses of uplifting shallow foundations on soil deposits with nonlinear behavior. The analyses are conducted to illustrate the sensitivity of load - deformation relationships of foundations to considered parameters.

In chapter seven, conclusions deduced from the study are presented.

CHAPTER 2

THE STATIC IMPEDANCE COEFFICIENTS OF SHALLOW FOUNDATION RESTING ON IDEALLY ELASTIC MEDIA

2.1. Introduction

The relation between the set of external loads applied on a rigid shallow foundation and the displacements of the foundation is

$$\begin{Bmatrix} H \\ V \\ M \end{Bmatrix} = [K(B,L)] \begin{Bmatrix} h \\ v \\ \theta \end{Bmatrix} \tag{2.1}$$

such that, B and L are respectively the width and length of an arbitrarily shaped foundation (Figure 2.1). H, V, and M are respectively the horizontal load (base shear), vertical load and overturning moment acting on the center of gravity of the foundation; and h and v are respectively the horizontal and vertical displacement of the center of gravity, and θ is the rocking angle (rotation) of foundation in the plane of H and M (Figure 2.2.). $K(B,L)$ is the matrix defining the static stiffness matrix of foundation. Figure 2.2 also shows the positive sign conventions for the load and displacement terms.

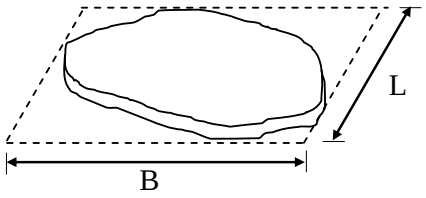

Figure 2.1 An arbitrarily shaped foundation

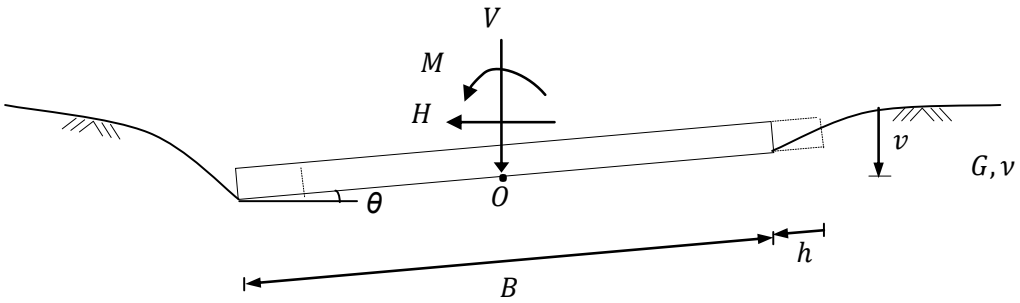

Figure 2.2 A shallow foundation with no separation

It is supposed that there are no coupling terms between H, V, and M for a shallow foundation in the absence of embedment (Gazetas, 1991). In that case, the matrix $K(B,L)$ involves only diagonal elements such as

$$K(B,L) = \begin{bmatrix} K_h(B,L) & 0 & 0 \\ 0 & K_v(B,L) & 0 \\ 0 & 0 & K_\theta(B,L) \end{bmatrix} \tag{2.2}$$

where, K_h, K_v and K_θ are the static stiffness (impedance) coefficients of shallow foundation. These coefficients are related to foundation dimensions and stiffness of load bearing soil. A number of the analytical and semi-empirical formulas for static stiffness coefficients have been proposed in literature. These formulas which will be used for calculation of impedance coefficients during uplifting foundation are presented in the following sections.

2.2. The Static Impedance Coefficients for a Shallow Foundation on an Elastic Half-space

For simplicity, a rigid foundation resting on a homogeneous and isotropic half space is considered. The half space extends infinitely in all directions except for the plane of free boundary. The material coefficients defining the rigidity of elastic half space are the shear modulus (G) and the Poisson's ratio (ν). The geometric properties (dimensions) of the system are the maximum width (B) and the maximum length (L) of the foundation, the contact area (f) of foundation, and the moment of inertia (I) around the axis of rotation. The static impedance coefficients for shallow foundations resting on homogeneous elastic half-space were simplified by Dobry and Gazetas (1986) and Gazetas (1991). The formulas for calculation of these coefficients are presented in Table 2.1 and Table 2.2. The formulas presented in Table 2.1 and Table 2.2 are used for derivation of the equations presented in next chapter.

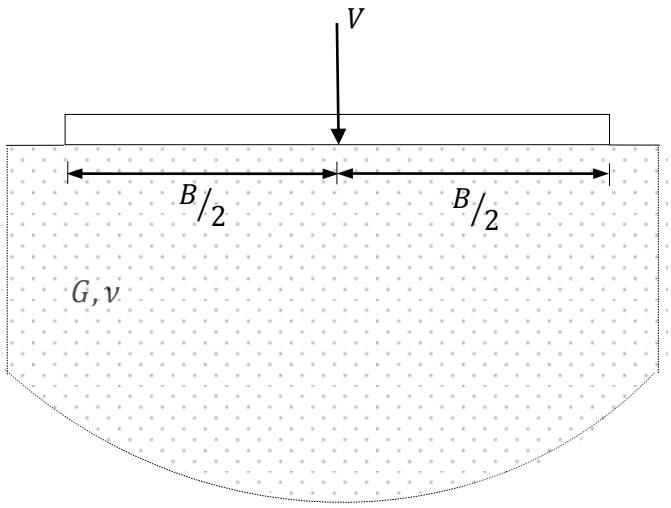

Figure 2.3 A shallow foundation resting on elastic halfspace

Table 2.1 The static impedance coefficients of arbitrarily shaped foundation on homogeneous halfspace (Dobry and Gazetas, 1986 and Gazetas, 1991)

Vibration Mode	Static Impedance Coefficients
Vertical (B<L)	$K_v = S_v \frac{GL}{1-\nu}$ $S_v = 0.8$ for $\frac{f}{L^2} < 0.02$ $S_v = 0.73 + 1.54\left(\frac{f}{L^2}\right)^{0.75}$ for $\frac{f}{L^2} > 0.02$
Vertical (B>L)	$K_v = S_v \frac{GB}{1-\nu}$ $S_v = 0.8$ for $\frac{f}{B^2} < 0.02$ $S_v = 0.73 + 1.54\left(\frac{f}{B^2}\right)^{0.75}$ for $\frac{f}{B^2} > 0.02$
Horizontal (B<L)	$K_h = S_h \frac{GL}{2-\nu}$ $S_h = 2.24$ for $\frac{f}{L^2} < 0.16$ $S_h = 4.5\left(\frac{f}{L^2}\right)^{0.38}$ for $\frac{f}{L^2} > 0.16$
Horizontal (B>L)	$K_h = S_h \frac{GB}{2-\nu} - \frac{0.105Gb}{0.75-\nu}\left(1-\frac{L}{B}\right)$ $S_h = 2.24$ for $\frac{f}{B^2} < 0.16$ $S_h = 4.5\left(\frac{f}{B^2}\right)^{0.38}$ for $\frac{f}{B^2} > 0.16$
Rocking (B<L)	$K_\theta = S_\theta \frac{G}{1-\nu}\left(\frac{L}{B}\right)^{0.25} I^{0.75}$ $S_\theta = 2.54$ for $\frac{B}{L} < 0.4$ $S_\theta = 3.2\left(\frac{B}{L}\right)^{0.25}$ for $\frac{B}{L} > 0.4$
Rocking (B>L)	$K_\theta = 3.2 \frac{G}{1-\nu} I^{0.75}$

Table 2.2 The static impedance coefficients of rectangular foundation, circular foundation and strip foundation on homogeneous halfspace (Dobry and Gazetas, 1986 and Gazetas, 1991)

Vibration Mode	Static Impedance Coefficients		
	Rectangular foundation	Circular foundation	Strip foundation
Vertical (B<L)	$K_v = \frac{GL}{1-\nu}\left(0.73 + 1.54\left(\frac{B}{L}\right)^{0.75}\right)$	$K_v = \frac{2GB}{1-\nu}$	$\frac{K_v}{2L} = \frac{0.8G}{1-\nu}$
Vertical (B>L)	$K_v = \frac{GB}{1-\nu}\left(0.73 + 1.54\left(\frac{L}{B}\right)^{0.75}\right)$	$K_v = \frac{2GB}{1-\nu}$	$\frac{K_v}{2L} = \frac{0.8G}{1-\nu}$
Horizontal (B<L)	$K_h = \frac{GL}{2-\nu}\left(2 + 2.5\left(\frac{B}{L}\right)^{0.85}\right)$	$K_h = \frac{4GB}{2-\nu}$	$\frac{K_h}{2L} = \frac{2.24G}{2-\nu}$
Horizontal (B>L)	$K_h = \frac{GB}{2-\nu}\left(2 + 2.5\left(\frac{L}{B}\right)^{0.85}\right) - \frac{0.1GB}{0.75-\nu}\left(1 - \frac{L}{B}\right)$	$K_h = \frac{4GB}{2-\nu}$	——
Rocking (B<L)	$K_\theta = \frac{GB^2L}{1-\nu}\left(0.372 + 0.078\frac{B}{L}\right)$	$K_\theta = \frac{GB^3}{3(1-\nu)}$	$\frac{K_\theta}{2L} = \frac{\pi GB^2}{2(1-\nu)} \cdot \left(1 + \left[\frac{\ln(3-4\nu)}{\pi}\right]^2\right)$
Rocking (B>L)	$K_\theta = \frac{0.465G(B^4L)^{0.6}}{1-\nu}$	$K_\theta = \frac{GB^3}{3(1-\nu)}$	——

2.3. The Static Impedance Coefficients for Rectangular Foundation on Elastic Layer

The static impedance coefficients of rectangular foundation resting on finite layer are presented by Sovinc (1969, quoted by Poulos and Davis, 1974). The soil comprises a homogenous layer of thickness D which rests on an ideally rigid geological formation (Figure 2.4). The range of D/B is from 0 to 2.5. For D/B greater than 2.5, the static impedance coefficients of rectangular foundation resting on finite layer are similar to those of resting on an elastic half space.

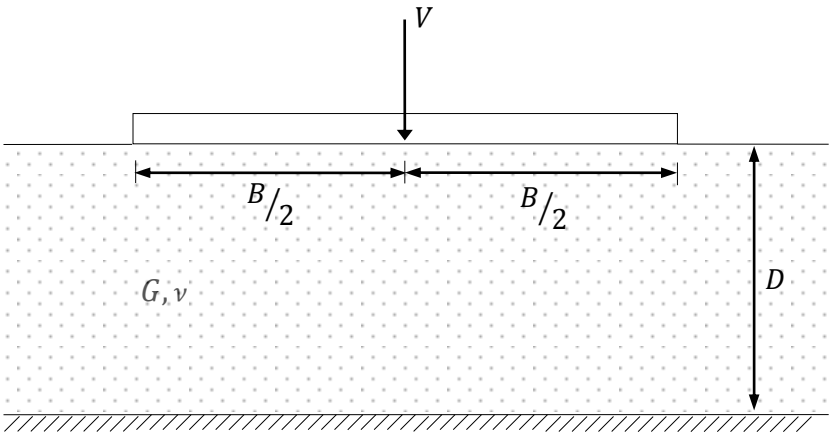

Figure 2.4 A shallow foundation resting on an elastic layer

The static foundation impedances are expressed in terms of dimensionless parameters β and γ.

$$\beta = \frac{3GL}{K_v} \tag{2.3}$$

$$\gamma = \frac{3GB^3}{8K_\theta} \tag{2.4}$$

The relationships between β, γ, D/B and B/L are shown in Figure 2.5.

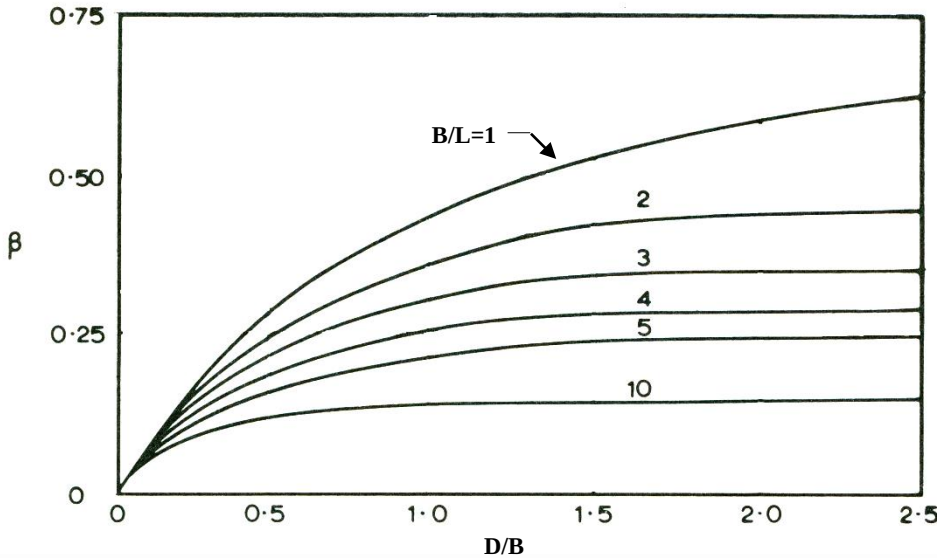

(a)

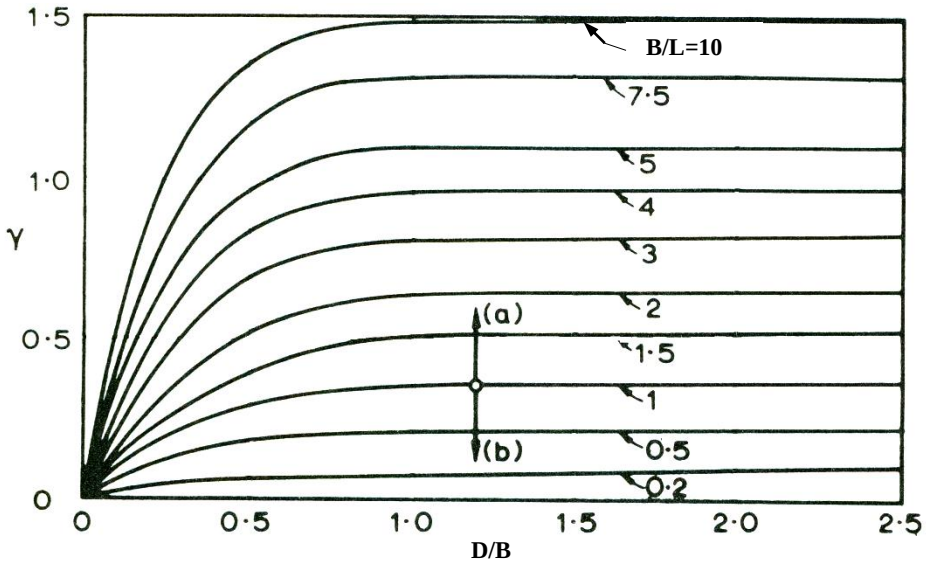

(b)

Figure 2.5 (a) $\beta - D/B$ relationship for a rectangular foundation resting on finite layer, (b) $\gamma - D/B$ relationship for a rectangular foundation resting on finite layer (Sovinc, 1969).

2.4. The Static Impedance Coefficients for a Strip Foundation resting on Deep Inhomogeneous Deposits

Vertical and horizontal stiffness coefficients for a shallow strip foundation resting on a heterogeneous soil medium with a constant gradient of shear modulus are (Gazetas, 1991)

$$K_v = \frac{0.73G_0}{1-\nu}(1 + 2\mathrm{a}) \qquad (2.5.a)$$

$$K_h = \frac{2G_0}{2-\nu}\left(1 + \frac{2\mathrm{a}}{3}\right) \qquad (2.5.b)$$

in vertical and horizontal directions respectively. The relationship between G and G_0 is

$$G = G_0\left(1 + a\frac{z}{\mathrm{B}}\right) \qquad (2.6)$$

where a is the gradient of G, the shear modulus of a particular point in an elastic medium (Gazetas, 1991). G increases by depth (z) linearly. Consequently, the rocking stiffness of foundation resting on an inhomogeneous medium (Gazetas, 1991) is

$$K_\theta = \frac{\pi G_0}{2-2\nu}\left(\frac{B^2}{4}\right)\left(1 + \frac{\mathrm{a}}{3}\right) \qquad (2.7)$$

2.5. The Static Impedance Coefficients for Shallow Foundation on Winkler Springs

Due to its simplicity Winkler foundation is among the most widely used models used for simulation of the behavior of shallow foundations interacting with soil. In

the Winkler foundation, the reaction of soil is simulated as a bed of independent nonlinear springs. In this study, particular emphasize is put on Winkler Foundation to show its limitations, and to justify theoretical relationships about foundation uplift. Despite its simplicity the critical limitation of Winkler foundation is that the relationship between K_V and K_θ is not consistent with that of a shallow foundation on elastic continuum (Table 2.1 and Table 2.2). Therefore, the model cannot correctly couple vertical displacement with rocking angle during foundation uplift.

The static impedance of a rigid rectangular foundation resting on (distributed) Winkler springs (Figure 2.6) with coefficient k_v and k_h are

$$K_v(B,L) = k_v BL \qquad (2.8.a)$$

and

$$K_h(B,L) = k_h BL \qquad (2.8.b)$$

in the vertical and horizontal directions respectively. The rocking impedance coefficient of foundation is

$$K_\theta(B,L) = \frac{1}{12} k_v B^3 L \qquad (2.9)$$

In order to simulate foundation behavior during uplift, it is supposed that the springs connected normal to the foundation (i.e. k_v) lack tensional resistance. When the normal stress reduces down to zero that part of foundation becomes separated from the elastic medium. It is assumed that the horizontally connected springs (k_h) on the separated section do not contribute to the rocking impedance. The foundation uplift will initiate when the normal stress on one side of foundation reduces to zero due to the increase in M.

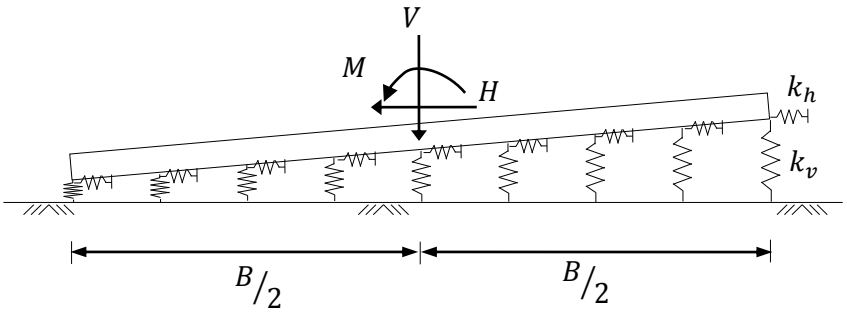

Figure 2.6 A rigid foundation resting on tensionless Winkler springs

CHAPTER 3

A SIMPLE MODEL ON FOUNDATION UPLIFT

3.1. Introduction

In this chapter, development of an analytical model to calculate the static response of arbitrarily shaped foundations during the uplift is presented. First, the main equilibrium equations are presented. Then, the theory of impedance for arbitrarily shaped foundations during uplift is presented. Finally, the relationship between the applied load and response parameters is derived.

3.2. Basic equations of equilibrium

The main equations on static equilibrium of a shallow foundation permitted to uplift is presented in this section. In the verge of foundation uplift, the section of a foundation that is in contact with soil may be considered as a shallow foundation of width b (shown as dashed section in Figure 3.1). Therefore, substitution of b for B in Equation 2.1 results in the equations of equilibrium for a foundation that is partially separated from the supporting elastic medium.

$$\begin{Bmatrix} H' \\ V' \\ M' \end{Bmatrix} = [K(b, L)] \begin{Bmatrix} h' \\ v' \\ \theta' \end{Bmatrix} \tag{3.1}$$

where, H', V' and M' are respectively the horizontal reaction, vertical reaction and moment acting on the centroidal axis of contact area, due to the horizontal

displacement (h'), vertical displacement (v') and rotation (θ') of the centroidal axis of contact area. The centroidal axis is shown by O in Figure 3.1.

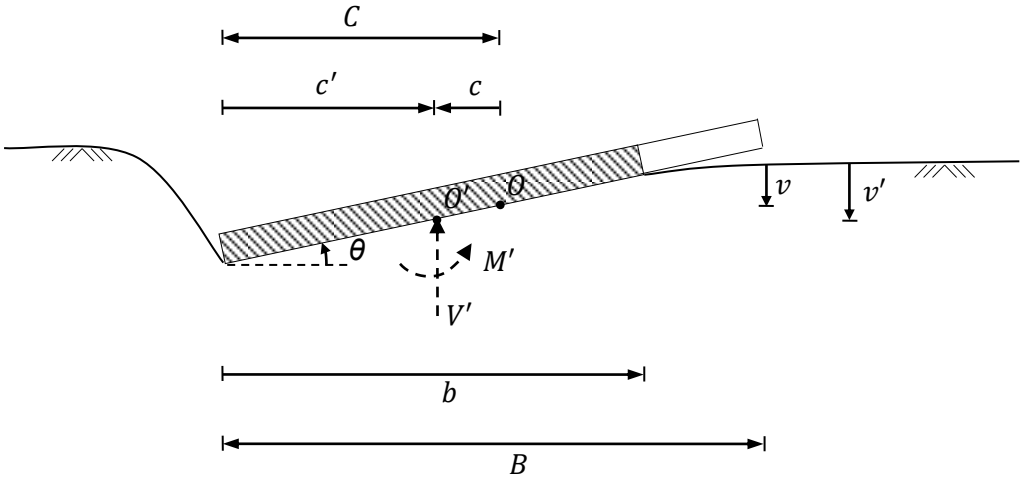

Figure 3.1 Reduction in effective foundation width due to loss of contact with load bearing medium

The relationship between the displacements on the centroidal axis of foundation (O in Figure 3.1) and the centroidal axis of contact area (point O' in Figure 3.1) is

$$\begin{Bmatrix} h' \\ v' \\ \theta' \end{Bmatrix} = [A] \begin{Bmatrix} h \\ v \\ \theta \end{Bmatrix} \tag{3.2}$$

Assuming small deflections (i.e., $\tan\theta \cong \theta$),

$$[A] = \begin{bmatrix} 1 & 0 & 0 \\ 0 & 1 & c \\ 0 & 0 & 1 \end{bmatrix} \tag{3.3}$$

where, c is the distance between the centroidal axis of the foundation (O in Figure 3.1) from the centroidal axis of contact area (point O' in Figure 3.1). v' is related

to both v and θ after initiation of uplift. Using general transformation rule (Cook et al., 1989), the relationship between resultant forces acting on the centroidal axis of the foundation and on the centroidal axis of contact area is

$$\begin{Bmatrix} H \\ V \\ M \end{Bmatrix} = [A]^T \begin{Bmatrix} H' \\ V' \\ M' \end{Bmatrix} \tag{3.4.a}$$

or

$$\begin{Bmatrix} H' \\ V' \\ M' \end{Bmatrix} = \begin{bmatrix} 1 & 0 & 0 \\ 0 & 1 & 0 \\ 0 & c & 1 \end{bmatrix} \begin{Bmatrix} H \\ V \\ M \end{Bmatrix} \tag{3.4.b}$$

Substitution of Equations 3.1 and 3.2 in Equation 3.4 results in the equations of equilibrium during uplift. The foundation stiffness is related to the contact width b and foundation length L. On the other hand, b is related to foundation displacements, v and θ.

$$\begin{Bmatrix} H \\ V \\ M \end{Bmatrix} = [A]^T [K(b, L)][A] \begin{Bmatrix} h \\ v \\ \theta \end{Bmatrix} \tag{3.5}$$

Equation 3.5 constitutes a nonlinear system of equations.

3.3. Theory for calculation of impedance for a foundation during uplift

The rocking motion of buildings due to horizontal loading may lead to partial separation of the shallow foundations from underlying soil, and consequently uplift of a side of foundation due to the lack of tensional strength in load bearing soil. During the uplift of shallow foundations, reduction of effective contact width of the foundation, b, modifies the reaction moment due to the varying location of the

foundation center. The section of the foundation that is not in contact with soil cannot contribute to the foundation impedance. The relation between the moment acting on foundation during the uplift and the applied vertical load is supposed to be

$$M' = \alpha . V . c' \tag{3.6}$$

where, M' is the moment acting on instantaneous central axis of the section in contact with soil (Figure 3.1), V is the applied vertical load, and α is a parameter dependent on the geometric properties of the foundation and mechanical properties of the deformable support.

For a shallow foundation uplift behavior may be described by two mechanisms that compensate each other. If the overturning moment exceeds a specific limit, tensional stresses will tend to occur beneath the foundation. A part of foundation will partially separate from the soil. Consequently, the contact width of the foundation with soil will decrease. The section of the foundation that is not in contact with soil cannot contribute to the foundation impedance. Therefore, the effective width of foundation reduces to the width of foundation that is in contact with soil. This will tend to reduce the reaction moment. The second mechanism is related to the change in load eccentricity. The increase in the distance between the geometric center and the center of the effective foundation width (Figure 3.1.) will tend to increase the eccentricity of applied vertical load, and consequently the moment acting on initial centroidal axis of foundation. Because the external load V and its eccentricity (i.e., M) are supposed to be given (or, constant) the change in contact width should not have any effect on the foundation reaction balancing the external load. In other words, it is postulated that there should be no change in reaction moment due to a differentially small change in contact area between soil and foundation during uplift. A physical explanation of this postulate can be presented by the stress distribution beneath a foundation during uplift. The normal

stress on the edge of foundation that is in merely contact width soil is zero. Therefore, a differentially small change in contact width should have no effect on reaction moment and vertical load acting on centroidal axis of contact width of foundation. Consequently, two mechanisms should compensate each other during increment of applied external loading. Hence,

$$\frac{dM'}{db} = 0 \tag{3.7}$$

By substituting Equation 2.1 in Equation 3.4b:

$$M' = c.V + K_\theta(b, L)\theta \tag{3.8}$$

The change in M' due to a differential change in b is

$$\frac{dM'}{db} = \frac{dc}{db}V + \frac{\partial K_\theta(b, L)}{\partial b}\theta \tag{3.9}$$

The rocking angle during initiation of uplift is equal to $M'/K_\theta(b, L)$. Substitution of Equation 3.6 and Equation 3.7 in Equation 3.9 yields

$$0 = \frac{dc}{db}V + \alpha\frac{Vc'}{K_\theta(b, L)}\frac{\partial K_\theta(b, L)}{\partial b} \tag{3.10}$$

or,

$$\alpha = -\frac{dc}{db}\frac{K_\theta(b, L)}{\frac{\partial K_\theta(b, L)}{\partial b}c'} \tag{3.11}$$

c' will tend to decrease; or, c will tend to increase by increasing load eccentricity, or M. Therefore, α is a function of b, and can be used for calculation of the relationship between b, θ and M during uplift.

In case of a prismatic section, $c' = b/2$ and $dc'/db = 1/2$, yielding a simpler relationship

$$\alpha = \frac{K_\theta(b, L)}{\frac{\partial K_\theta(b, L)}{\partial b} b} \tag{3.12}$$

For non-prismatic sections, the derivatives (Equation 3.11) should be analytically or numerically derived, by expressing c' in terms of b. Equation 3.11 and Equation 3.6 will provide a formula for M that will initiate separation of foundation from load-bearing medium, if $c' = B/2$ is substituted in Equation 3.11 to calculate α at the initiation of uplift. α at the verge of initial uplift was studied in the past by a number of researchers. Several values have been proposed for α at the initiation of uplift, which are explained in the following paragraph.

The moment initiating uplift, M_{uplift}, is equal to M', when the effective width, b, is equal to the true width of the foundation, B. c' is equal to the distance between the center of the foundation and the edge of the foundation, C.

$$M_{uplift} = \alpha . V . C \tag{3.13}$$

C is equal to $B/2$ for sections symmetric around centroidal axis (Figure 3.1). If a rigid foundation resting on an ideally rigid support was considered, the uplift would initiate as soon as M reaches to an ultimate value M_{ult}, such that

$$M_{ult} = V . C \tag{3.14}$$

Consequently, the threshold moment for the initiation of uplift for rigid foundations resting on deformable medium will be proportional to M_{ult}, such that

$$M_{uplift} = \alpha . M_{ult} \tag{3.15}$$

which was previously suggested by Apostolou et al. (2007). The theoretical values of α on the verge of uplift for strip, rectangular and circular foundations on elastic support are compared with those reported in the literature in Table 3.1. The derivations of theoretical values of α for these basic foundation shapes are shown in Appendix D. It is observed that the theoretical values of α according to Equation 3.11 are reasonably consistent with the fraction $1/3$ reported by Chopra and Yim (1985) for rectangular foundations resting on a Winkler type support. Parameter α according to Equation 3.11 agrees with the figures reported by Wolf (1976) for circular and strip foundation on elastic half space. Although the solution for strip foundation on elastic half space is consistent with that of Gazetas et al. (2013), M_{uplift} is 11% and 5% lower than that reported by Gazetas et al. (2013) in the cases of a rectangular foundation having an aspect ratio 5, and for a circular foundation respectively. These limited differences may be attributed to the assumptions in the finite element models of Gazetas et al. (2013) or to the assumption that the boundary between the part of foundation that is in contact with soil and the part that is not supported by soil is linear (Figure 3.2). Hence, Equation 3.11 is reasonably supported by these comparisons and can be used for computation of α and for the relationship between θ and M during uplift of an arbitrarily shaped foundation.

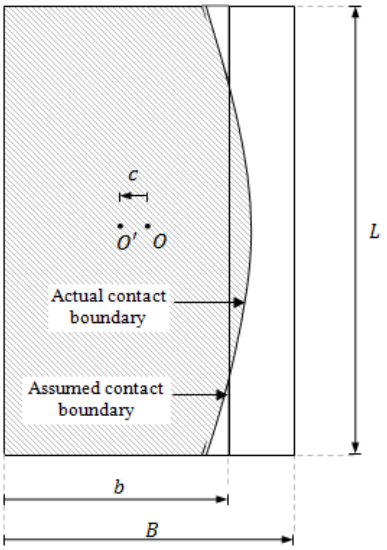

Figure 3.2 Actual and assumed contact boundaries during the uplift of foundation

Table 3.1 Comparative results for α on the verge of uplift

Foundation	$\boldsymbol{\alpha}$	
	Equation 3.11	**Literature**
Rectangular foundation (on Winkler springs)	$1/3$	$1/3$ (Chopra and Yim,1985)*
Rectangular foundation (B=5L) (on elastic halfspace)	$1/2.25$	$1/2$ (Gazetas et al., 2013)
Circular foundation (on elastic halfspace)	$1/3$	$1/3$ (Wolf,1976) $1/2.85$ (Gazetas et al., 2013)
Strip foundation (on elastic halfspace)	$1/2$	$1/2$ (Wolf,1976) $1/2$ (Gazetas et al., 2013)

* Equation showing $\alpha = 1/3$ is shown in Appendix C.

3.4. The relationship between M, v and θ during uplift

In this section the theory behind the equations used for calculation of the relationship between external load and foundation displacements is introduced. Also, a procedure for calculations is presented by using a flow chart and its step by step explanation.

Only the section of foundation that is in contact with soil contributes to the impedance of foundation after the initiation of uplift. The load bearing section of the foundation, c', varies with each increment in overturning moment acting on foundation. It was postulated that for the initiation of uplift the condition

$$M' = \alpha . V . c' \qquad (3.16a)$$

or

$$\frac{M'}{V} - \alpha . c' = 0 \qquad (3.16b)$$

should be satisfied for any c'.

$$\frac{M'}{V} - \left(- \frac{dc}{db} \frac{K_\theta(b,L)}{\frac{\partial K_\theta(b,L)}{\partial b}_{c'}} \right) . c' = 0 \qquad (3.17)$$

A computer program is developed for computation of the static response of arbitrarily shaped shallow foundations during uplift. The computing language of Matlab (The MathWorks Inc., 2008) is used. The flowchart of main program is shown in Figure 3.2a. The program calculates the displacement response of a shallow foundation to an external load vector. Basically, the program calculates c'

for any given set of M and V. Moreover, V is supposed to be a constant and M is incrementally increased up to an ultimate value.

In the solution algorithm, the geometric foundation properties (i.e. b, c, f, I, L), explained in Section 2.2 are required to calculate the rotational, vertical and horizontal stiffness of foundation. Such properties of foundations are calculated by employing cubic-spline interpolation, and used in the solution algorithm as input values.

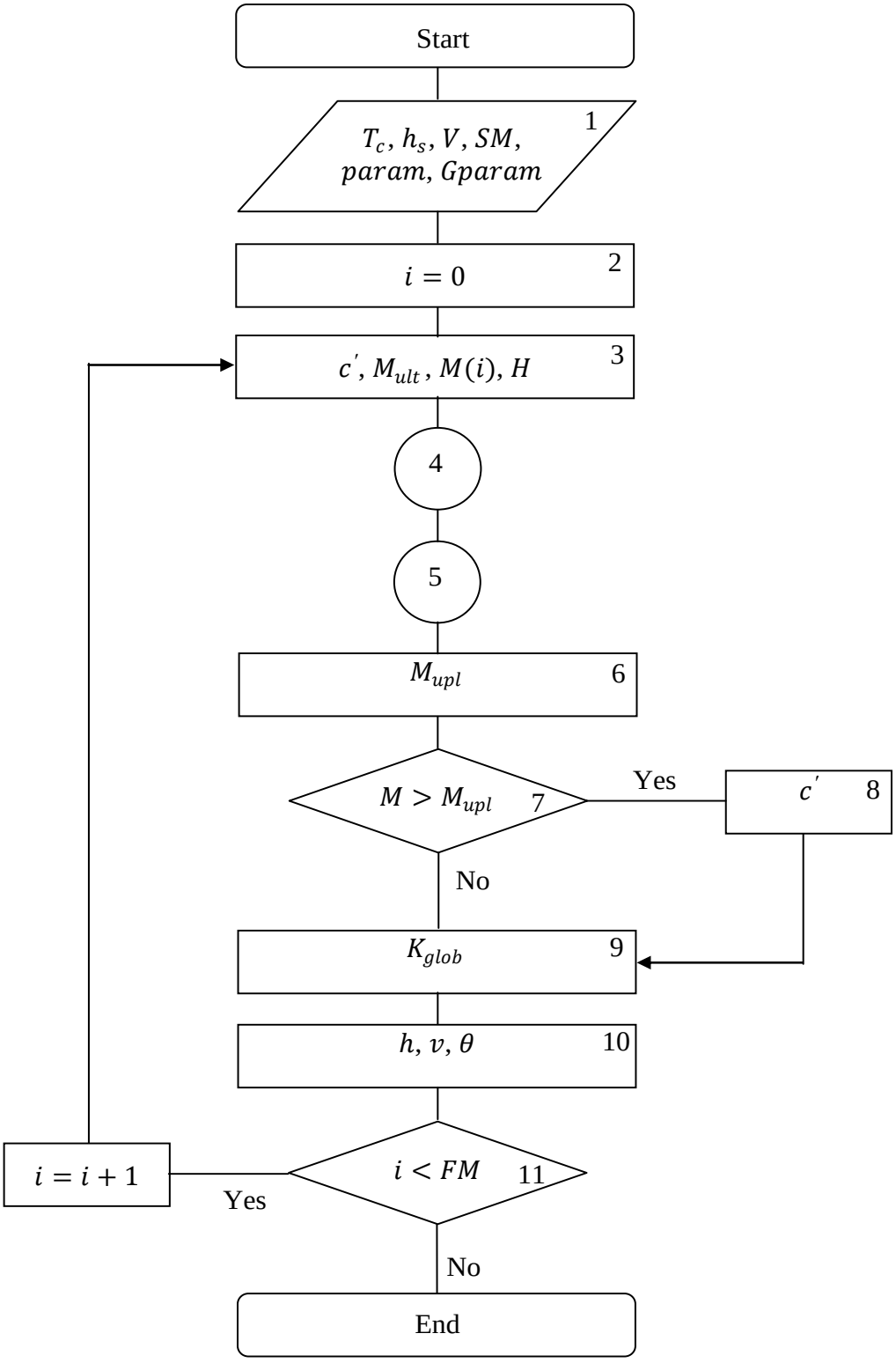
Start
$T_c, h_s, V, SM,$
$param, Gparam$
1
$i = 0$
2
$c', M_{ult}, M(i), H$
3
4
5
M_{upl}
6
$M > M_{upl}$
7
Yes
c'
8
No
K_{glob}
9
h, v, θ
10
$i = i + 1$
$i < FM$
11
Yes
No
End

(a)

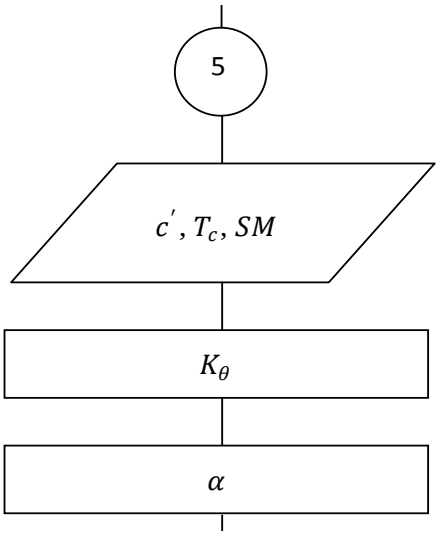

(b)

Figure 3.3 Flow Chart: (a) main program, (b) routine to calculate α

The algorithm of computer program is presented in Figure 3.2. The details of the algorithm are presented below step by step.

1. The parameters necessary for the computer program are entered. T_c is a six column matrix showing the relationships between the geometric parameters c', b, c, f, I and L in a tabulated form. Typical geometric relationships between the normalized parameters (i.e. $b_N - c'_N$, $c_N - c'_N$, $f_N - c'_N$, $I_N - c'_N$, $L_N - c'_N$) are shown in Figures A.4 to A.8 in Appendix A. These parameters are presented in Section 3.2, and in Appendix A).

SM is an integer value that is equal to the number of steps considered in generation of the incremental moment array for M. V is the vertical load acting on foundation. h_s is the moment arm, the vertical distance between the foundation and the point of application of the horizontal load.

$param$ is an array defining the properties of foundation and the soil. $param(1)$ defines the methodology to simulate the soil conditions, as shown in Table 3.2.

Table 3.2 Options to simulate the soil conditions in the computer program

param(1)	Support type
1	Winkler
2	Elastic halfspace (rectangular foundation)
3	Elastic halfspace (circular foundation)
4	Elastic halfspace (arbitrarily shaped foundation)
5	Heterogeneous soil medium (strip foundation)
6	Finite thickness elastic layer (rectangular foundation)

$param(2)$ defines the coefficient k_0 that is used in the calculation of static impedance matrix for a foundation on Winkler springs.

$param(3)$ gives the Poisson's ratio of soil.

$param(4)$ defines depth of finite thickness layer in case $param(1) = 6$.

$param(5)$ is used to select the shape of foundation among the foundations shapes presented in Table 3.3.

Table 3.3 Options for $param(5)$ in the computer program

param(5)	Foundation shape
1	Square
2	Rectanqular (b>L)
3	Rectangular (b<L)
4	Circular
5	Square*
6	Strip

*2 way eccentricity (see Appendix A)

$param$ (6) is used to give the gradient of G, a applicable only for a strip foundation (see Section 2.4).

$Gparam$ is shear modulus of elastic layer or halfspace.

2. i is the current value of the counter used in computer program. The starting value of the counter is zero (i.e. $i = 0$).

3. c' is taken from the first row of Table T_c, and is used for calculation of M_{ult} by Equation 3.14. The array of moments (M) having length of SM is generated in the range from 0 to M_{ult} with constant intervals. Then the magnitude of the applied horizontal load (H) is calculated by dividing the current value of M, $M(i)$, by h_s.

4. Shear modulus of elastic layer or halfspace (G) is equal to $Gparam$.

5. The rotational impedance coefficient (K_θ) of a foundation is calculated. K_θ of a foundation resting on homogeneous elastic half-space is calculated by using Table 2.1, K_θ depends on $param(3)$ and $Gparam$. Similarly, K_θ of foundations resting on a (i) finite layer, depending on $param(1)$ and $Gparam$, (ii) heterogeneous soil medium, depending on $param(6)$ and $Gparam$, and (iii) Winkler springs, depending on $param(2)$, are calculated by Equation 2.4, Equation 2.7, and Equation 2.9, respectively.

α is calculated using Equation 3.11. α is calculated by calculating the derivative of c with respect to b. The forward difference approximation (Chapra and Canale, 2010) is used for the application of numerical derivation. b, c, f, I and L corresponding to c' are taken from T_c. b, c, f, I and L corresponding to any c' is calculated using the cubic spline interpolation method (Chapra and Canale, 2010). Then an infinitesimal value, $eps.$, is calculated. eps, is calculated by taking reciprocal of SM multiplied with 100. Next, the new value of c' is calculated by

subtracting eps from the initial value of c'. Then, new values of b, c, f, I and L corresponding to new c' are calculated together with a new K_θ. Finally, the numerical derivation procedure is applied by using forward difference approximation.

6. The threshold moment for the initiation of uplift (M_{uplift}) is calculated using Equation 3.15.

7. Then a new variable, $MCOUNT$, with a length equal to the length of the moment array M is used to activate a counter, $ICOUNT$, used to distinguish between the moment values smaller and higher than the M_{uplift}. Next, a conditional if function is used, such that;

a) If the overturning moment is smaller than M_{uplift} $(i.e.\ M(i) < M_{uplift})$, go to step 9.

b) If the overturning moment is greater than M_{uplift} $(i.e.\ M(i) > M_{uplift})$ go to step 8 and then go to step 9.

8. First the transformation matrix A is calculated using Equation 3.3. To calculate A, the value of c corresponding to c' is taken from T_c. Then, the moment acting on centroidal axis of contact area, $M(i)'$ is calculated using Equation 3.4b. Finally, c' is calculated using Equation 3.17. In Equation 3.17, the c' is updated by calling a built-in Matlab function, $fzero$. $fzero$, determines the root of a function. The initial estimate for the iterative method employed by $fzero$ is set to be equal to c' computed for the previous load combination. α is also updated in each iteration due to the variation of c' in the procedure.

9. The new geometric properties of foundation (b, c, f, I, L) corresponding to new

value of c' are taken from T_c. Then, using these new geometric properties, the impedance coefficients of foundation (K_h, K_v, K_θ) are calculated using (i) Table 2.1 for arbitrarily shaped foundations resting on homogeneous half-space, (ii) Equation 2.3 and Equation 2.4 for rectangular foundations resting on finite layer and (iii) Equation 2.8-2.9 for rectangular foundations resting on Winkler Springs. Furthermore, the transformation matrix A is also updated using the new value of c'. A and the stiffness matrix K (i.e. formed by using K_h, K_v, K_θ) is used together and the global stiffness matrix K_{glob} is obtained.

10. The horizontal displacement (h), the vertical displacement (v) and rotation (θ) are calculated using Equation 3.5 for the load step. Finally, the $M(i)$, H and V values of the load step is used together with K_{glob} (Equation 3.18) to calculate h, v and θ. K_{glob} is the matrix defining the static stiffness of the uplifting foundation.

$$K_{glob} = [A]^T[K(b, L)][A] \tag{3.18}$$

11. The current value of the counter i is compared with the length of generic load array, FM.

a) if $i < FM$, the counter is increased by 1 and the computational process goes to Step 3.

b) if $i = FM$, the computer program ends.

This solution procedure is repeated for each incremental step of applied overturning moment.

CHAPTER 4

JUSTIFICATIONS AND APPLICATIONS

In this chapter, theoretical responses of shallow foundations on elastic halfspace, elastic layer, uniformly distributed springs, and deep inhomogeneous soil deposits to excessive eccentric loading are presented. The theoretical method proposed in this study is justified by comparisons with available solutions. Also, the effect of foundation dimensions, thickness of deformable layer, and the nonlinear behavior of soil on the relationships between M and θ, and v and θ are investigated in the chapter.

4.1. Normalization

The reaction forces and the foundation displacements are normalized to compare the effect of geometric (i.e., shape and dimensions of foundation) and soil parameters (i.e., the thickness of elastic layer) on the response of foundation. The normalized reaction forces and the foundation displacements are compared with the results obtained from different theoretical approaches, such as Winkler foundation and elastic half space. The overturning moment is normalized by

$$M_N = \frac{M}{M_{ult}} \qquad (4.1a)$$

or

$$M_N = M\frac{2}{VB} \tag{4.1b}$$

The rocking angle is normalized by

$$\theta_N = \theta\frac{K_\theta(B,L)}{M_{ult}} \tag{4.2a}$$

or

$$\theta_N = \theta\frac{2K_\theta(B,L)}{VB} \tag{4.2b}$$

The vertical displacement is normalized by

$$v_N = v\frac{K_v(B,L)}{V} \tag{4.3}$$

Hence the normalized overturning moment (M_N), the normalized rocking angle (θ_N) and the normalized vertical displacement (v_N) are used for comparisons with the other theoretical or numerical solutions presented in literature.

4.2. Verifications

In this section, results of the proposed theoretical method are compared with those available in the literature obtained using several benchmark studies focused on the response of uplifting shallow foundations. In the comparisons, M_N - θ_N, v_N - θ_N and α - θ_N relationships are considered. The results are presented for shallow foundations with rectangular, circular and strip foundations.

Figure 4.1 shows the relationships between M_N and θ_N calculated for a square foundation resting on elastic half-space and Winkler springs. The rotational stiffness of the foundation, K_θ, resting on elastic half space is calculated using the input parameters. The vertical impedance of a Winkler foundation, K_v, (Equation 2.8a) is proportional to K_θ (Equation 2.9). Such an assumption provided the comparison of the M_N and θ_N relationships plotted for foundations resting on elastic half space and Winkler springs. It is observed that the M_N and θ_N relationships follow the same trend until the initiation of uplift. However, after the initiation of uplift, the range of M_N forms two different lines with a maximum error of 13%. This deviation may be attributed to well known drawbacks of the Winkler springs (Pender, 2007; Figini et al., 2012). Some of these drawbacks are the lack of accurate interaction between Winkler springs and lack of accurate modeling of the coupling between various degrees of freedom of the system (Figini et al., 2012). Such drawbacks result in inaccurate relationships between K_θ and K_v, and assuming uniform spring stiffness in contrary to the actual conditions.

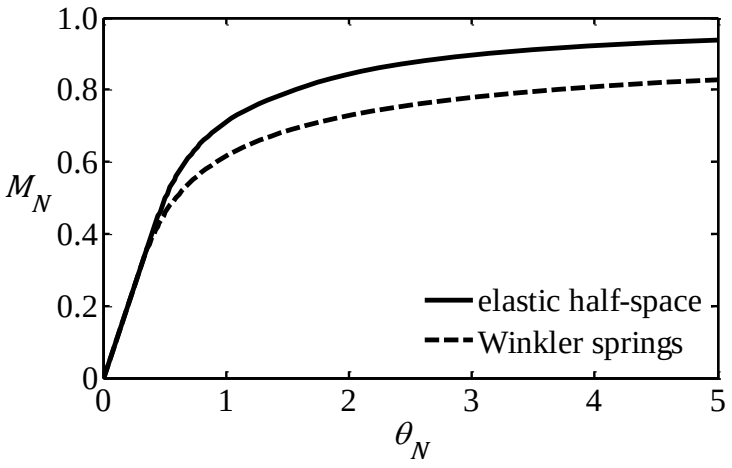

Figure 4.1 The relationship between M_N and θ_N for a square foundation under static loading on elastic half-space and Winkler springs

The v_N and θ_N relationship of a square foundation on elastic half-space and Winkler springs are presented in Figure 4.2. It is observed that the relationships between v_N and θ_N coincide until the initiation of uplift. After the initiation of uplift, v_N is calculated by two models deviate from each other. This figure shows that the Winkler model cannot yield accurate results in terms of vertical and rotational response of a foundation simultaneously, because of the incorrect relationship between K_θ and K_v.

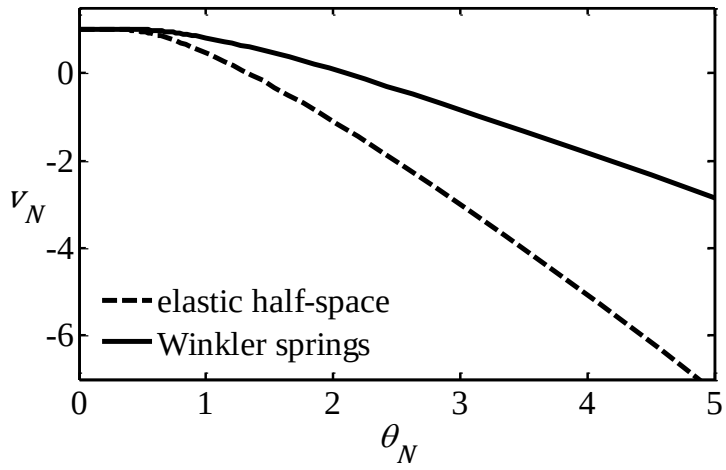

Figure 4.2 The relationship between v_N and θ_N for a square foundation under static loading on elastic half-space and Winkler springs

The relation between α and θ_N for circular foundation resting on elastic half-space is presented in Figure 4.3 to observe the variation of α with the normalized rotation values, θ_N, in circular foundations. Before initiation of uplift, α obtained from Equation 3.11 remains constant (i.e., $1/3$). It is worth noting that Wolf (1976) and Gazetas et al. (2013) proposed two different α for circular foundations (i.e. α=1/3 (Wolf, 1976) and α=1/2.85 (Gazetas et al., 2013)). However, after the initiation of uplift α obtained by Equation 3.11 continuously changes. The continuous variation of α is attributed to the formation of arbitrarily shaped foundations during the uplift of circular foundations (Appendix A) which results in variations in the rotational stiffness of foundation. These variations in the rotational stiffness

necessitate the use of different formulations in solution algorithms. Different solution algorithms to calculate the rotational stiffness create sudden change in α.

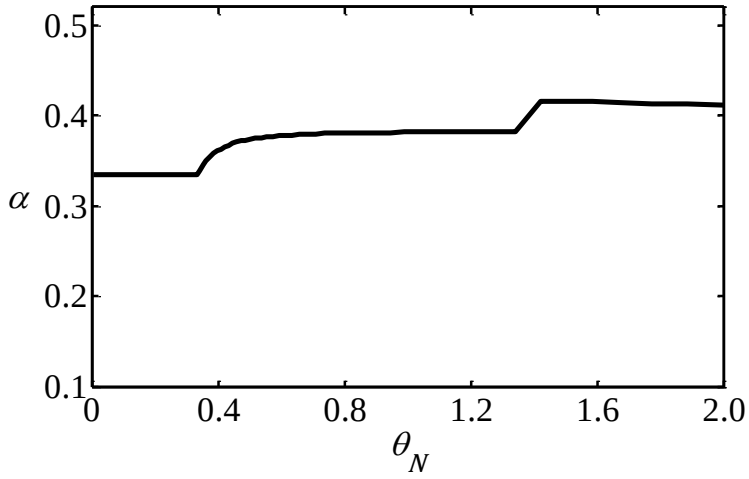

Figure 4.3 The relationship between α and θ_N obtained using Equation 3.11 for circular foundations resting on homogeneous half-space.

In Figure 4.4, the variation of M_N as a function of θ_N is compared with those given by Wolf (1976). It may be observed that the maximum difference between the results of this study and that of the Wolf (1976) is 6.7%. This difference may be attributed to the approximations in the study of Wolf (1976). One of these approximations may be due to the transformation of actual irregular contact area to an equivalent circular area in calculations. Another reason can be the assumption made in this study, such that the boundary between contact zone and separated zone beneath foundation is linear.

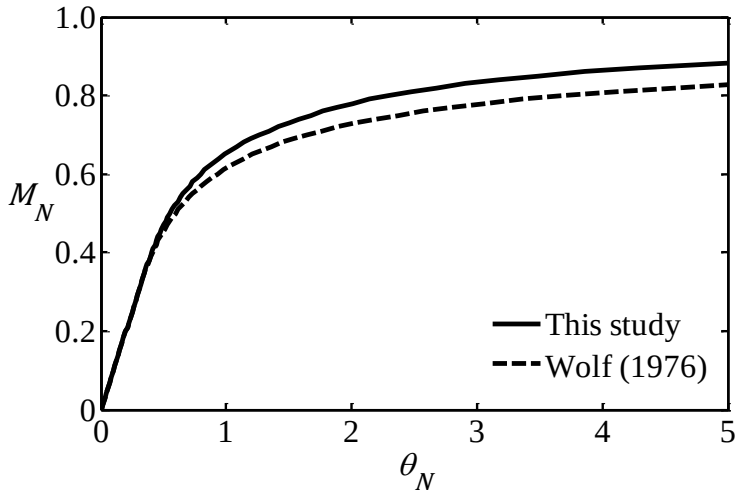

Figure 4.4 The relationship between M_N and θ_N for a circular foundation on homogeneous half-space

In Figure 4.5, the variation of v_N as a function of θ_N is compared with those given by Wolf (1976). There is a difference between the relationship developed in this study and that of Wolf (1976). The differences between the results of Wolf (1976) and this study are calculated as 42%, 29% and 22% for θ_N values 3, 4 and 6, respectively. The relative difference is smaller at the initial stage of uplift. However, the difference shows an increasing trend by increasing of θ_N. On the other hand, the opposite is true in terms of percent relative error. As stated in the previous paragraph, this trend of difference may be attributed to the approximations in the study of Wolf (1976) or to the assumption of a linear boundary between contact and separated zone beneath foundation.

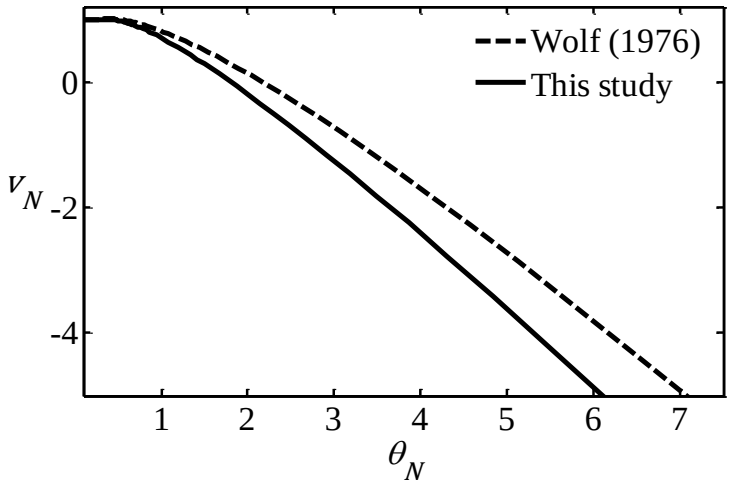

Figure 4.5 The relationship between v_N and θ_N for a circular foundation on homogeneous half-space

In Figure 4.6 the α - θ_N relationship for a strip foundation resting on elastic half-space is presented. α obtained by Equation 3.11 remains constant during eccentric loading (i.e. $\alpha = 1/2$) as proposed by Wolf (1976) and by Gazetas et al. (2013), because the shape of strip foundations remains unchanged during foundation uplift.

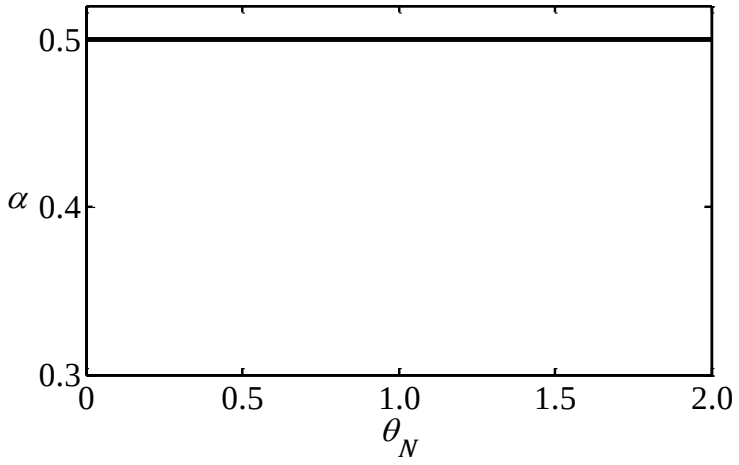

Figure 4.6 The relationship between α and θ_N (Equation 3.11) for strip foundations on homogeneous half-space

In Figure 4.7, the relationships between M_N and θ_N for strip foundations resting on elastic half-space are presented. It is observed that the results obtained from this study and those of Cremer et al. (2001) are in good agreement. The equations proposed by Cremer et al. (2001) are summarized in Appendix B.

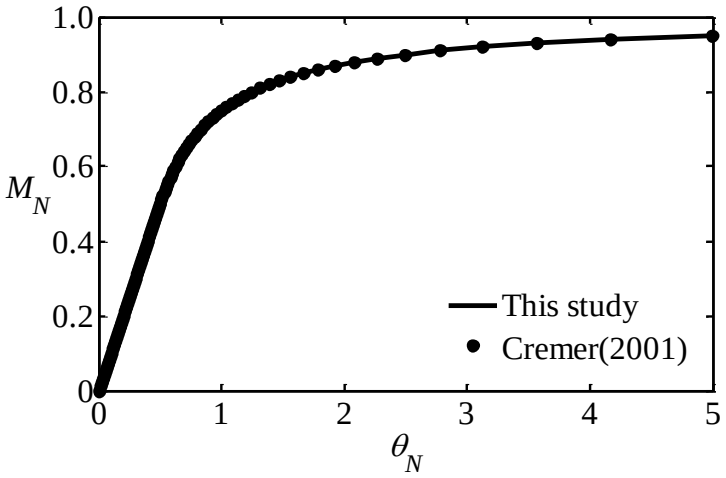

Figure 4.7 The relationship between M_N and θ_N for strip foundations on elastic half-space

4.3. Applications

In this section, figures showing the effect of several parameters on the response of shallow foundations are presented. The relationships presented in the figures are illustrating the effect of geometric properties of shallow foundations that of underlying soil properties, and that of using variable α on the response of shallow foundations.

4.3.1. A Comparison of Rocking Impedances for Rectangular Foundations Resting on Different Types of Elastic Supports

A rectangular foundation resting on elastic half-space, Winkler springs and, elastic layer is considered in this section to compute impedance with increasing θ.

In Figure 4.8, the relationships between α and θ_N are compared for rectangular foundations resting on elastic half-space. α for a rectangular (i.e., $B = 5L$ and $B = L/2$) and for a square ($B = L$) shaped foundation (Equation 3.11) approaches to $1/2$ due to their similarity with strip foundations in case of uplift (Table 3.1). The main reason for the abrupt change of α is the change in K_θ at a particular B/L ratio (Table 2.1).

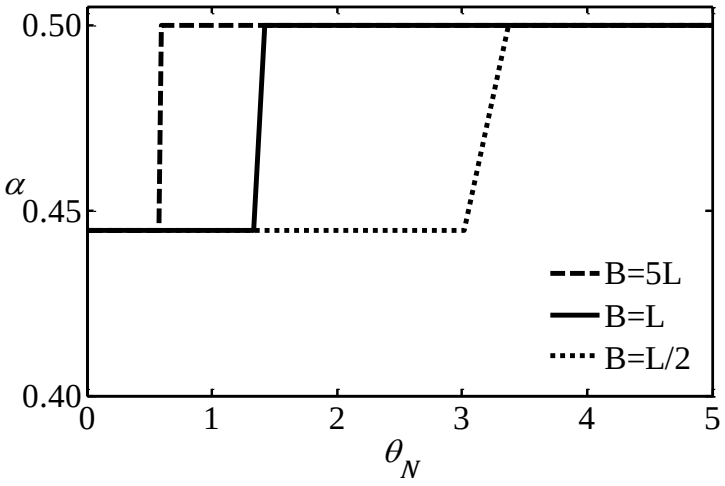

Figure 4.8 The relationship between α and θ_N for various rectangular foundations resting on homogeneous half-space

In Figure 4.9, the relationships between M_N and θ_N of the rectangular foundations are compared for a set of α. In the figure, the relationship between M_N and θ_N is also plotted for α varying according to Equation 3.11. It is observed that the relation between M_N and θ_N pertinent to variable α yields a smooth transition between the regions before and after uplift.

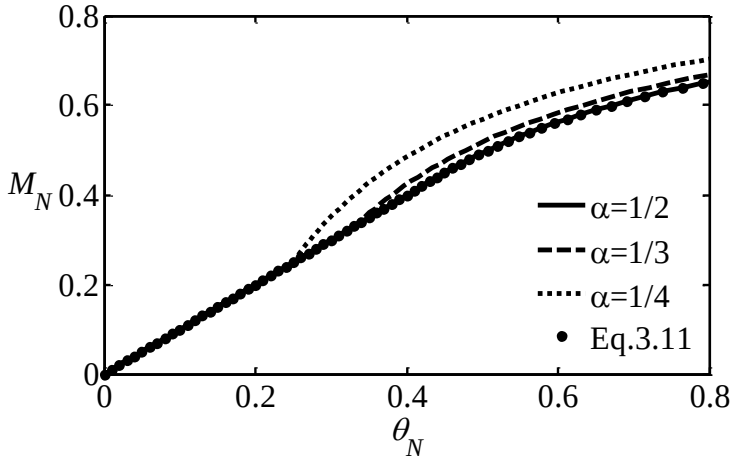

Figure 4.9 The relationship between M_N and θ_N for rectangular ($B = 5L$) foundations on homogeneous half-space

Next, the ratio of homogeneous layer thickness, *D*, to the width of the foundation is considered. For this purpose, the relationship between M_N and θ_N for a rectangular foundation resting on elastic layer is presented Figure 4.10 for a set of D/B in. The effect of D/B ratio on the variation of $M_N - \theta_N$ relationship diminishes in case D/B is greater than 1, such that the solution reaches to the solution for a foundation on elastic half space. Hence the models assuming an elastic half-space are applicable provided that the practically rigid geological formation is not shallower than B. Rectangular foundations resting on elastic layer were considered in Section 2.3 in detail.

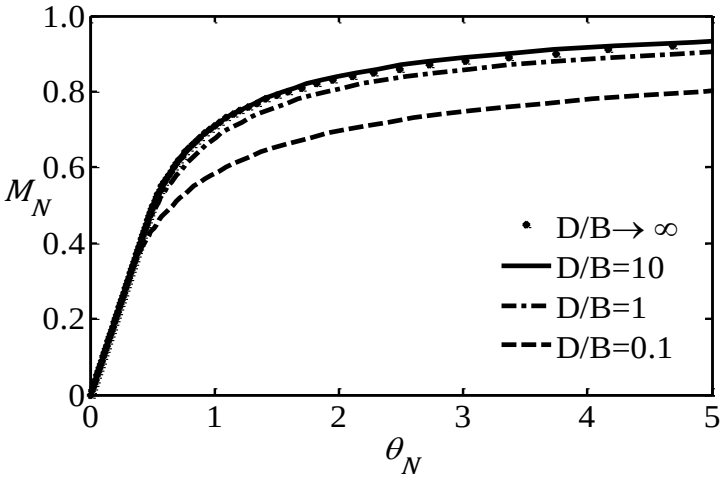

Figure 4.10 The relationship between M_N and θ_N for a rectangular ($B = 5L$) foundation under static loading

In Figure 4.11 the relationship between M_N and θ_N for rectangular foundations resting on elastic half-space with variable B/L are presented to observe the effect of the ratio of foundation dimensions on its impedance. In the figure, length of the foundation is represented by L, and width of the foundation is represented by B. It is observed that the variation of B/L does not have any significant effect on the relationship between M_N and θ_N for rectangular foundations resting on an elastic half-space.

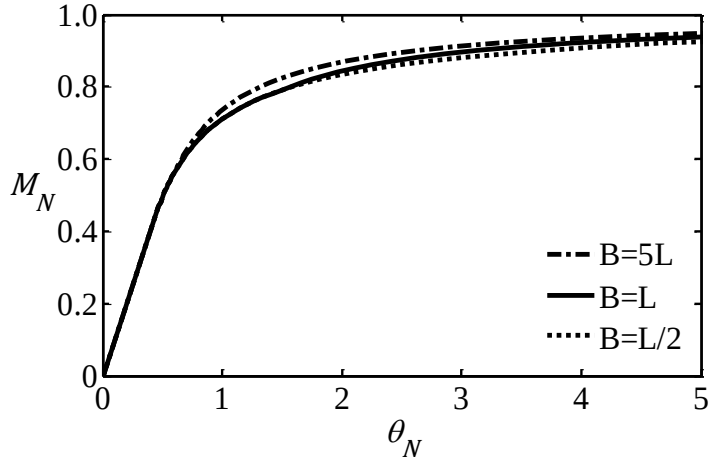

Figure 4.11 The relationship between M_N and θ_N for various rectangular foundations resting on an elastic half-space for cases

In Figure 4.12, the relationship between v_N and θ_N for rectangular foundations, with varying B/L, resting on elastic half-space are presented. It is observed that v_N and θ_N relationships coincide until the initiation of uplift. But, after this point, it is observed that v_N for foundations with higher b/L ratios deviate from each other. Such a deviation may be attributed to the deviation of center of contact area from the geometric center of the foundation in a large amount even at small rotation angles.

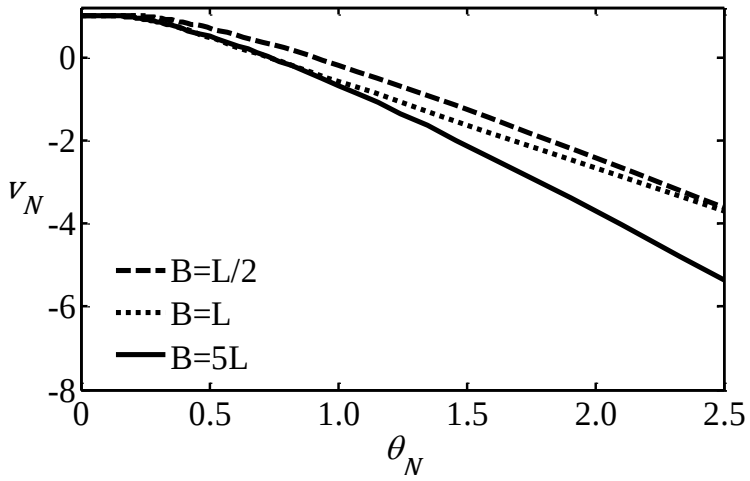

Figure 4.12 The relationship between v_N and θ_N for various rectangular foundations resting on elastic half-space

4.3.2. A Circular Foundation Resting on Elastic Half-space

The relationships between M_N and θ_N for circular foundations are compared in Figure 4.13. In the figure, these relationships are plotted for a set of α and for a variable α calculated by Equation 3.11. It is observed that $M_N - \theta_N$ relationship for the continuously varying α yield a smooth transition between the impedance before and after uplift.

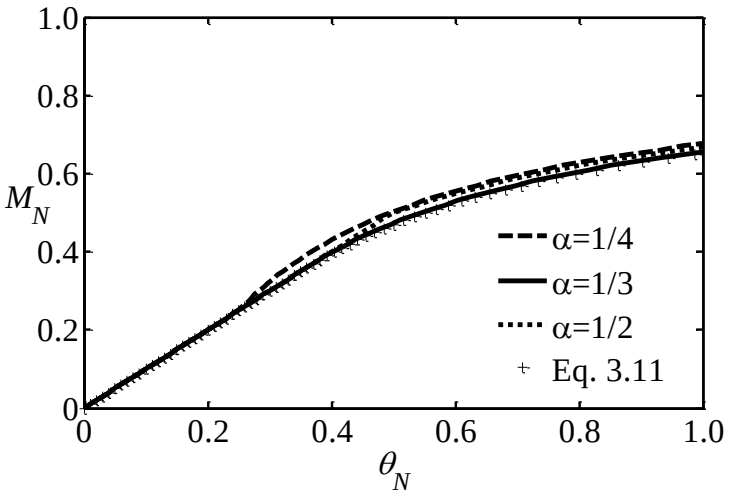

Figure 4.13 The relationship between M_N and θ_N for circular foundations on homogeneous halfspace

4.3.3. A Strip Foundation Resting on Deep Inhomogeneous Deposits and Elastic Half-space

Response of a strip foundation resting on elastic half-space and resting on deep inhomogeneous deposits are considered. The relationships between M_N and θ_N for strip foundations are compared in Figure 4.14. The $M_N - \theta_N$ relationships are compared for a set of α and for a variable α calculated by Equation 3.11. It is observed that $M_N - \theta_N$ relationship for the continuously varying α yield a smooth impedance transition between the regions before and after uplift.

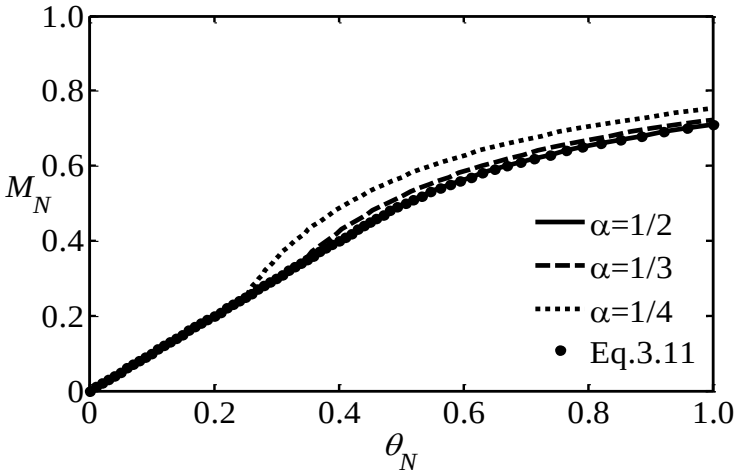

Figure 4.14 The relationship between M_N and θ_N for strip foundations on homogeneous half-space

In Figure 4.15, the relationship between M_N and θ_N for a strip foundation resting on deep inhomogeneous deposits is presented as a function. In Section 2.4, the impedance relalationships for foundations are presented for constant foundation widths without considering the effect of uplift behavior. Consequently, the shear modulus of the shallow foundations is given for constant foundation width (Equation 2.6). However, for the uplifting shallow foundations, the effective width of foundation continuously varies due to the uplift behavior. The relationship between instantaneous and initial shear modulus should involve the variation in the effective contact width between load bearing medium and foundation. For this purpose a variable form of a is used to provide identical shear modulus for uplifting and linear foundations for the same depth of soil. This is achieved by modifying Equation 2.6 as

$$\mathrm{G} = \mathrm{G}_0 \left(1 + a_{sec} \frac{z}{b}\right) \tag{4.4}$$

where $\mathrm{a}_{\mathrm{sec}}$is defined as

$$a_{sec} = a\frac{b}{B} \tag{4.5}$$

In Figure 4.15, the relationship between M_N and θ_N of strip foundation is plotted as a function of the initial value of a. The figure shows that the depth dependent increase in shear modulus can yield an significant increase in the stiffness of foundations during uplift. This is explained by the increasing rigidity of load bearing medium, which moves the M_N in greater ranges of θ_N to the ultimate value for a foundation on rigid support.

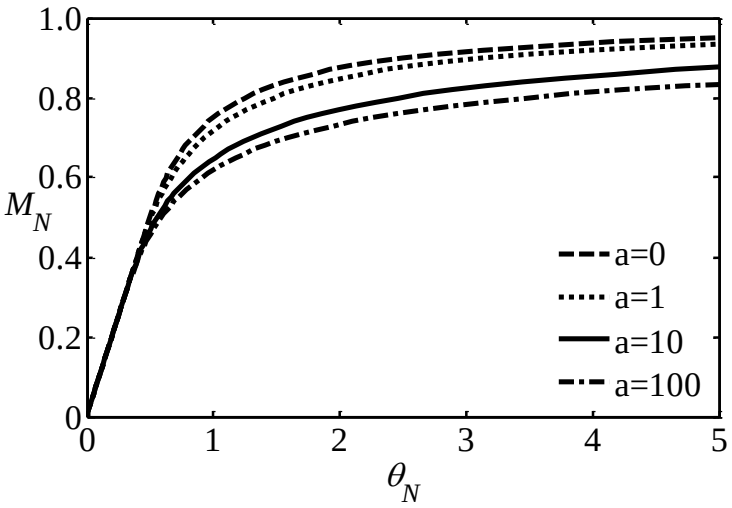

Figure 4.15 The relationship between M_N and θ_N for strip foundations on deep inhomogeneous deposits

4.3.4. A Square Foundation Subjected to 2 Way Eccentric Loading Resting on Elastic Half-space

The method presented in this study is applicable to any arbitrary shaped foundation as long as the geometric properties of foundation are provided. A square foundation subjected to 2 way eccentric loading resting on elastic half-space is considered as an example. The geometric properties of this foundation is

calculated and implemented in the computer program with the aid of an external routine. Details about the calculation of these properties are presented in the Appendix A.

In Figure 4.16, the relationship between α and θ_N is plotted for a square foundation subjected to 2 way eccentric loading resting on elastic half-space. Before initiation of uplift, α calculated by Equation 3.11 remains constant. However, after the initiation of uplift α continuously varies due to the changing shape of foundation section that is in contact with the load bearing medium during uplift.

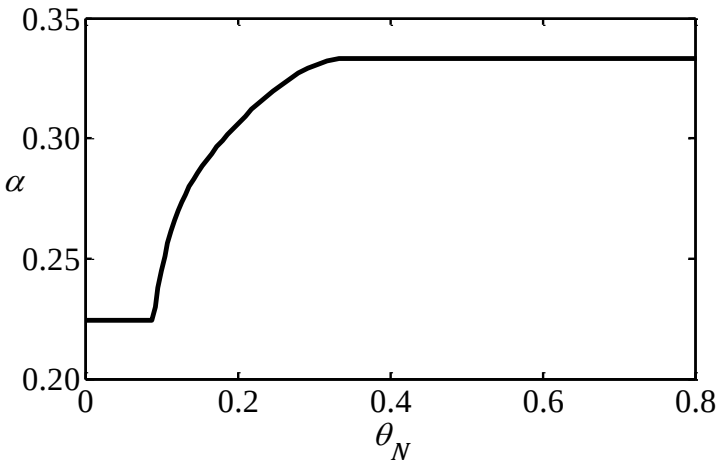

Figure 4.16 The relationship between α and θ_N for square foundations subjected to 2 way eccentric loading resting elastic halfspace

The relationships between M_N and θ_N for square foundations subjected to 1 way and 2 way eccentric loading, and resting on an elastic half-space are shown in Figure 4.17. In the figure, a linear relationship followed by a nonlinear curve is observed showing the effect of uplift on the variation of M_N as a function of θ_N for 1 way eccentric loading. A similar relationship with lower moment magnitudes is observed for 2 way eccentric loading.

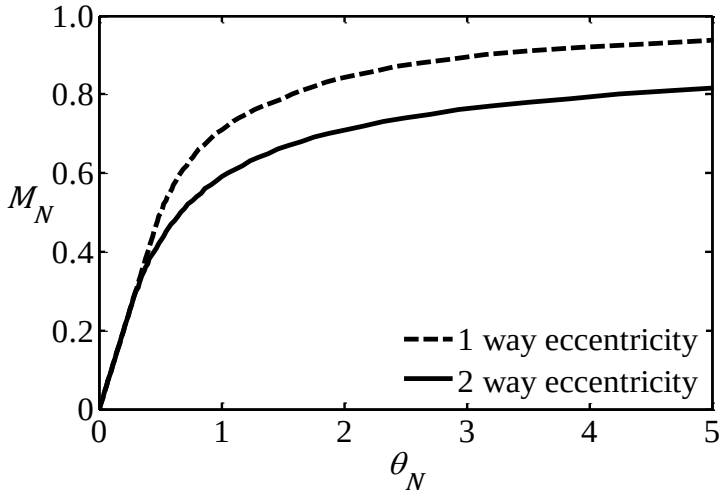

Figure 4.17 The relationships between M_N and θ_N for square foundations subjected to 1 way and 2 way eccentric loading resting elastic halfspace

Figure 4.18 shows the relationships between v_N and θ_N for a square foundation subjected to 1 way and 2 way eccentric loading. In the figure, a flat plateau observed until the initiation of uplift is followed by sloping curve due to the increasing effect of foundation uplift on stiffness of foundation. The θ_N defining the transition between these two parts is consistent with θ_N corresponding to this transition in Figure 4.17.

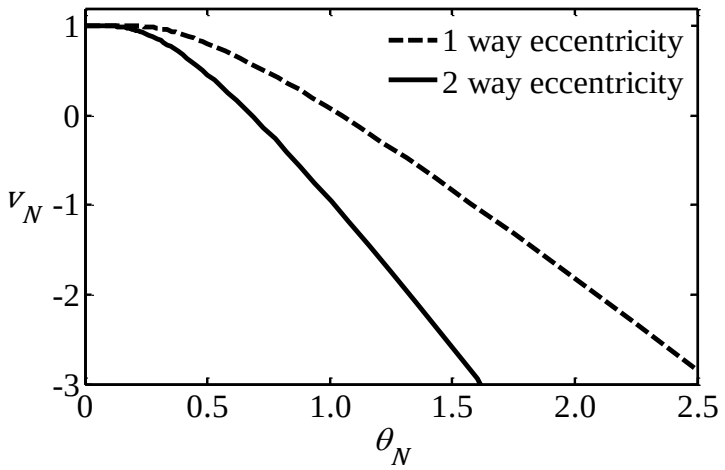

Figure 4.18 The relationships between $v_N$and θ_N for square foundations subjected to 1 way and 2 way eccentric loading resting elastic halfspace

CHAPTER 5

EFFECT OF SOIL NONLINEARITY ON BEARING CAPACITIES OF SHALLOW FOUNDATIONS

5.1 Introduction

The effect of soil nonlinearity on the stiffness of an arbitrarily shaped shallow foundation is investigated in this chapter. A brief literature review on the modeling techniques of soil nonlinearity in the problems involving soil-structure interaction is presented. The method for calculation of the nonlinear response of a shallow foundation resting on soil deposits is illustrated. The results obtained from the proposed theoretical method are compared with those of former experimental studies to verify the accuracy of the proposed theoretical method.

In an analysis of foundation uplift, the behavior of soils can be considered as linear if the foundation is resting on very stiff soils, or if the foundation is subjected to light loading conditions (Apostolou, 2011). Otherwise, the nonlinear behavior of soil is inevitable due to excessive stress levels concentrated particularly at the corners of the foundations (Pecker and Pender, 2000; Anastasopoulos and Kontourpi, 2014). Figure 5.1 shows the reduction of shear modulus of a Toyoura sand sample with increasing shear strain (Kokusho, 1980). In the figure, ratio between the instantaneous shear modulus, G, and initial shear modulus, G_0, of soil is plotted with respect to the cyclic amplitude of the shear strain in soil. Significant degradation of shear modulus of soil with increasing shear strain is clearly observed. The nonlinear soil behavior may result in nonlinearity of foundation response even if a foundation is completely in contact with the load bearing soils

(Apostolou, 2011). An accurate technique accounting for the nonlinear behavior of soil deposits should be adopted to estimate the nonlinear response of foundations to severely eccentric loads.

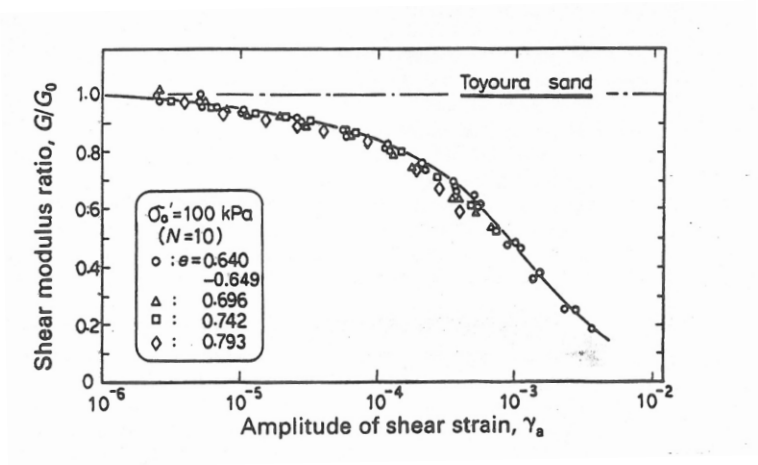

Figure 5.1 Normalized shear modulus versus shear strain for Toyoura sand (Kokusho, 1980)

Finite element modeling techniques are used by researchers considering the nonlinear behavior of soil in soil-structure interaction analyses (Apostolou, 2011). In these techniques, using kinematic hardening models with appropriate failure criteria and associated flow rules is a way to simulate the nonlinear soil behavior (Gelagoti et al., 2012a,b; Gazetas et al., 2013; Zafeirakos and Gerolymos, 2013; Adamidis et al., 2014; Kourkolis et al.,2012a; Ntritsos et al. 2015). Advances in the computer technology motivated the researchers using finite element methods to focus on nonlinear soil-structure interaction analyses (Gazetas and Apostolou, 2004; Gazetas et al., 2013). Whereas, these analyses are computationally expensive to be considered for practical engineering purposes, due to the necessity for domain discretisation.

In macro element modeling method, bounding surface plasticity model is a way to simulate the nonlinear soil behavior (Figini et al., 2012; Gajan and Kutter, 2009; Chatzigogos et al., 2009, 2011; Cremer et al. 2001, 2002). The bounding surface

plasticity model was developed by Dafalias and Popov (1975) to simulate the nonlinear behavior of materials when subjected to complex loading conditions. In this model, the nonlinear deformation at a loading point is calculated by defining the modulus of plasticity as a function of the distance between the loading point and the image point lying on a bounding surface. Such an approach provides a smooth shift in the response from elastic to plastic state (Kan et al. 2014). In the bounding surface, any combination of the load vectors lying out of the bounding surface leads to an unstable condition. On the other hand, any combination of the loads lying in the bounding surface corresponds to a potential by stable condition (Pecker and Pender, 2000). Paolucci (1997) simulated the inelastic behavior of the soil deposit by assuming a linear visco-elastic soil behavior until reaching the failure surface. This assumption was based on the fact that possible plastic behavior of soil in the failure surface can be disregarded with respect to the plastic deformations occurring at failure.

As an alternative to bounding surface plasticity models, equivalent linearization is a technique that can be employed to take soil nonlinearity in account soil-structure interaction analyses (Adamidis et al. 2014). The pioneering studies that developed the theory of approximation of real nonlinear soil behavior by equivalent linear method were performed by Idriss and Seed (1968) and Schnabel et al. (1972). In the equivalent linear modeling of soil behavior, the empirical relationships describing the variation of secant shear modulus (Figure 5.2) and hysteretic damping ratio with shear strain are iteratively used for modifying the parameters of linear elasticity. However, equivalent linearization method cannot capture the actual behavior of soil deposits in the presence of excessive soil nonlinearity.

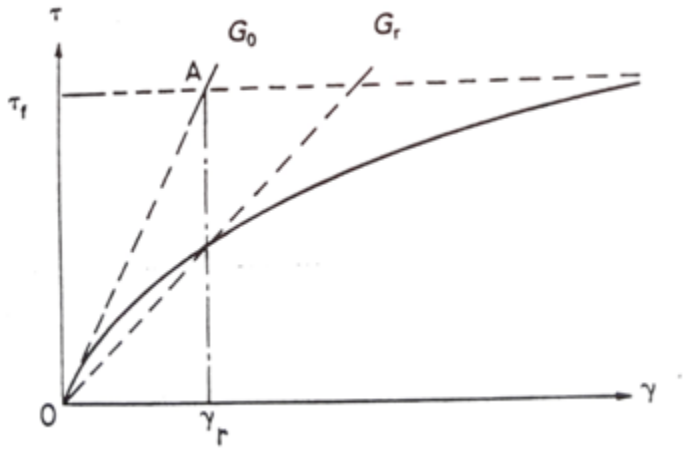

Figure 5.2 Variation of secant shear modulus with shear strain

In this study, the effect of soil nonlinearity on the static response of arbitrarily shaped shallow foundations is modeled by continuously modifying the shear modulus of load-bearing soil as a function of magnitude of vertical load acting on the foundation due to the simplicity of equivalent linearization method. It was numerically and experimentally shown that the hyperbolic and exponential functions are suitable to describe the relationship between vertical load and vertical displacement for a foundation resting on homogenous medium (Kohno et al., 2009; Apostolou, 2011; Uzielli and Mayne, 2012). The vertical load-displacement relationship of a shallow foundation is described by using hyperbolic and exponential functions (Figure 5.3). Details of this methodology are presented in the following section.

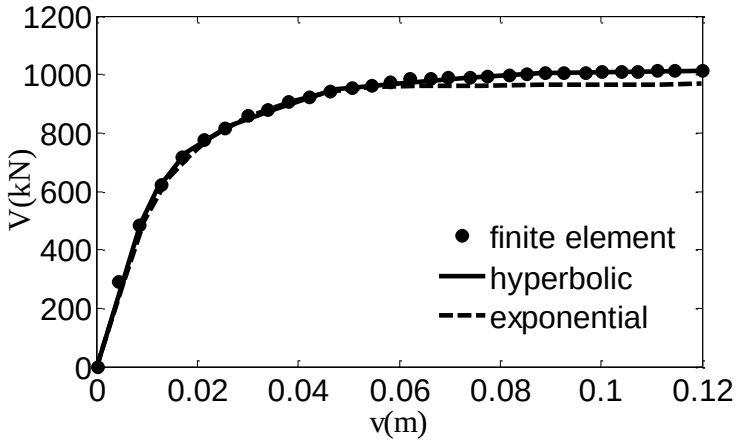

Figure 5.3 Comparison of the vertical load – displacement relationships calculated using exponential and hyperbolic law with those calculated using the finite element analyses (Apostolou, 2011)

5.2. Methodology

The effect of soil nonlinearity on the static response of shallow foundations is considered by continuously modifying the shear modulus of the load-bearing soil deposit. The calculations are performed by employing the method of equivalent linearization. Hence, the shear modulus of load bearing soil is reduced by increasing load eccentricity. It is supposed that the secant shear modulus is related to the ratio of vertical load to ultimate bearing capacity (V/V_{ult}) under any given load eccentricity (M/V) and load inclination (H/V). The relationship between G_{sec} and V/V_{ult} is estimated by using vertical loading tests on model foundations. In practice, this is possible by plate loading tests on a site where a shallow foundation will be constructed (Chen et al., 2004).

The hyperbolic and the exponential functional forms were used to simulate the static vertical load–vertical displacement relationships of shallow foundations. Two functional forms can be used optionally, because no superiority of one to the other was observed.

5.2.1 The Hyperbolic Model

The hyperbolic functional form is expressed as:

$$V = \frac{v}{m + nv} \tag{5.1a}$$

or

$$\frac{1}{V} = \frac{m}{v} + n \tag{5.1b}$$

where V is the applied vertical load, v is the vertical displacement of the foundation and m and n are constants of functional form. The differentiation of the hyperbolic function (Equation 5.1) with respect to v results in the initial vertical stiffness of the shallow foundation (K_{v0}):

$$\left.\frac{dV}{dv}\right|_{v=0} = K_{v0} \tag{5.2}$$

which yields

$$m = \frac{1}{K_{v0}} \tag{5.3}$$

V reaches to its ultimate value by increasing v, such that

$$\lim_{v \to \infty} \frac{v}{m + nv} = V_{ult} \tag{5.4}$$

so

$$n = \frac{1}{V_{ult}} \tag{5.5}$$

By substituting Equation 5.3 and Equation 5.5 in Equation 5.1, the vertical load V is related to v by

$$V = \frac{v}{\frac{1}{K_{v0}} + \frac{1}{V_{ult}} v} \tag{5.6}$$

Substitution of Equation 2.1 and Equation 2.2 ($K_v = V/v$) in Equation 5.6 yields the relation between the secant vertical stiffness (K_v) and initial vertical stiffness (K_{v0}), such that

$$\frac{K_v}{K_{v0}} = 1 - \frac{V}{V_{ult}} \tag{5.7}$$

Because K_v is proportional to G for a foundation on a linearly elastic medium (Table 2.1), the relationship between maximum shear modulus (G_0), the secant shear modulus (G_{sec}), K_v and K_{v0} is

$$\frac{G_{sec}}{G_0} = \frac{K_v}{K_{v0}} \tag{5.8}$$

or, by substituting Equation 5.7 in Equation 5.8 the relation between the secant shear modulus (G_{sec}) and initial shear modulus (G_0) is

$$\frac{G_{sec}}{G_0} = 1 - \frac{V}{V_{ult}} \tag{5.9}$$

5.2.2 Exponential Model

The experimental relationship between vertical load and displacement is (Nova and Motrasio, 1991)

$$\frac{V}{V_{ult}} = 1 - \exp\left(-\frac{K_{v0}v}{V_{ult}}\right) \tag{5.10}$$

By substituting Equation 2.1 and Equation 2.2 (i.e. $K_v = V/v$) in Equation 5.10, relationship between the simultaneous vertical stiffness (K_v) and initial vertical stiffness (K_{v0}) is calculated by

$$\frac{K_v}{K_{v0}} = -\frac{V}{V_{ult}\ln\left(1 - \frac{V}{V_{ult}}\right)} \tag{5.11}$$

Consequently, the relationship between G_{sec} and G_0 for the exponential model is

$$\frac{G_{sec}}{G_0} = -\frac{V}{V_{ult}\ln\left(1 - \frac{V}{V_{ult}}\right)} \tag{5.12}$$

5.2.3 Estimation of V_{ult}

Distribution of contact stresses under a rigid foundation is non-uniform (Schultz and Ing, 1961; Terzaghi and Peck, 1967). For a rigid foundation resting on elastic cohesive soil deposit, theoretical level of stresses at the outer edges is infinite. In actual case, the level of stress at the outer edges is limited with the shear strength of soil deposit (Figure 5.4). For a rigid foundation resting on a granular soil

deposit, a parabolic stress distribution with zero stress at each corner occurs (Terzaghi and Peck, 1967; Holtz, 1991). In contrast to the nonlinear distribution of actual contact stresses, in structural design of footings, generally, uniform contact stress distribution is assumed by the designers (Holtz, 1991, Yamin et al., 2016). The ultimate vertical load resisting capacity of a shallow foundation is calculated by using this uniform contact stress under the foundation and the area of contact.

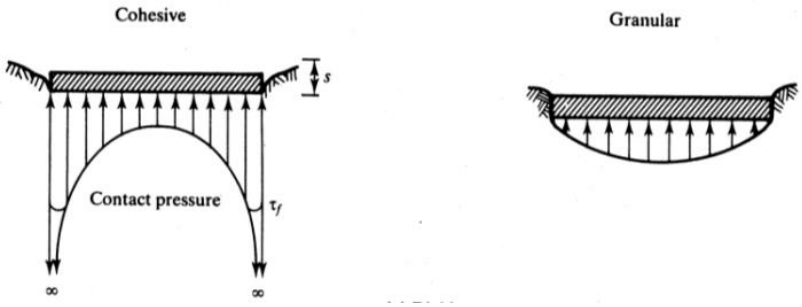

(a) (b)

Figure 5.4 Contact pressures for cohesive and granular soils under rigid foundations (Holtz, 1991)

The bearing capacity of a strip foundation (q_u) on soil with cohesion, friction and self weight was proposed by Terzaghi (1943):

$$q_u = c_s N_c + qN_q + \frac{1}{2}\gamma_s b N_\gamma \tag{5.13}$$

where, c_s is unit cohesion, q is effective overburden pressure at the base level of the foundation, γ_s is effective unit weight of soil below the foundation base, and b is the width of the foundation. The terms N_c, N_q and N_γ are the bearing capacity factors to scale the contribution of the variables c_s, q and γ_s respectively to q_u as a function of internal angle of friction, ϕ. In this study, the bearing capacity factors

proposed by Reissner (1924), Prandtl (1921) and Hansen (1970) are used for estimation of q_u, such that

$$N_q = e^{\pi \tan \phi} \left(\frac{1 + \sin \phi}{1 - \sin \phi} \right) \tag{5.14a}$$

$$N_c = \left(N_q - 1 \right) \cot \phi \tag{5.14b}$$

$$N_\gamma = 1.5 N_c \tan^2 \phi \tag{5.14c}$$

The bearing capacity equation for a strip foundation (Equation 5.13) was generalized by Meyerhof (1963) for foundations with rectangular and circular geometries, embedded foundations and foundations subjected to inclined loading, such that

$$q_u = c_s \lambda_{cs} \lambda_{cd} \lambda_{ci} N_c + q \lambda_{qs} \lambda_{qd} \lambda_{qi} N_q + \frac{1}{2} \lambda_{\gamma s} \lambda_{\gamma d} \lambda_{\gamma i} \gamma_s b N_\gamma \tag{5.15}$$

where, $\lambda_{*s}, \lambda_{*d}$ and λ_{*i} are shape, depth and inclination factors. The depth factors ($\lambda_{cd}, \lambda_{qd}$ and $\lambda_{\gamma d}$) are equal to unity for a foundation resting on ground surface. The load inclination factors presented by Hansen (1970) are in the following equations

$$\lambda_{qi} = \left(1 - \frac{0.5 q_u \sin \beta_i}{q_u \cos \beta_i + c_s \cot \beta_i} \right)^5 \tag{5.16a}$$

$$\lambda_{ci} = \lambda_{qi} - \left(\frac{1 - \lambda_{qi}}{N_q - 1} \right) \tag{5.16b}$$

$$\lambda_{\gamma i} = \left(1 - \frac{0.7 q_u \sin\beta_i}{q_u \cos\beta_i + c_s \cot\beta_i}\right)^5 \qquad (5.16c)$$

where β_i (rad) is the angle of load inclination defined as

$$\beta_i = \text{atan}\frac{H}{V} \qquad (5.17)$$

The shape factors in Equation 5.15 are suggested by DeBeer (1970) as

$$\lambda_{cs} = 1 + \frac{N_q}{N_c}\frac{b}{L} \qquad (5.18a)$$

$$\lambda_{qs} = 1 + \frac{b}{L}\tan\phi \qquad (5.18b)$$

$$\lambda_{\gamma s} = 1 - 0.4\frac{b}{L} \qquad (5.18c)$$

These expressions are used for estimation of ultimate vertical load on a shallow foundation, V_{ult}, such that

$$V_{ult} = q_u f \qquad (5.19)$$

f is the contact area of the shallow foundation.

The flow chart shown by Figure 5.5 and explained in the following paragraphs is developed to account for the effect of soil nonlinearity on the load - displacement response of foundations. This algorithm is substituted into step 4 in the main flow chart (Figure 3.2) to reduce shear modulus due to nonlinear behavior of load

bearing soils. The parameters required by the subroutine implemented in the computer program (see Appendix E) are explained in the following paragraphs.

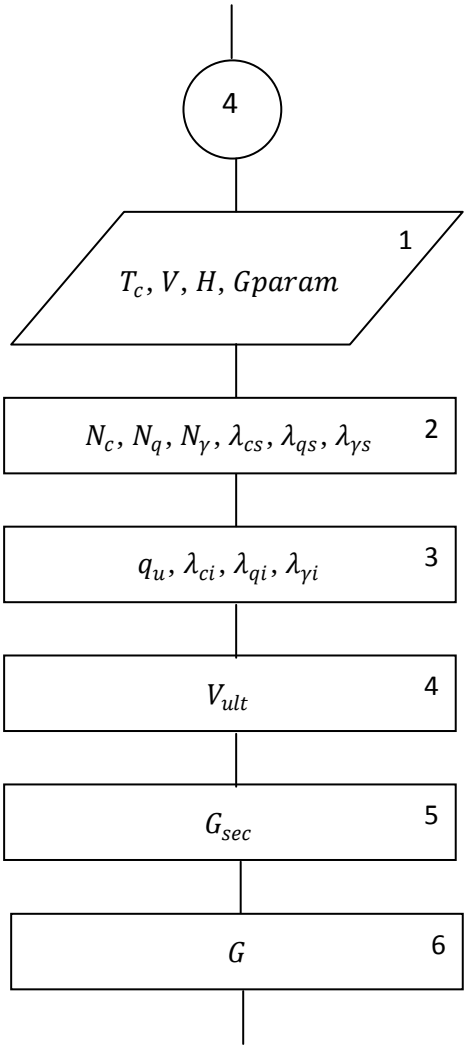

Figure 5.5 Flow Chart to calculate G

1. $Gparam(1)$ is the shear modulus of elastic layer or half-space (G_0). $Gparam(2)$ is unit cohesion (c_s). $Gparam(3)$ is internal angle of friction (ϕ), in degrees. $Gparam(4)$ is effective unit weight of soil below the foundation (γ_s). $Gparam(5)$ is effective overburden pressure at the base level of the foundation

(q). $Gparam(6)$ is used to select the functional form to fit the static vertical load-vertical displacement relationship of shallow foundations presented in Table 5.1.

Table 5.1 Functional forms in the proposed method

$Gparam(6)$	Functional form
1	Hyperbolic
2	Exponential

2. ϕ (in degrees) is converted to radians. N_c, N_q and N_γ are calculated by using ϕ (Equations 5.14a-c). Then λ_{cs} is calculated by using N_c and N_q and dimensions of the foundation (Equation 5.18a). λ_{qs} and $\lambda_{\gamma s}$ are calculated using ϕ and dimensions of the foundation (Equations 5.18b,c).

3. Initial guess for q_u (Equation 5.15), q_{uold} is calculated by assigning 1 to $\lambda_{ci}, \lambda_{qi}$ and $\lambda_{\gamma i}$. The new value of q_u is calculated by using $fzero$ calibrated to find the root of q_u around q_{uold}. λ_{ci} is a factor used to account for the load inclination (β_i) to modify the cohesion given by $Gparam(2)$. Similarly, λ_{qi} is a factor used to account for β_i to modify the effective overburden pressure given by $Gparam(5)$ and $\lambda_{\gamma i}$ is a factor used to consider the effect of β_i to modify the effective unit weight of soil deposit given by $Gparam(4)$.

4. V_{ult} is calculated by multiplying q_u with the contact area, f, obtained by T_c (Equation 5.19). If the calculated instantaneous value of V_{ult} is smaller than V, value of V is assigned to V_{ult} .

5. Finally, G_{sec} is calculated by using Equation 5.9 and Equation 5.12.

6. G_{sec} is used as the shear modulus, G, in calculation of foundation impedance.

5.3. Model Validations

The accuracy of theoretical model developed in this study is justified by comparisons with experiments. In the justification of the theoretical model, results of three experimental studies are used. Experimental studies used to justify the developed theoretical model were presented by Shirato et al. (2008), Negro et al. (2000), and Kokkali et al. (2014).

5.3.1. Foundation model of PWRI

The Public Works Research Institute of Japan (PWRI) tests were conducted to measure the response of shallow foundations subjected to monotonic and cyclic loading conditions (Shirato et al., 2008). The tests were conducted on square footings with 0.5 m width, as shown in Figure 5.6.

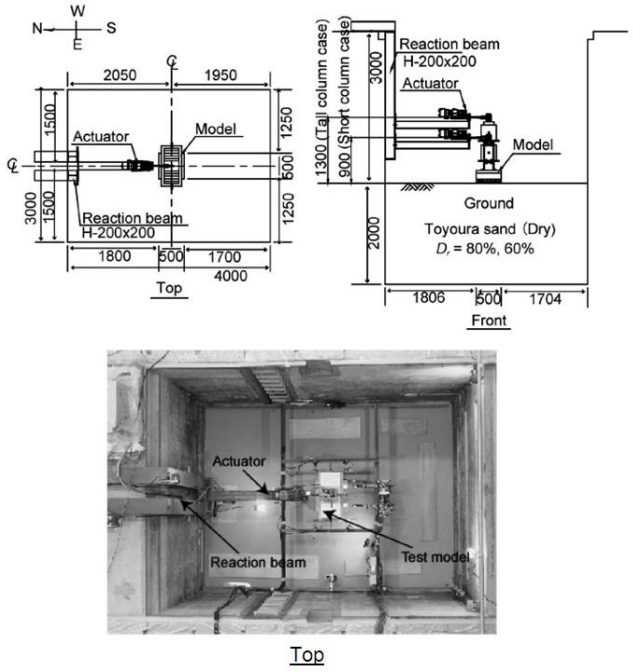

Figure 5.6 Sketches and photo of the test setup used for cyclic loading experiments (Shirato et al., 2008)

In the experiments, soil deposit lying under the test specimens was composed of a 2 m deep layer of air-dried Toyoura standard sand. The tests were conducted by using a sand deposit with two relative densities. Unit weights of the air-dried Toyoura standard sand layers were γ = 15.1 kN/m^3 and γ = 15.7 kN/m^3 for relative densities of D_r = 60% (i.e. loose condition) and D_r = 80% (i.e. dense condition), respectively. In the experimental study, vertical and horizontal loading tests were conducted on test specimens. The vertical loading tests are considered for determination of parameters used in the theoretical model, and horizontal loading tests are considered for verification of model predictions. The summary information about the PWRI tests are presented in Table 5.2.

Table 5.2 Selected load cases in the experiments of PWRI

Loading Case	**Model**	**Load Pattern**	$\boldsymbol{D_r}$(%)
1	V	Vertical load	80
2	V	Vertical load	60
3	T	Monotonic horizontal load	80
5	T	Cyclic horizontal load	80
6	S	Monotonic horizontal load	80
8	S	Cyclic horizontal load	80
9	S	Monotonic horizontal load	60
11	S	Cyclic horizontal load	60

S: short pier

T: tall pier

V: vertical loading on base plate

The vertical loading tests were conducted by applying vertical forces on tested foundations as shown in Figure 5.7. Consequently, the relationship between V and v of the test specimens were determined as shown in Figure 5.8.

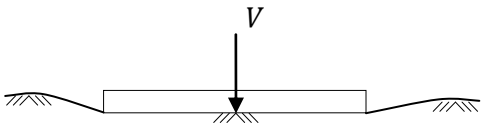

Figure 5.7 The experimental model for vertical loading

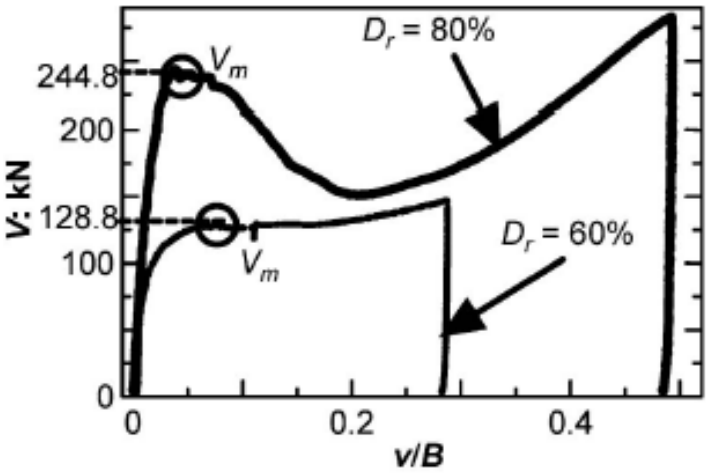

Figure 5.8 Results of the vertical loading tests (Shirato et al., 2008; $V_m = V_{ult}$)

In the proposed theoretical method, the maximum shear modulus, G_0, of sand deposit underlying the footing is a parameter required to perform the numerical analyses. The G_0 of the Toyoura standard sand layer is calculated by using the initial vertical stiffness, K_{v0}, of the test specimens. Figure 5.9 shows that the relationship between V and v is empirically estimated. K_{v0} and V_{ult} of the test models are calculated by applying a curve fitting procedure (see Sections 5.2.1 and 5.2.2 for further information about exponential and hyperbolic functions). In the curve fitting procedure, the regression coefficients are selected to make the coefficient of determination, R^2, close to 1. For this purpose the principle of least squares (Chapra and Canale, 2010) is applied on the data pairs of $1/V$ and $1/v$.

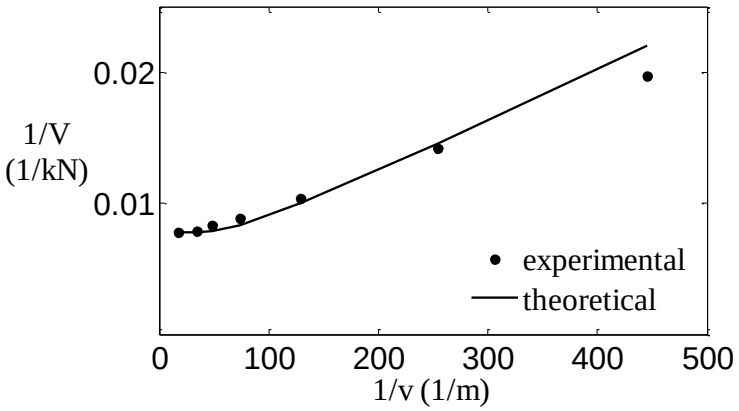

Figure 5.9 Typical $V - v$ relationship of a shallow foundation in exponential form

K_v values are used for calculation of G_0 for Toyoura sand with different relative densities by Equation 5.8. The internal angle of friction, ϕ, is calculated by using the ultimate load, V_{ult}, via Equations 5.13-5.19. The parameters used in the theoretical model are presented in Table 5.3.

Table 5.3 Calculated parameters used in the theoretical model for PWRI tests

Load Case	$\boldsymbol{\phi}(°)$	$\boldsymbol{G_0}$ (kN/m^2)	$\boldsymbol{\gamma}$ (kN/m^3)	$\boldsymbol{N_q}$	$\boldsymbol{N_c}$	$\boldsymbol{N_\gamma}$
1	48.8	21701	15.7	256	223	437
2	45.5	15380	15.1	146	143	221

Shear wave velocities, V_s, of the soil deposits are calculated. V_s of the Toyoura sand with different relative densities are estimated by using the well known relationship between V_s, G_0, and unit mass of the soil, ρ, such that

$$V_s = \sqrt{\frac{G_0}{\rho}} \tag{5.20}$$

The calculated V_s for the test specimens are given as a function of the relative density of sand. V_s is estimated by the fitted functional form of the $V - v$ relationship of the model foundation. It is observed that the shear wave velocities obtained using exponential and hyperbolic functions are slightly different. V_s values of Toyoura sand for a D_r of 80% are calculated as 116 m/s and 128 m/s by using exponential and hyperbolic functional forms, respectively. Similarly, V_s values of Toyoura sand for D_r =60% are calculated as 100 m/s and 122 m/s by using exponential and hyperbolic functional forms, respectively.

In this study either a hyperbolic (Equation 5.8) or exponential (Equation 5.9) functional form is used to simulate the degradation of shear modulus of soil deposit. The difference in the calculated V_s for hyperbolic and exponential cases is negligible. In the horizontal loading tests, horizontal displacement patterns were applied at the cap of the pier (Figure 5.10). In the tests, two foundation models with different pier lengths were used. The height of the pier was 0.9 m in the Model H and 1.3 m in the Model L. The total weight of Model H was 8.924 kN and, that of Model L was 8.728 kN.

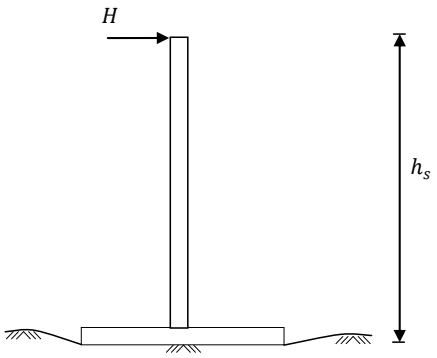

Figure 5.10 The schematic view of the horizontal loading experiment

The results of the proposed theoretical model are compared with the results of PWRI tests, in terms of normalized moment - rotation, $M_N - \theta_N$, (Equations 4.1b, 4.2b) and normalized vertical displacement – rotation, $v_N - \theta_N$, (Equation 4.3) relationships. Theoretical $M_N - \theta_N$ relationships are compared with the experimentally obtained $M_N - \theta_N$ envelopes gathered from the monotonic and cyclic - loading tests. Details about the normalization procedure are presented in Section 4.1.

In the calculation of the theoretical $M_N - \theta_N$ relationships, the parameters (i.e. G_0, ϕ) required to conduct numerical analyses are obtained by using parameters based on fitted $V - v$ relationships (Figure 5.8). The $M_N - \theta_N$ relationships calculated without considering the soil nonlinearity are also presented with other experimental and theoretical relationships to clearly observe the effects of soil nonlinearity on the response of shallow foundations.

In Figure 5.11, theoretical and experimental $M_N - \theta_N$ relationships obtained from Load Case 3 are presented. Both of the proposed nonlinear theoretical relationships (i.e. estimated based on the parameters calculated using exponential and hyperbolic functional forms of vertical load displacement relationships) agree with the experimental results. On the other hand, the theoretical relationship calculated without considering the effects of soil nonlinearity coincided with the other relationships until the initiation of uplift. However, for the higher values of θ_N, an increasing discrepancy between the linear and other relationships is observed. Such discrepancy is indicative of amplified effects of soil nonlinearity in higher ranges of θ_N. In the figure, M_N representing the initiation of uplift is identified for load Case 3. This is achieved by using the theoretical rotational stiffness of the foundation (K_θ) which is normalized with its initial stiffness ($K_{\theta 0}$).

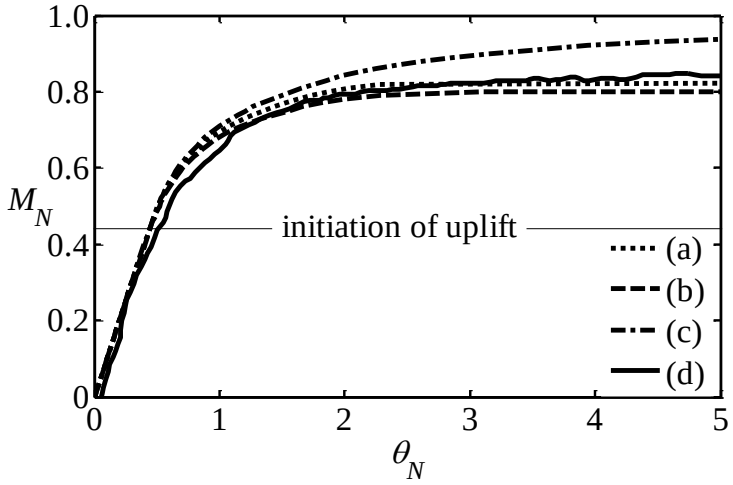

Figure 5.11 The relationship between M_N and θ_N calculated by considering (a) an exponential function, (b) a hyperbolic function, (c) a linear response, and (d) the experimental data for load Case 3.

In Figure 5.12, $K_\theta/K_{\theta 0}$ of foundation is plotted as a function of θ_N. The end of flat plateau shows the initiation of uplift. θ_N corresponding this transion marks the initiation of uplift. M_N corresponding to this specific value of θ_N is shown in Figure 5.11.

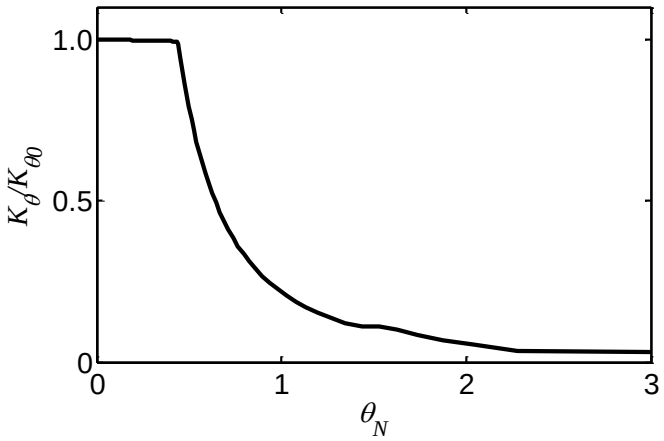

Figure 5.12 Variation of $K_\theta/K_{\theta 0}$ with θ_N for load Case 3

The theoretical and experimental $M_N - \theta_N$ relationships are compared for the Load Case 6 in Figure 5.13. The test specimen was subjected to monotonic horizontal loading. It is observed that the theoretical $M_N - \theta_N$ relationships considering the nonlinearity of soil were in reasonable agreement with the experimental results. On the other hand, the accuracy of the theoretical model is more satisfactory for higher θ_N.

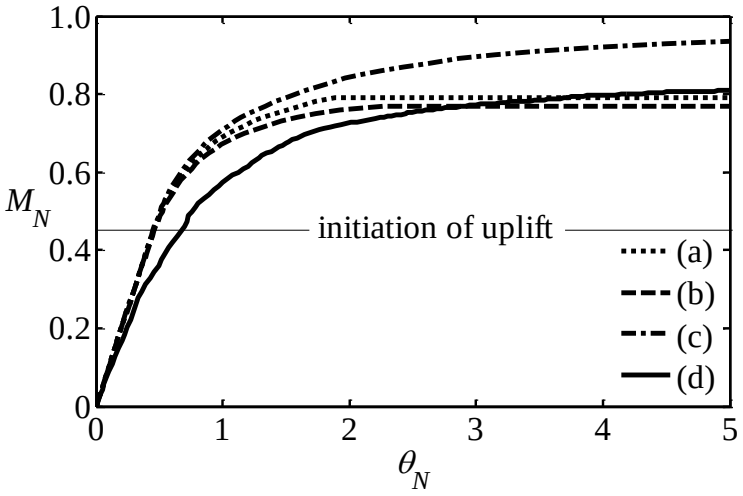

Figure 5.13 The relationship between M_N and θ_N calculated by considering (a) an exponential function, (b) a hyperbolic function, (c) a linear response, and (d) the experimental data for load Case 6

The experimental and theoretical $M_N - \theta_N$ relationships of the Load Case 9 are presented in Figure 5.14. It is observed that the proposed theoretical model yields slightly different results than those obtained from the experiments. On the other hand, the experimental data do not show a smoothly changing trend in this experiment, implying a possible problem in the set up.

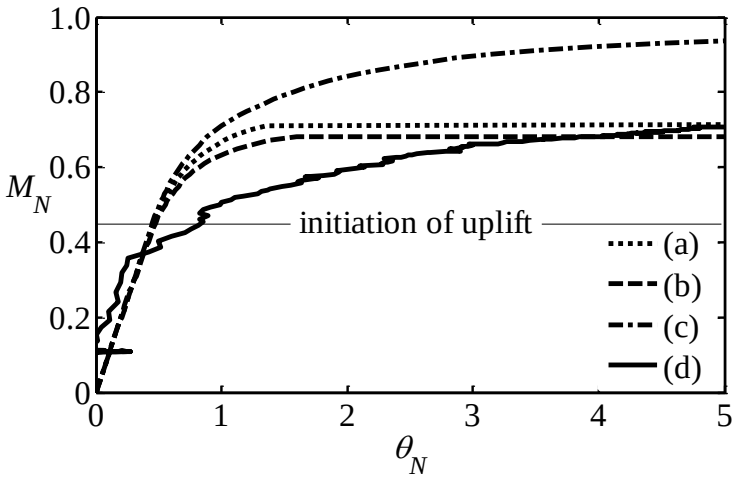

Figure 5.14 The relationship between M_N and θ_N calculated by considering (a) an exponential function, (b) a hyperbolic function, (c) a linear response, and (d) the experimental data for load Case 9

In Figure 5.15, $K_{\theta(experimental)}/K_{\theta(theoretical)}$ is compared for Case 6 and Case 9 for a range of θ. $K_{\theta(theoretical)}$ was computed according to Table 2.1 and $K_{\theta(experimental)}$ was computed by substituting Equation 2.1 in Equation 2.2. The ratios of two parameters are ranging between 0.75 and 1.05, which indicates a reasonable agreement between experimental and theoretical results. Such alterations in the ratio may be attributed to the variability in test conditions, such as the densification of sand.

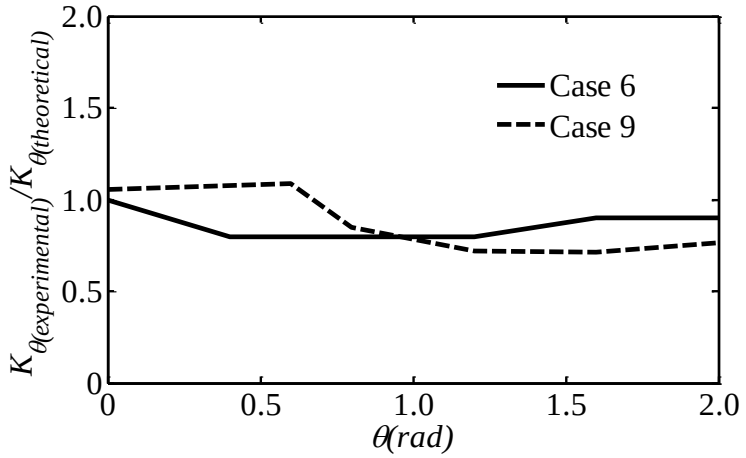

Figure 5.15 Comparison of ratio of experimental to theoretical (exponential function) K_θ for Load Cases 6 and 9

Normalized relationships of theoretical and experimental v_N vs. θ_N are compared in Figures 5.16-5.18 for load Cases 3, 6 and 9, respectively. The settlement behavior is represented by the positive (upward) direction, and the separation of foundation center and load bearing soil (i.e., uplift) is represented by the negative (downward) direction.

In Figure 5.16, theoretical and experimental relationships between v_N and θ_N are presented for Case 3. A reasonable agreement between the experimental and theoretical relationships is observed until the severe plastic flow of the load bearing soil (the theoretical relationship is calculated by using the parameters obtained from the exponential form of the vertical load displacement relationship). The theoretical v_N - θ_N relationships calculated (i) without considering the soil nonlinearity and, (ii) by considering a hyperbolic $V - v$ relationship are not in good agreement with the experimental one. During the experiment of specimen tested under the conditions of load Case 3, probably a premature settlement occurred due to possible errors in the compaction process of the underlying soil. Such premature settlement created a discrepancy between the theoretical and the

experimental results at the beginning of the test. The theoretical relationships between v_N and θ_N is applicable until the excessive plastic flow of the load bearing soil. Consequently, the experimental and theoretical relationships are not compared after the formation of this plastic flow.

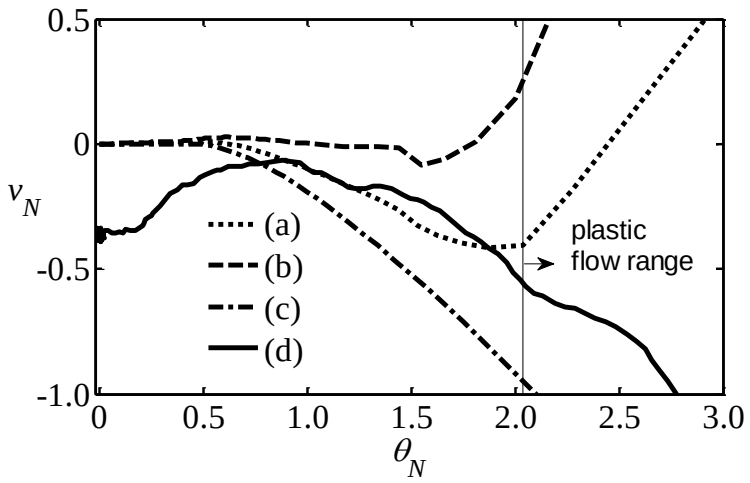

Figure 5.16 The relationship between v_N and θ_N calculated by considering (a) an exponential function, (b) a hyperbolic function, (c) a linear response, and (d) the experimental data for load Case 3

In Figure 5.17, the relationships between v_N and θ_N of short pier are compared for case 6. It is observed that the experimental response of the foundation reasonably agree with the theoretical response calculated by ignoring the effect of soil nonlinearity. Such behavior indicates that the nonlinear behavior of soil was not significantly effective on the $v_N - \theta_N$ relationship of the foundation. Consequently, a discrepancy is observed between the experimental and theoretical results obtained by both of nonlinear relationships between $v_N - \theta_N$.

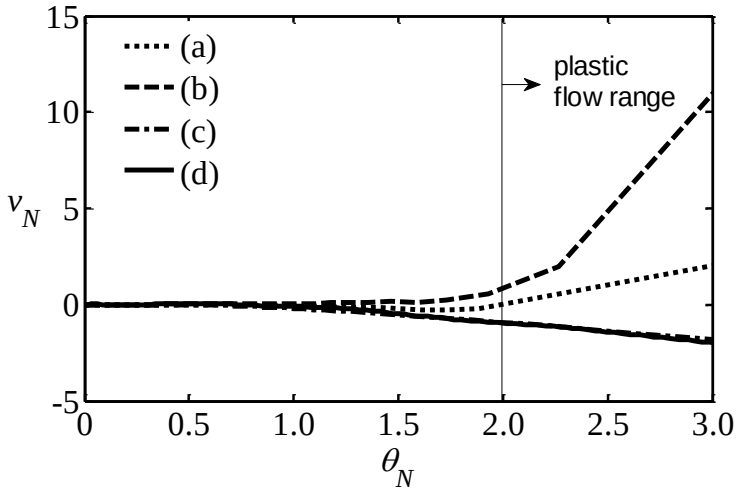

Figure 5.17 The relationship between v_N and θ_N calculated by considering (a) an exponential function, (b) a hyperbolic function, (c) a linear response, and (d) the experimental data for load Case 6

The relationship between v_N and θ_N are presented in Figure 5.18 for Case 9. It is observed that the most accurate theoretical relationship is the one calculated using the exponential function. This accuracy illustrates that the theoretical values of ϕ and G_0calculated using exponential function (Table 3) is more convenient than those calculated by using hyperbolic function for this experimental study.

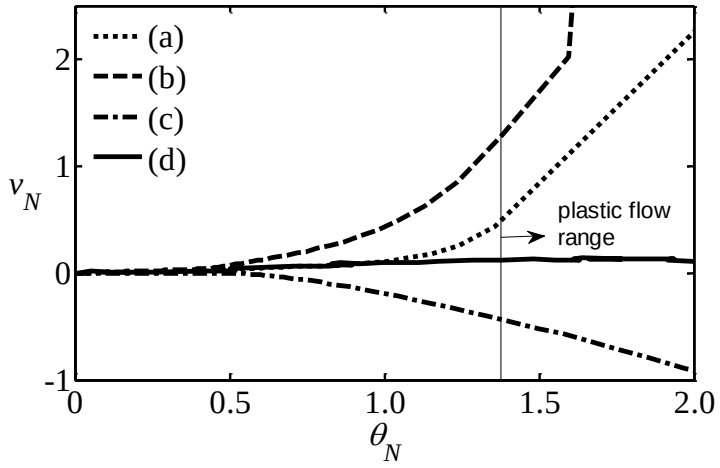

Figure 5.18 The relationship between v_N and θ_N calculated by considering (a) an exponential function, (b) a hyperbolic function, (c) a linear response, and (d) the experimental data for load Case 9

It was observed that use of exponential function (Equation 5.12) in calculating the theoretical relationship between M_N and θ_N generally yielded more consistent results with the experimental ones than the hyperbolic function (Equation 5.9). Therefore, only the theoretical results obtained by the exponential functional form are plotted.

The theoretical relationships between M_N and θ_N are compared with the experimental cyclic $M_N - \theta_N$ relationships in Figures 5.19, 5.20, and 5.21. In Figure 5.19, a complete number of loading cycles is used to observe the general behavior and associated accuracy of the theoretical relationships in longer ranges of θ_N for load cases 3 and 5. It is observed that the theoretical $M_N - \theta_N$ envelope is in reasonable agreement with the peak points of experimental results.

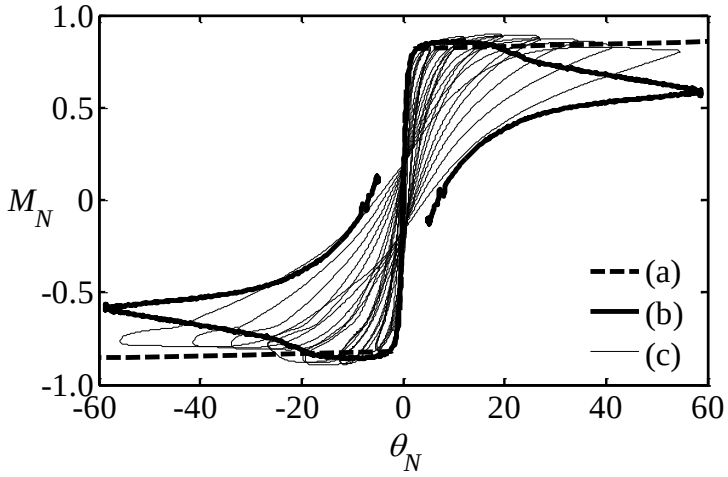

Figure 5.19 The relationship between M_N and θ_N calculated by considering (a) an exponential function and by experimental data for (b) Case 3 and (c) Case 5

In Figure 5.20 complete loading cycles are used to observe the accuracy of the proposed theoretical relationships for load cases 6 and 8. Figure 5.20 shows that the theoretical $M_N - \theta_N$ envelope is in reasonable agreement with the experimental results for relatively small values of θ_N (i.e., $\theta_N = 10$). On the other hand, for higher values of θ_N agreement between the theoretical and experimental relationships decays.

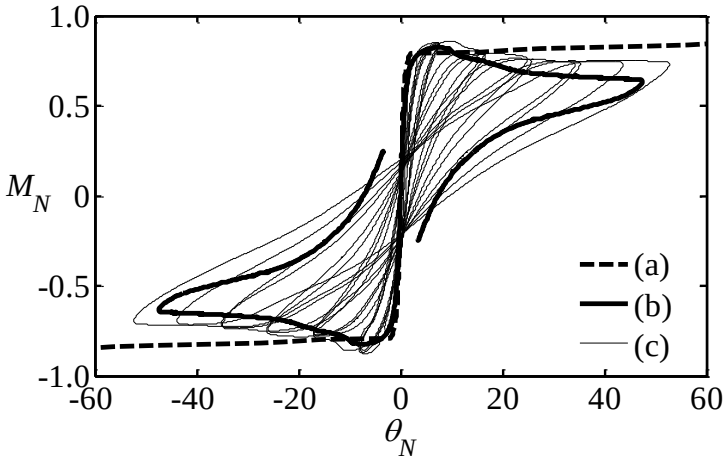

Figure 5.20 The relationship between M_N and θ_N calculated by considering (a) an exponential function and by experimental data for (b) Case 6 and (c) Case 8

Figure 5.21 compares the proposed theoretical M_N and θ_N relationships with experimental ones for load cases 9 and 11. Figure shows that the theoretical $M_N - \theta_N$ envelope follows a similar trend with the experimental data until $\theta_N = 10$. For higher ranges of θ_N, the agreement between the theoretical and experimental relationships decays.

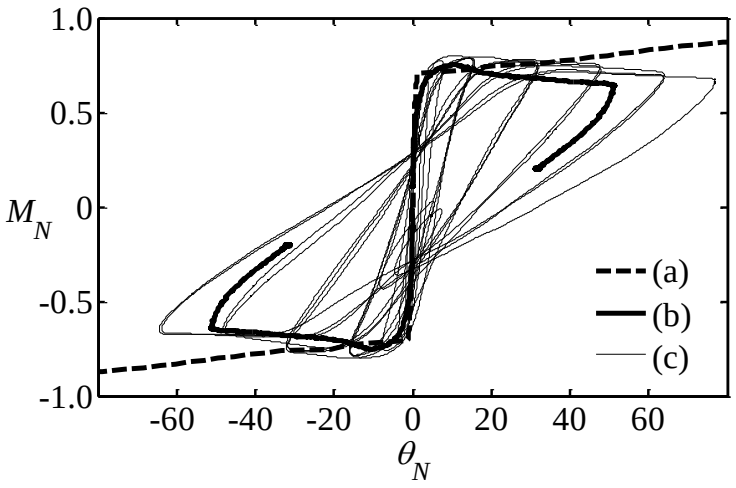

Figure 5.21 The relationship between M_N and θ_N calculated by considering (a) an exponential function and by experimental data for (b) Case 9 and (c) Case 11

In Figures 5.22, 5.23 and 5.24, only the first three cycles of cyclic loading experiments are used to observe the accuracy of the theoretical relationships in lower ranges of θ_N. In Figure 5.22, the closer views of the cyclic $M_N - \theta_N$ relationships show a reasonable accuracy for load cases 3 and 5. The peak points of each load cycle are almost on the theoretical relationship.

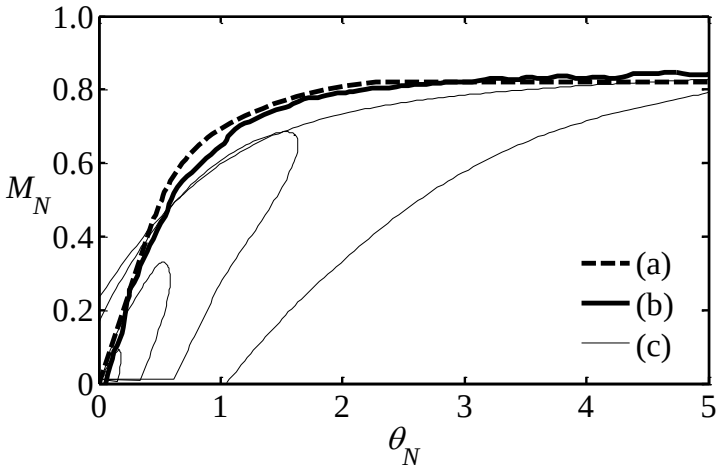

Figure 5.22 The relationship between M_N and θ_N in the lower range of θ_N calculated by considering (a) an exponential function and by experimental data for (b) Case 3 and (c) Case 5

In Figure 5.23, the closer views of the cyclic $M_N - \theta_N$ relationships are compared with the theoretical relationship. In the figure, a reasonable accuracy is observed for load cases 6 and 8. The maximum difference between theoretical and experimental values of M_N is approximately 20% appearing around $\theta_N = 1$. For the longer range of θ_N, theoretical and experimental M_N show better agreement.

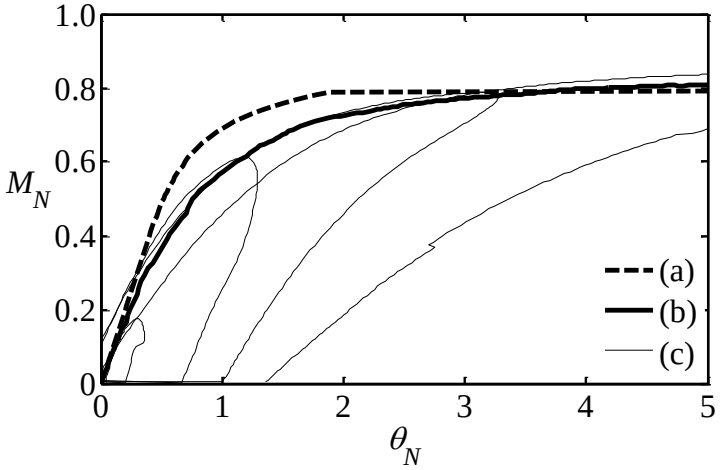

Figure 5.23 The relationship between M_N and θ_N in the lower range of θ_N calculated by considering (a) an exponential function and by experimental data for (b) Case 6 and (c) Case 8

Figure 5.24 shows the closer views of the cyclic $M_N - \theta_N$ relationships for load cases 9 and 11. It is observed that the experimental value of M_N initiating the uplift is smaller than that calculated by using the proposed theoretical model. The relative difference between these two M_N values is approximately 10%. Furthermore, the maximum difference between theoretical and experimental values of M_N for the same θ_N is approximately 40% in the range $0 < \theta_N < 5$.

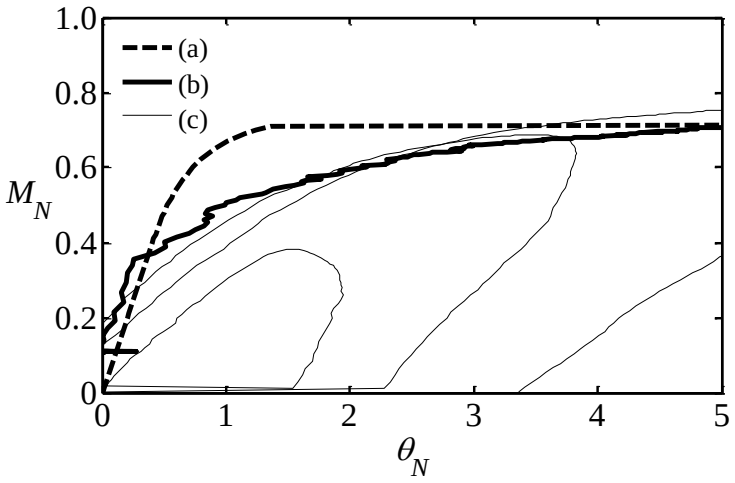

Figure 5.24 The relationship between M_N and θ_N in the lower range of θ_N calculated by considering (a) an exponential function, and by experimental data for (b) Case 9 and (c) Case 11

Another important observation on Figures 5.19 to 5.24 is the increase in the moment values in cyclic loading cases with respect to the monotonic loading cases. Such increase is explained with the densification of the soil by Drosos et al. (2012).

5.3.2. Simulation of TRISEE tests

Large scale, dynamic loading experiments (TRISEE) were performed in scope of the European research project "3D Site Effects and Soil-Foundation Interaction in

Earthquake and Vibration Risk Evaluation" to examine the response of rigid shallow foundations subjected to dynamic loads (Negro et al., 2000). Results obtained from this experimental study were used by a number of researchers for the validation of proposed analytical procedures (Allotey and El Naggar, 2008; Grange et al., 2008; Figini et al. 2012). The results of TRISEE tests are used to verify the results obtained by the proposed theoretical method.

In TRISEE experiments, 1 m length square shallow foundations were embedded by 1m in the Ticino sand with two relative densities: (i) $D_r = 85\%$ (high density) and (ii) $D_r = 45\%$ (low density). ϕ and FS for loose and dense sand conditions are obtained by Harden et al. (2005). In the study, ϕ values are recommended as 42 and 38 degrees, respectively for the dense and loose Ticino sand. In this study, the ϕ values for loose and dense sand conditions are also calculated. The calculated ranges of ϕ values are identical with those presented by Harden et al. (2005). Similarly, vertical factors of safety are given as 12.5 and 20.7 for the dense and loose sand conditions, respectively. G_0 is calculated by using the horizontal stiffness, K_h, and by using pertinent equation in Table 2.1. In the study of Faccioli et al. (2001), K_h is given as 110000 kN/m for TRISEE experiments. By using this recommended value of K_h, G_0 is calculated as 41555 kN/m^2 for TRISEE experiments.

In the experimental procedure, tests were conducted with variable loading conditions. In the tests, three types of cyclic loading patterns were used: Type 1 loading – small amplitude force controlled cyclic loading; Type 2 loading – ground motion like cyclic loading; and Type 3 loading - sinusoidal displacement cycles with increasing amplitude. In this study, results obtained from Type 3 loading for loose and dense sand conditions are used for verification purposes. Other details of the experimental study are presented by Faccioli and Paolucci (1998). All parameters required to conduct the analyses are summarized in Table 5.4.

Table 5.4 Calculated parameters used in the theoretical model for TRISEE tests

D_r (%)	ϕ (°)	G_0 (kN/m^2)	γ (kN/m^3)	N_q	N_c	N_γ
45	38	15000	14.5	49	61	56
85	42	41555	16.2	84	93	112

The results of the theoretical model are compared with the experimental results, in Figure 5.25 for loose soil conditions. The peak points of the experimental cyclic curves are marked with solid circles for comparisons with the theoretical relationship. It is observed that the maximum difference between the theoretical experimental relationships is approximately 40% appearing at θ=0.01 rad. The figure shows that there is a constant increase in the peak *M* of experimental *M* - θ relationship. The theoretical model calculates an average theoretical *M* value lying between the peak *M* values of experimental *M* - θ relationship. This difference between the theoretical and experimental relationship can be explained by the effect of limited foundation embedment in the experiments. More detailed numerical analyses involving discretization of nonlinear continuous load-bearing medium can be necessary for clarification of the reasons. Such a study is left as a future study.

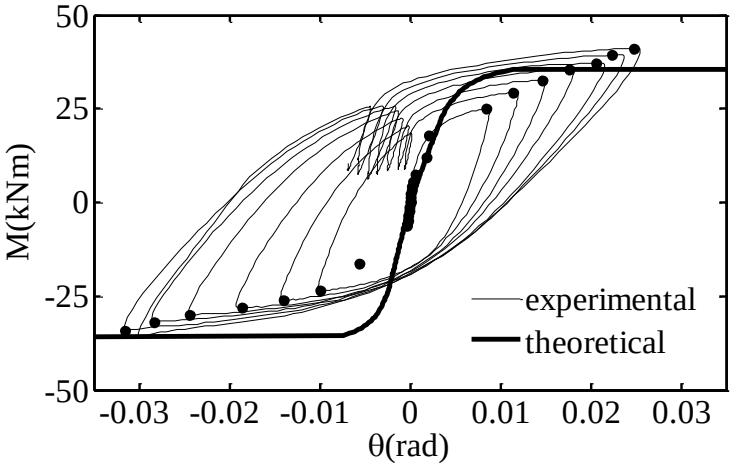

Figure 5.25 The relationship between M and θ for loose sand conditions and loading Type 3

Similarly, the results of the theoretical model, in terms of M and θ relationship, are compared with the experimental M and θ relationships for dense soil conditions in Figure 5.26. Figure 5.26 shows a reasonable agreement until θ= 0.01 rad. After this point, the theoretical model cannot capture the increasing values of M for higher values of θ. Nevertheless, the agreement between the theoretical and experimental results is better that that shown in Figure 5.25.

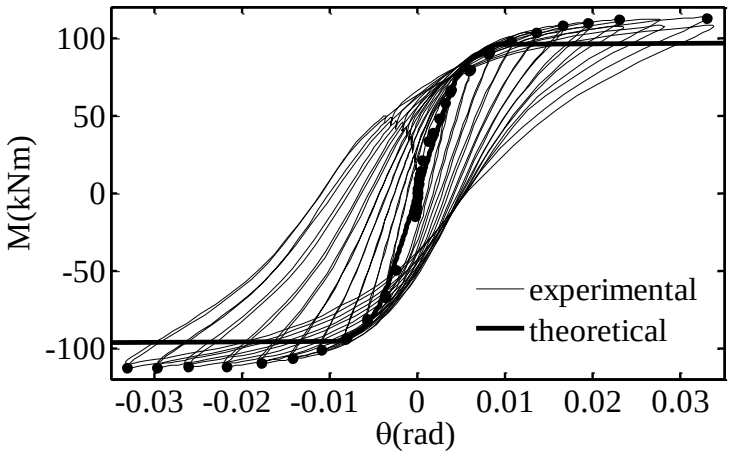

Figure 5.26 The relationship between M and θ for dense sand conditions and loading Type 3

5.3.3. Simulation of the tests conducted by Kokkali et al. (2015)

Kokkali et al. (2015) conducted centrifuge experiments of shallow foundations resting on dry Nevada sand. Results of the tests conducted in scope of experimental study are used for validation of the proposed theoretical model.

In the centrifuge experiments, Kokkali et al. (2015) simulated the tests of a square shallow foundation with a prototype width of 3 m. The actual dimensions of the tested foundation surfaces were 6 cm x 6 cm. The test specimens were placed on dry Nevada sand with relative densities of D_r =45% (loose) and D_r =90% (dense). The physical properties of the dry Nevada sand are presented in Table 5.6. The factor of safety against bearing failure against V for loose and dense sand conditions are given as 5 and 11, respectively. ϕ is 44.5 and 48 degrees for loose and dense conditions of sand, respectively. G_0 values are calculated by considering the relationships between V and v of the experimental data (Figure 5.27), and FS was reported by Kokkali et al. (2015). Details of the calculation procedure of ϕ and G_0 are identical to the aforementioned procedure in Section 5.3.1.

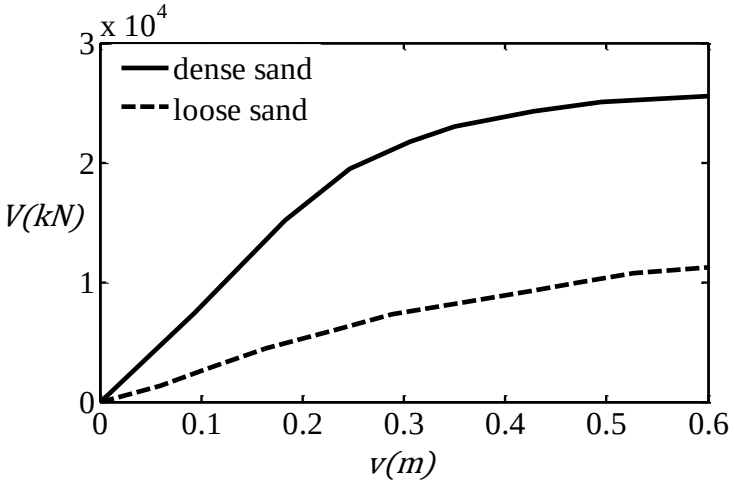

Figure 5.27 Results of the vertical loading tests (Kokkali et al., 2015)

It should be noted that calculated ϕ values are later modified to improve the agreement between theoretical and experimental relationships between M_N and θ_N. On the other, Kokkali et al. (2015) does not present any further information on the effective value of ϕ in the model, whereas this parameter is sensitive to the preparation and other conditions in testing. In Table 5.5, ϕ values derived using experimental vertical load-displacement relationships are presented instead of ϕ that provides a good agreement between the theoretical and the experimental relationships.

Table 5.5 Calculated parameters used in the theoretical model for the tests conducted by Kokkali et al. (2015)

D_r (%)	ϕ (°)	G_0 (kN/m^2)	γ (kN/m^3)	N_q	N_c	N_γ
45	44.5	19176	15.25	43	56	47
90	48	74800	16.9	85	94	114

Experimental relationships between M_N and θ_N of the test specimens are presented in Figure 5.28. The figure shows that the M_N obtained for the dense soil conditions are higher than the M_N values obtained for the loose soil conditions. These experimental relationships between M_N and θ_N of the test specimens are compared with relationships between M_N and θ_N calculated by using the theoretical relationship in Figures 5.29 and 5.30 for loose and dense soil conditions respectively.

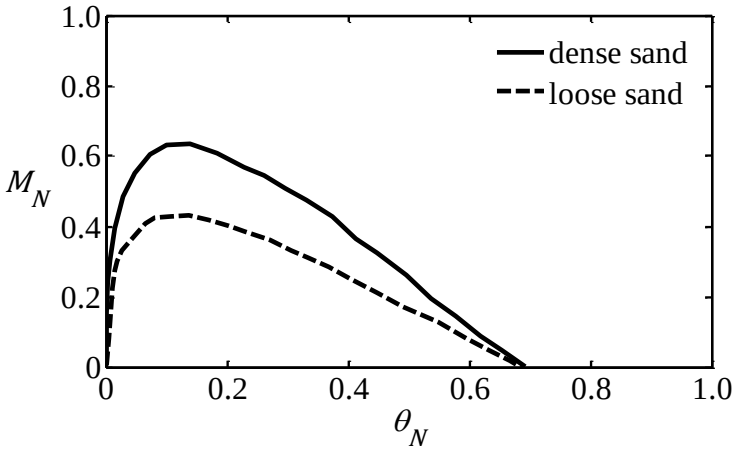

Figure 5.28 The relationships between M_N and θ_N according to the results of the monotonic loading tests (Kokkali et al., 2015)

Figure 5.29 shows that the theoretical relationship between M_N and θ_N is not consistent with the experimental datas. It is known that the results obtained from reduced scale tests may suffer from scaling effects (Perkins and Madson, 2000). Possible problems associated with scaling effects may arise due to: (i) the nonlinearity of Mohr Coulomb failure envelope for soil deposits; (ii) progressive-failure mechanism leading to different mobilized $\emptyset$ values in different locations on failure plane; (iii) inherent anisotropic deformation and strength (Siddiquee et al., 2001); and (iv) highly nonlinear stress-hardening or softening of in stress strain relationship (Siddiquee et al., 2001). In relation to that the discrepancy between the experimental and theoretical curves may be due to such scaling effects in the experimental study. A more detailed numerical simulation of the test model is necessary for clarification of the reasons of inconsistency. These studies, involving numerical discretization of nonlinear medium, are left as future studies.

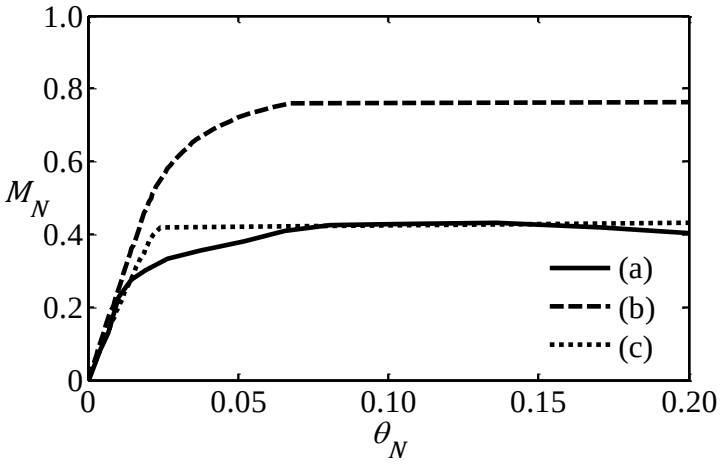

Figure 5.29 Comparison of the relationship between M_N and θ_N for loose sand conditions: (a) experimental, (b) theoretical with $\phi = 44.5°$, (c) theoretical with $\phi = 37°$

Figure 5.30 illustrated that the theoretical relationship between M_N and θ_N is not in good agreement with the experimental relationship. The differences between the theoretical and experimental results may be attributed to the questionable test results obtained by using small scale test specimens (Perkins and Madson, 2000). On the other hand, if the calculated ϕ values are modified to yield compatible theoretical results with the experimental data (Figures 5.29 and 5.30), ϕ of dry Nevada sand appear as 37^{o} for loose sand and 41.5^{o} for dense sand. These observations may imply an uncertainty about the presumed test conditions, or a limitation of theoretical model.

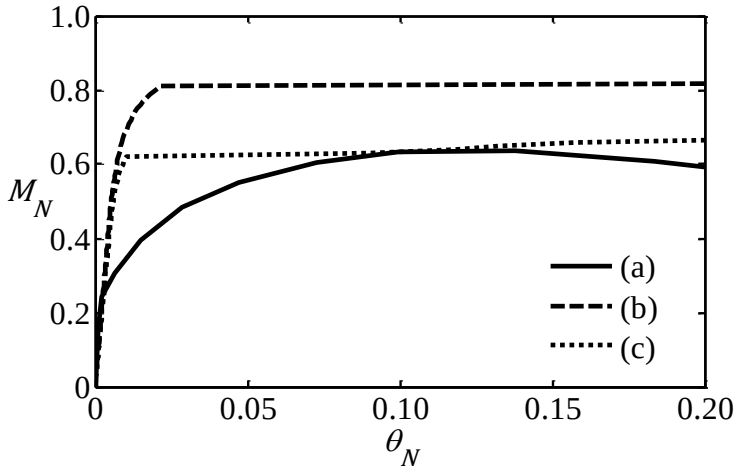

Figure 5.30 Comparison of the relationship between M_N and θ_N for dense sand conditions: (a) experimental, (b) theoretical with $\phi = 48°$, (c) theoretical with $\phi = 41.5°$

CHAPTER 6

APPLICATIONS

6.1. Introduction

Parametric analyses are conducted to observe the sensitivity of $M/M_\infty - \theta_N$ and $v/v_\infty - \theta_N$ relationships to model parameters. In the analyses, the moment and vertical displacement of the foundations are normalized by the moment reaction of a foundation resting on a linearly elastic halfspace. M_∞ represents the moment on the foundation calculated without considering the material nonlinearity. Similarly v_∞ represents the vertical displacement of the foundation without considering the material nonlinearity. It should be noted for $FS \rightarrow \infty$, M/M_∞ ratio and v/v_∞ ratio are equal to 1. In the analyses, the principal parameters are the length of moment arm (h_s), the internal friction angle of load bearing soil (ϕ), the cohesion of soil (c_s), factor of safety against bearing failure (FS), shape and dimensions of shallow foundations. The parametric theoretical analyses are conducted by using an exponential function for the $V - v$ relationship, because this function was shown to provide better agreement with the experimental data (section 5.3.1).

6.1.1. The Effect of h_s on the variation of $M/M_\infty - \theta_N$ and $v/v_\infty - \theta_N$ relationships

Effect of h_s on the variation of the relationships between M/M_∞ and θ_N (Figure 6.1), and that between v/v_∞ and θ_N (Figure 6.2) relationships are presented in this section. The parametric analyses are conducted by considering a square shaped (i.e., 1 m x 1 m) shallow foundation with a factor of safety, FS, equal to 5. In

Figure 6.1, the relationships between M/M_∞ and θ_N of a square foundation are plotted for a set of h_s. An increase in h_s, increases moment capacity. This is attributed to the observation that a small amount of H will be required to initiate uplift if h_s is relatively long. The decrease in load inclination yields to relatively higher bearing capacity due to decreasing load inclination factor (section 5.2.3) leading to a smaller soil nonlinearity.

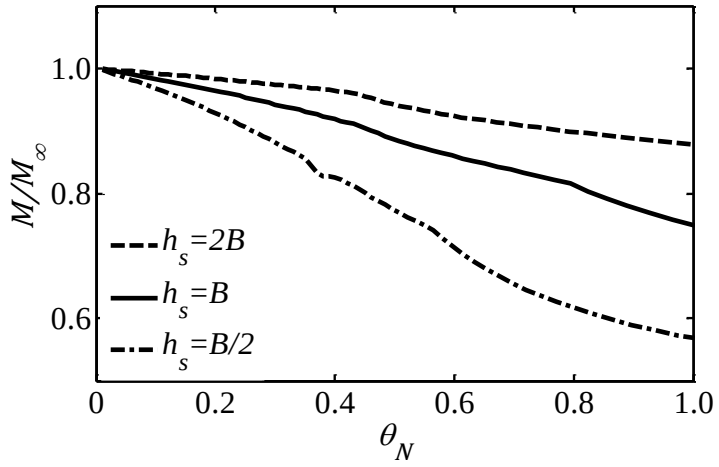

Figure 6.1 Variation of the relationship between M/M_∞ and θ_N by h_s

Similar explanation is also valid for the relationship between v/v_∞ and θ_N presented in Figure 6.2. For a shallow foundation with a long column, a smaller H is required to have the rotation value causing uplift. Such a smaller disturbance leads to a small amount of settlement. Consequently, the foundation displays only upward displacement (i.e., decreasing v/v_∞) in case h_s is as large as two times the width of the foundation.

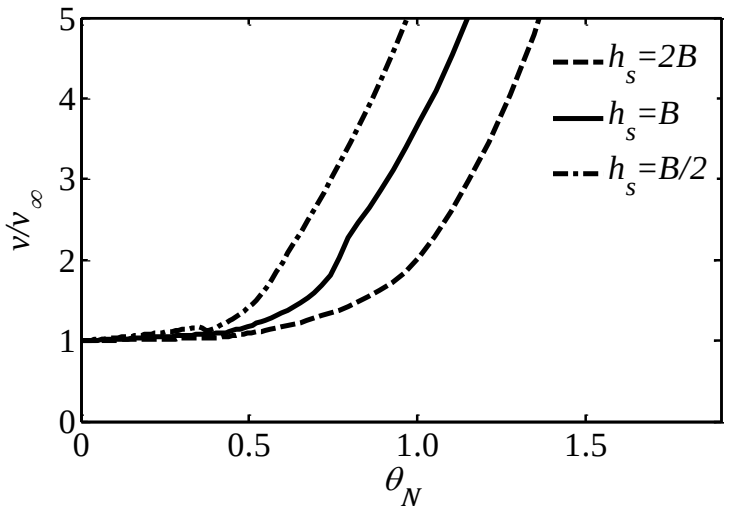

Figure 6.2 Variation of the relationship between v/v_∞ and θ_N with h_s

6.1.2. Effect of ϕ on the $M/M_\infty - \theta_N$ and $v/v_\infty - \theta_N$ relationships

Effects of ϕ on the variation of $M/M_\infty - \theta_N$ (Figure 6.3), and $v/v_\infty - \theta_N$ (Figure 6.4) relationships are presented. The parametric analyses are conducted by using a square shaped shallow foundation (i.e., 1 m x 1 m). In Figure 6.3, the relationship between M/M_∞ and θ_N of foundation are plotted as a function of ϕ for a load bearing soil with zero cohesion, c_s. As known, ϕ is an effective factor on the variation of FS. Varying ϕ used in the analyses lead to varying FS which are also shown in this figure. It is observed that increasing ϕ leads to higher ranges of FS. An increase in FS reduces the effect of soil nonlinearity on the variation of the response.

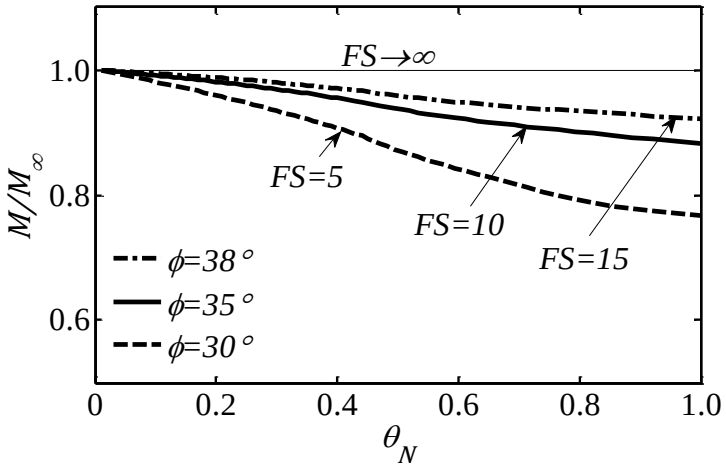

Figure 6.3 Variation of the relationship between M/M_∞ and θ_N with ϕ

Figure 6.4, shows the relationship between v/v_∞ and θ_N of the foundation as a function of ϕ for a load bearing soil with zero cohesion. Behavior similar to that observed in Figure 6.3 is also observed from this figure. Increasing ϕ leads to higher ranges of FS. An increase in FS reduces the effect of soil nonlinearity on the variation of the response. In conclusion, increasing ϕ leads to a decrease in v/v_∞ due to reduced effect of soil nonlinearity.

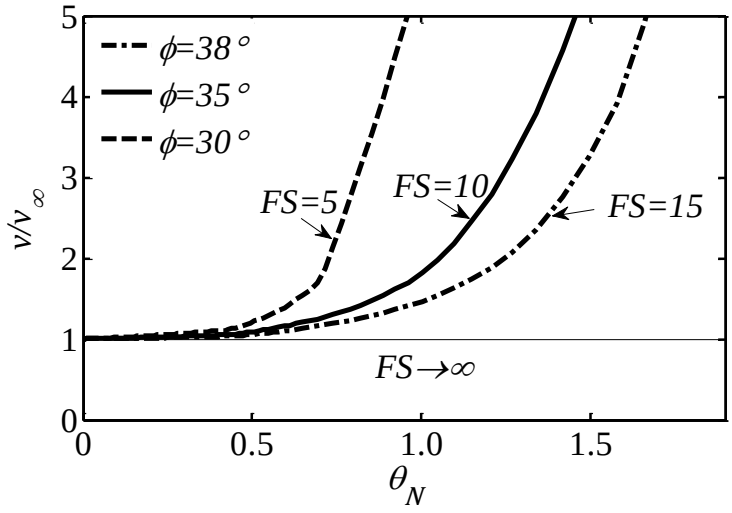

Figure 6.4 Variation of the relationship between v/v_∞ and θ_N with ϕ

6.1.3. Effect of c_s on the variation of $M/M_\infty - \theta_N$ and $v/v_\infty - \theta_N$ relationships

The effects of c_s on the variation of the relationships between M/M_∞ and θ_N (Figure 6.5), and v/v_∞ and θ_N (Figure 6.6) are presented. The parametric analyses are conducted by using a square shaped foundation (i.e., 1 m x 1 m). The M/M_∞ and θ_N relationships of foundation are plotted as a function of c_s (Figure 6.5). c_s is effective on the variation of FS of a foundation. Varying c_s used in the analyses lead to varying FS. It is observed that M/M_∞ increases with increasing c_s and leads to higher ranges of FS. Such an increase illustrates the reduced effect of soil nonlinearity on the relationship between M/M_∞ and θ_N.

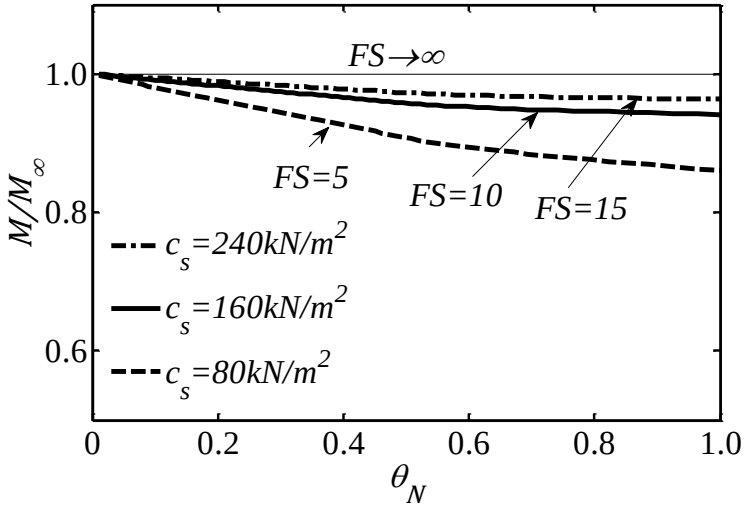

Figure 6.5 Variation of the relationship between M/M_∞ and θ_N as a function of c_s

The relationships between v/v_∞ and θ_N of foundation are plotted as a function of c_s, cohesion of soil, in Figure 6.6. As explained before, variability of c_s used in the analyses lead to variability in FS. It is observed in Figure 6.6 that v/v_∞ decreases with increasing c_s and with decreasing FS due to the reduced soil nonlinearity.

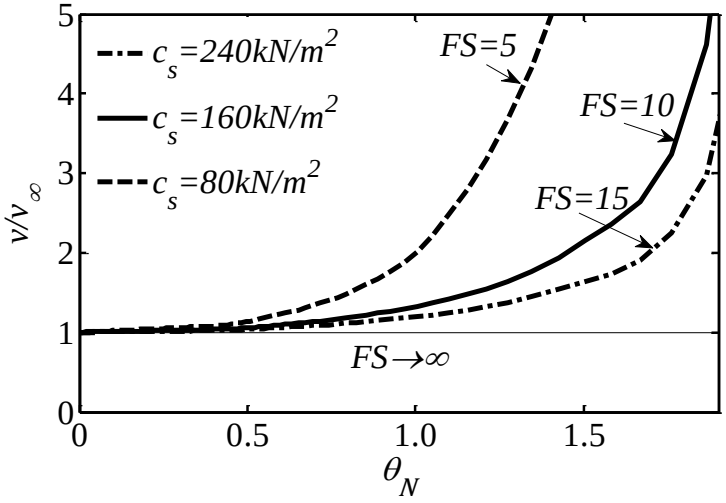

Figure 6.6 Variation of the relationship between v/v_∞ and θ_N as a function of c_s

6.1.4. The effect of foundation shape and loading direction on the relationship between $M/M_\infty - \theta_N$ and $v/v_\infty - \theta_N$

Effect of foundation shape and loading direction on the variation of the relationship between M/M_∞ and θ_N (Figure 6.7, Figure 6.8), and that between v/v_∞ and θ_N (Figure 6.9, Figure 6.38) are presented in this section. The analyses are conducted on square and circular shallow foundations. The foundations with different shapes but identical properties (i.e., K_v, K_r and FS) are considered to observe the effect of theoretical parameters. The identical properties of foundations are obtained by modifying the parameters G, B and ϕ. In the analyses, square-shaped shallow foundations are subjected to one and two-way eccentric loadings (Appendix A). The results are compared in terms of load eccentricity and are presented in Figure 6.8 and Figure 6.10 for $M/M_\infty - \theta_N$, and $v/v_\infty - \theta_N$ relationship, respectively.

Figure 6.7 shows that the range of M/M_∞ for the square shaped foundations are greater than those of their circular counterparts with identical FS. It should be

noted that higher ranges of ϕ are assigned for comparisons (i.e., to have identical FS for circular and square foundations). Higher ranges of ϕ results in relatively higher ranges of M/M_∞ for square shaped foundations due to the increased load bearing capacity of the soil deposit.

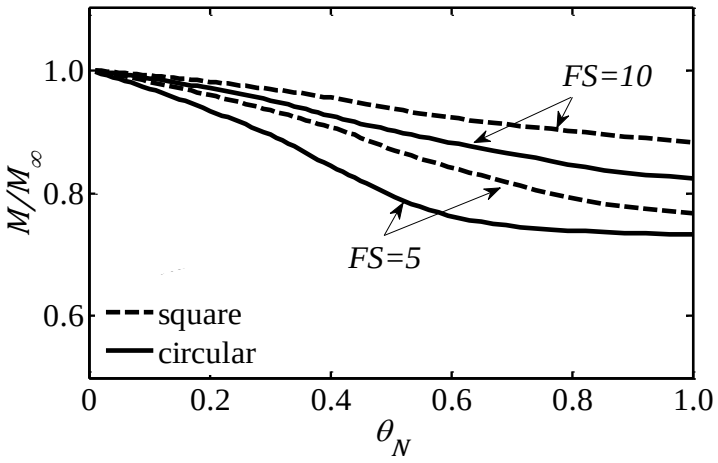

Figure 6.7 Variation of the relationship between M/M_∞ and θ_N by the shape of foundation

Figure 6.8 shows that M/M_∞ for the square shaped foundations subjected to one-way eccentric loading are greater than those of their counterparts subjected to two-way eccentric loading with identical FS. It is observed that two-way eccentric loading leads to a higher soil nonlinearity with respect to one-way eccentric loading. The increase in the soil nonlinearity may be attributed to the relatively higher disturbance of load bearing soil deposit in two-way eccentric loading conditions.

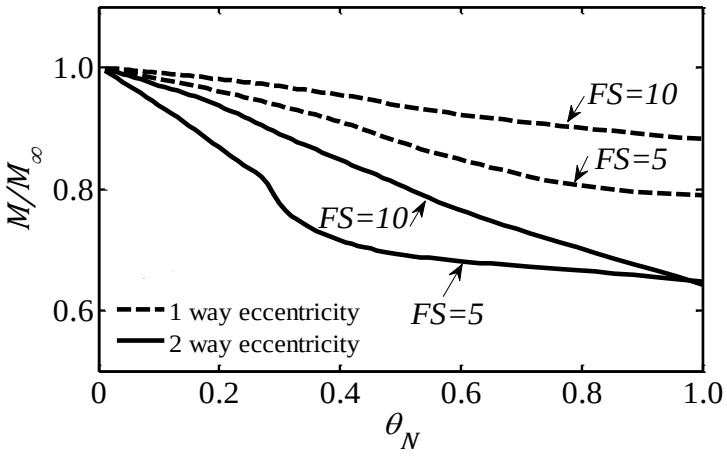

Figure 6.8 Variation of the relationship between M/M_{∞} and θ_N as a function of loading direction

It is observed in Figure 6.9 that the settlement of a circular foundation is higher than that of square foundation with identical *FS*. Higher ranges of ϕ resulted in relatively smaller ranges of v/v_{∞} for square shaped foundations due to the increased load bearing capacity of the soil deposit. Moreover, the ranges of v/v_{∞} of the foundations with higher *FS* are smaller than those of foundations with smaller *FS*.

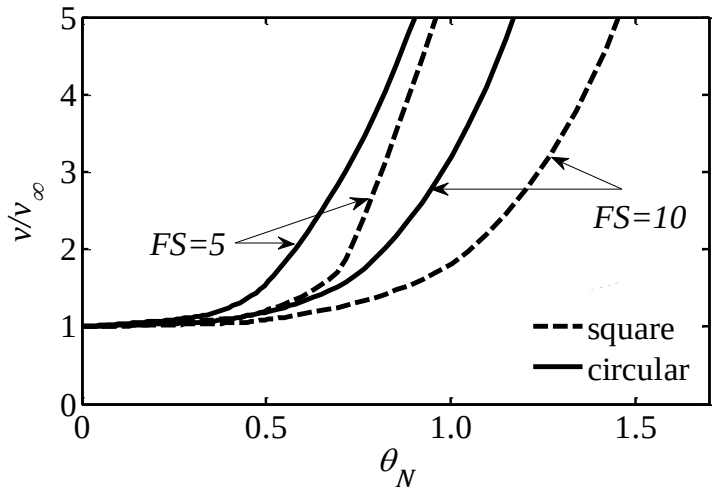

Figure 6.9 Variation of the relationship between v/v_{∞} and θ_N by the foundation shape

Figure 6.10 shows that the settlement of the foundations subjected to two-way eccentric loading are higher than those of foundations subjected to one way eccentric loading. Amplified soil nonlinearity due to two-way eccentric loading leads higher ranges of v/v_∞ as expected. Figure 6.10 shows that the settlement of the foundations subjected to two-way eccentric loading are higher than those of foundations subjected to one way eccentric loading. Amplified soil nonlinearity due to two-way eccentric loading leads higher ranges of v/v_∞ as expected.

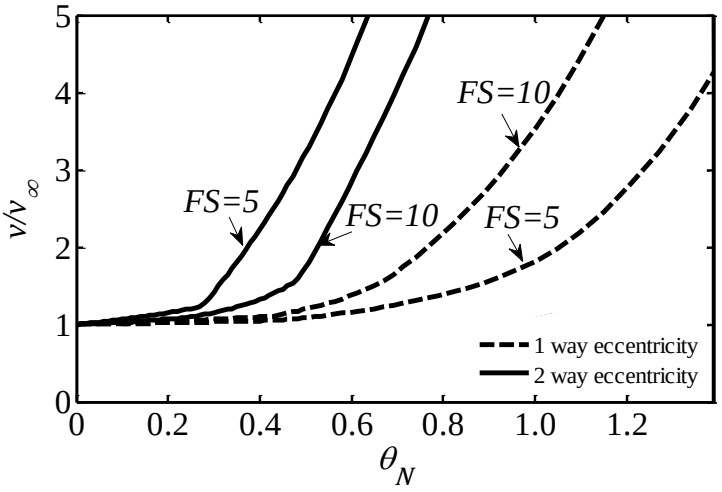

Figure 6.10 Variation of the relationship between v/v_∞ and θ_N by loading direction

6.1.5. The effect of foundation dimensions on $M/M_\infty - \theta_N$ and $v/v_\infty - \theta_N$ relationships

Effect of foundation dimensions on the variation of M/M_∞ and θ_N (Figure 6.11), and on the relationship between v/v_∞ and θ_N (Figure 6.12) are presented for rectangular foundations. In the analyses, *FS* of the model foundations are equal to *5*. Figure 6.11 shows that the ratio M/M_∞ the foundation with dimensions *L=2B* is close to 1. This is attributed to the higher cross sectional area of the foundation which results in smaller stresses on the load bearing soil deposit. Due to reduced

stress values, the shear modulus of the underlying soil deposit degrades slower than that of a load bearing soil deposit underlying a foundation with smaller area. Consequently, the effect of soil plasticity becomes less pronounced in a relatively large foundation. On the other hand, a high amount of H will be required to initiate uplift if the cross sectional area of the foundation is relatively large. The increase in the load inclination yields to relatively smaller bearing capacity due to increasing load inclination factor (section 5.2.3) leading to a higher soil nonlinearity. Thus, negative effect of the increased foundation length reduces the positive effect of the smaller stress and consequently, a limited difference may be observed in the response of shallow rectangular foundations with varying lengths in the direction of uplift.

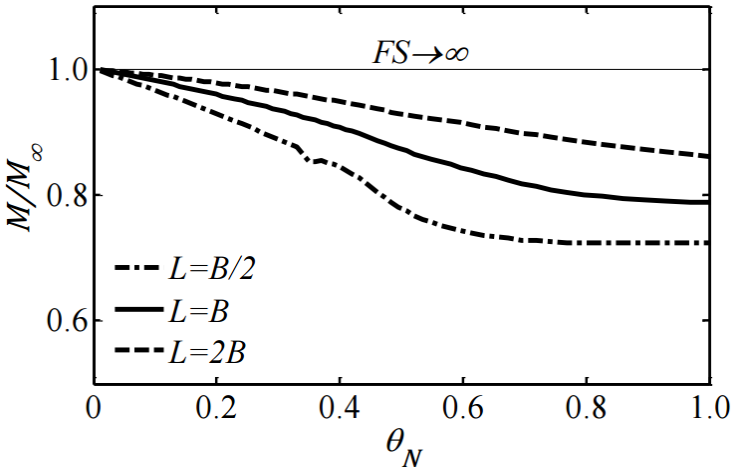

Figure 6.11 Variation of the relationship between M/M_∞ and θ_N as a function of rectangular foundation dimensions for $FS = 5$

Figure 6.12 shows that the v/v_∞ ratio of the foundation with smaller length is greater than those with greater length. This may be attributed to the higher cross sectional area of the larger foundation which results in smaller stresses on the load bearing soil deposit. These reduced stress values lead to a small decrease in the shear modulus of the underlying soil deposit. Consequently, the effect of soil plasticity becomes less pronounced in a relatively large foundation.

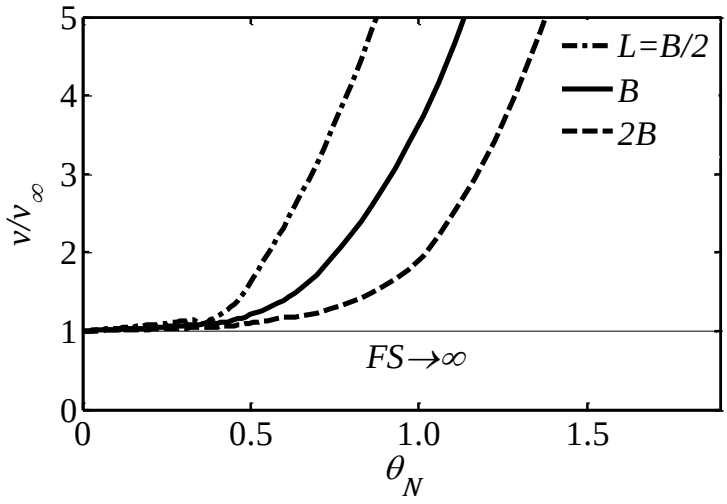

Figure 6.12 Variation of the relationship between v/v_∞ and θ_N as a function rectangular foundation size for $FS = 5$

CHAPTER 7

SUMMARY AND CONCLUSIONS

7.1. Summary

Eccentric loading on foundations can cause partial separation of shallow foundations from load bearing soil due to the lack of tensional strength on the interface between soil and foundation. The partial separation, namely the uplift of foundation, may significantly alter the foundation stiffness to be considered in structural design. The nonlinear response of shallow foundations partially loosing contact with underlying soil due to eccentric loading is important for an accurate estimation of foundation stiffness in structural analyses.

This study presents an approximate theoretical method to calculate the displacements of arbitrarily shaped ideally-rigid shallow foundations subjected to inclined and eccentric loading. The theoretical method is mainly based on two assumptions such that (i) the static impedance coefficients used in the calculations are accurate; and (ii) the boundary between the part of foundation that is in contact with soil and the part that is not supported by soil is linear.

The proposed method is a computationally simple yet robust technique, and is capable of involving the effects of material and geometrical nonlinearities on the response of shallow foundations to monotonic loading conditions. The threshold moment for the initiation of foundation uplift for ideally rigid foundations resting on deformable medium is proportional to the ultimate moment that can be applied on a foundation resting on a rigid support. The moment on foundation after

initiation of uplift is related to the geometric properties of the instantaneous shape of the foundation that is in contact with soil, and to the mechanical properties of the deformable support. In the study, the material nonlinearity (i.e. inelasticity of the soil) is taken into account by using an equivalent shear modulus to simulate the lumped stiffness of load bearing medium.

The approximate theoretical method is justified by comparing the results with the available solutions in the literature. Furthermore, parametric analyses are conducted to investigate the effect of geometric and material properties of the problem on the response of shallow foundations. Finally, the accuracy of the approximate theoretical method is tested by using the results of several experimental studies presented in literature.

7.2. Conclusions

The following conclusions are deduced.

- The response of a foundation to eccentric load is related to a non-dimensional parameter α which is the ratio of moment acting on a foundation to the ultimate moment that can be applied on a foundation resting on a rigid support.
- The effect of the thickness of a finite elastic layer on the relationship between overturning moment (M_N) and the rocking angle (θ_N) is insignificant in the case that the layer thickness is not less that the foundation width. Hence, the theoretical solutions on the rocking stiffness of foundations resting on a uniform medium is applicable provided that the layer thickness is not less than the foundation width.

- The proposed theoretical model can be used for computation of the response of an arbitrarily shaped foundation during uplift with reasonable accuracy.

- The calculated theoretical range of α initiating the foundation uplift is consistent with those reported by Chopra and Yim (1985) and Wolf (1976). A reasonable agreement between the theoretical relationships for α proposed in this study and that given by Gazetas et al. (2013) is also observed. So the alternative solutions presented by these researchers are supported.
- The theoretically calculated the relationship between M_N and θ_N are in reasonable agreement with those calculated using methods of Wolf (1976) and Cremer (2001).

- Factor of safety against bearing capacity failure significantly effects the relationship between M_N and θ_N, provided that this factor is not greater than 15.

7.3. Future Studies

The observed inconsistencies between the theoretical relationships proposed in this study and the results of some of experiments is showing the need for a more detailed numerical analysis of continuum, so that further improvements in the computationally simple method presented in this study will be possible.

REFERENCES

Adamidis O., Gazetas G., Anastasopoulos I. and Argyrou Ch. (2014). Equivalent-linear stiffness and damping in rocking of circular and strip foundations. *Bull Earthquake Eng*, *12*, 1177-1200.

Allotey N.K. and El Naggar M. H. (2008). An investigation into the Winkler modeling of the cyclic response of rigid footings. *Soil Dynamics and Earthquake Engineering, 28 (1),* 44–57.

Allotey N. K., El Naggar M. H. (2003). Analytic moment–rotation curves for rigid foundations based on a Winkler model. *Soil Dynamics and Earthquake Engineering*, *23*, 367–81.

Anastasopoulos I. (2010). Beyond conventional capacity design: towards a new design philosophy. *Soil–Foundation–Structure Interaction.* NewYork: CRCPress, Taylor & Francis Group.

Anastasopoulos I., Gazetas G., Loli M., Apostolou M. and Gerolymos N. (2010). Soil failure can be used for seismic protection of structures. *Bulletin of Earthquake Engineering, 8,* 309–26.

Anastasopoulos I., Loli M., Gelagoti F., Kourkoulis R. and Gazetas G. (2012). Nonlinear soil–foundation interaction: numerical analysis. *Second International Conference On Performance-Based Design In Earthquake Geotechnical Engineering*, 28-30 May, Taormina (Italy).

Anastasopoulos I., Loli M., Georgarakos T. and Drosos V. (2013). Shaking table testing of rocking−isolated bridge pier on sand. *Journal of Earthquake Engineering*, *17*, 1–32.

Anastasopoulos I. and Kontoroupi Th. (2014). Simplified approximate method for analysis of rocking systems accounting for soil inelasticity and foundation uplifting. *Soil Dynamics and Earthquake Engineering, 56*, 28–43.

Anastasopoulos I., Drosos V. and Antonaki N. (2015). Three-storey building retrofit: rocking isolation versus conventional design. *Earthquake Engineering and Structural Dynamics, 44*, 1235–1254.

Applied Technolgy Council, ATC (1996). Seismic evaluation and retrofit of concrete buildings. Volume 1 and 2, Report No. ATC-40, Redwood City, CA.

Apostolou M. (2011). Soil–structure interaction under strong seismic moment: material and geometric nonlinearity. PhD Thesis, National Technical University, Athens.

Apostolou M., Gazetas G. and Garini E. (2007). Seismic response of slender rigid structures with foundation uplifting. *Soil Dynamics and Earthquake Engineering, 27*, 642–654.

Biondi G., Massimino M. R. and Maugeri M. (2015). Experimental study in the shaking table of the input motion characteristics in the dynamic SSI of a SDOF model. *Bulletin of Earthquake Engineering*, *13*, 1835–1839.

Celep Z. and Güler K. (1991). Dynamic response of a column with foundation uplift. *Journal of Sound and Vibration*, *149 (2)*, 285–96.

Chapra S.C. and Canale R.P. (2010). Numerical Methods for Engineers, Sixth edition, Mc Graw-Hill.

Chatzigogos C. T., Pecker A. and Salençon J. (2009). Macro-element modeling of shallow foundations. *Soil Dynamics and Earthquake Engineering, 29*, 765–781.

Chatzigogos C. T., Figini R., Pecker A. and Salençon J. (2011). A macroelement formulation for shallow foundations on cohesive and frictional soils. *International Journal for Numerical and Analytical Methods in Geomechanics, 35 (8),* 902-931.

Chen X. C. and Lai Y. M. (2003). Seismic response of bridge piers on elasto-plastic Winkler foundation allowed to uplift. *Journal of Sound and Vibration, 266 (5),* 957-965.

Chen Q., Tominaga K. and Xu T. (2004). An analysis method for nonlinear behavior of rigid plate on soil under cyclic load. *13th World Conference on Earthquake Engineering,* Vancouver, B.C., Canada, 780.

Chopra A. K. and Yim S. C. S. (1985). Simplified earthquake analysis of structures with foundation uplift. *Journal of Structural Engineering, 111 (4),* 906-30.

Chapra S. C. and Canale R. P. (2010). Numerical Methods for Engineers, 6th edition, Mc Graw-Hill.

Cook R., Malkus D. S. and Plesha M. E. (1989). Concepts and Applications of Finite Element Analysis, Third edition, Wiley.

Cremer C., Pecker A. and Davenne L. (2001). Cyclic macro-element for soil–structure interaction: material and geometrical nonlinearities. *International Journal for Numerical and Analytical methods in Geomechanics*, *25 (12),* 1257–84.

Cremer C., Pecker A. and Davenne L. (2002). Modelling of nonlinear dynamic behavior of a shallow strip foundation with macro-element. *Journal of Earthquake Engineering, 6 (2),* 175-211.

Dafalias Y. and Popov E. (1975). A model of nonlinearly hardening materials for complex loading. *Acta Mechanica, 21(3),* 173-192.

DeBeer E. E. (1970). Experimental determination of the shape factors and bearing capacity factors on sand. *Geotechnique, 20 (4),* 387-411.

Deng L. and Kutter B. L. (2012). Characterization of rocking shallow foundations using centrifuge model tests. *Earthquake Engineering and Structural Dynamics*, 41(5), 1043–1060.

Deng L., Kutter B. and Kunnath S. (2012). Centrifuge modeling of bridge systems designed for rocking foundations. *Journal of Geotechnical and Geoenvironmental Engineering, 138(3),* 335–344.

Dobry R. and Gazetas G. (1986). Dynamic response of arbitrarily shaped foundations. *Journal of Geotechnical Engineering, 112 (2),* 109–35.

Drosos V., Georgarakos T., Loli M., Anastasopoulos I., Zarzouras O. and Gazetas G. (2012). Soil-foundation-structure interaction with mobilization of bearing capacity: experimental study on sand. *Journal of Geotechnical and Geoenvironmental Engineering, 138*, 1369-1386.

Faccioli E. and Paolucci R. (1998). TRISEE - 3D site effects and soil-foundation interaction in earthquake and vibration risk evaluation. Technical Report. European Commission. Directorate General XII for Science. Research and Development. 1994–98 Environment and Climate Programme. Climate and Natural Hazards Unit.

Faccioli E., Paolucci R. and Vivero G. (2001). Investigation of seismic soil-footing interaction by large scale cyclic tests and analytical models. *Fourth International Conference on Recent Advances in Geotechnical Earthquake Engineering and Soil Dynamics*, San Diego, California, March 26-31.

FEMA 273 (1997). NEHRP guidelines for the seismic rehabilitation of buildings, Washington, DC.

Figini R. (2010). Non-linear dynamic soil-structure interaction: application to seismic analysis and design of structures on shallow foundations. PhD Thesis, Politecnico di Milano, Italy.

Figini R., Paolucci R. and Chatzigogos C. T. (2012). A macro-element model for non-linear soil–shallow foundation–structure interaction under seismic loads: theoretical development and experimental validation on large scale tests. *Earthquake Engineering and Structural Dynamics*, *41*, 475–93.

Gajan S., Phalen J. D., Kutter B. L., Hutchinson T. C. and Martin G. (2005). Centrifuge modeling of load deformation behavior of rocking shallow foundations. *Soil Dynamics and Earthquake Engineering, 25 (7–10),* 773–83.

Gajan S. and Kutter B. L. (2008). Capacity, settlement and energy dissipation of shallow footings subjected to rocking. *Journal of Geotechnical and Geoenvironmental Engineering, 134 (8),* 1129–41.

Gajan S. and Kutter B. L. (2009). Contact interface model for shallow foundations subjected to combined cyclic loading. *Journal of Geotechnical and Geoenvironmental Engineering, 135(3),* 407-419.

Gazetas G. (1991). Formulas and charts for impedances of surface and embedded foundations. *Journal of Geotechnical Engineering, 117 (9),* 1363-81.

Gazetas G., Apostolou M. and Anastasopoulos I. (2003). Seismic uplifting of foundations on soft soil, with examples from Adapazari (Izmit 1999, Earthquake). *BGA international conference of foundations: innovations, observations, design and practice*. Scotland: University of Dundee, 37–50.

Gazetas G. and Apostolou M. (2004). Nonlinear soil-structure interaction: Foundation uplifting and soil yielding. *3rd U.S.-Japan Workshop on Soil-Structure Interaction*, 29–30 March 2004, Menlo Park, CA.

Gazetas G., Anastasopoulos I., Adamidis O. and Kontoroupi Th. (2013). Nonlinear rocking stiffness of foundations. *Soil Dynamics and Earthquake Engineering*, *47*, 83–91.

Gelagoti F., Kourkoulis R., Anastasopoulos I. and Gazetas G. (2012a). Rocking isolation of low rise frame structures founded on isolated footings. *Earthquake Engineering and Structural Dynamics, 41(1),* 1177–1197.

Gelagoti F., Kourkoulis R., Anastasopoulos I. and Gazetas G. (2012b). Rocking-isolated frame structures: margins of safety against toppling collapse and simplified design approach. *Soil Dynamics and Earthquake Engineering, 32 (1),* 87–102.

Gottardi, G., Houlsby, G. T., and Butterfield, R. (1995). The displacement of a model rigid surface footing on dense sand under general planar loading, *Soils and Foundations, 35,* 71–82.

Grange S., Kotronis P. and Mazars J. (2008). A macro-element for a circular foundation to simulate 3D soil–structure interaction. *International Journal for Numerical and Analytical methods in Geomechanics, 32,* 1205–1227.

Hansen J. B. (1970). A revised and extended formula for bearing capacity, Danish Geotechnical Institute, Bulletin 28, Copenhagen.

Harden H., Hutchinson T., Martin G.R. and Kutter B.L. (2005). Numerical Modeling of the Nonlinear Cyclic Response of Shallow Foundations. PEER Report 2005/04, Pacific Earthquake Engineering Research Center, College of Engineering, University of California, Berkeley.

Harden H., Hutchinson T. and Moore M. (2006). Investigation into the effects of foundation uplift on simplified seismic design procedures. *Earthquake Spectra, 22 (3),* 663–92.

Hayashi Y., Tamura K. and Takahashi I. (1999). Simulation analyses of buildings in 1995 Kobe Japan earthquake considering soil-structure interaction. *Earthquake Engineering and Structural Dynamics*, *28*, 371-391.

Holtz R. (1991). Stress Distribution and Settlement of Shallow Foundations. In: H. Fang, ed. Foundation Engineering Handbook. 2nd ed. New York: Chapman and Hall Inc., 167-222.

Houlsby G. T., Cassidy M. J. and Einav I. (2005). A generalised Winkler model for the behaviour of shallow foundations, *Geotechnique*, *55 (6)*, 449–460.

Hung H. H., Liu K. Y., Ho T. H. and Chang K. C. (2011). An experimental study on the rocking response of bridge piers with spread footing foundations, *Earthquake Engineering and Structural Dynamics*, *40*, 749–769.

Hung H. H., Liu K. Y. and Chang K. C. (2014). Rocking behavior of bridge piers with spread footings under cyclic loading and earthquake excitation. *Earthquakes and Structures*, *7 (6)*, 1001-1024.

Ibrahimbegovic A. and Wilson E. L., (1990). A methodology for dynamic analysis of large structure-foundation systems with local nonlinearities. *Earthquake Engineering and Structural Dynamics*, *19 (8)*, 1197-1208.

Idriss I. M. and Seed H. B. (1968). Seismic response of horizontal soil layers. *Journal of the Soil Mechanics and Foundations Division*, *94 (4)*, 1003-1031.

Jennings P. C., and Bielak J. (1973). Dynamics of building–soil interaction. *Bulletin of the Seismological Society of America*, *63 (1)*, 9–48.

Kan M. E., Taiebat H. A. and Khalili N. (2014). Simplified mapping rule for bounding surface simulation of complex loading paths in granular materials. *International Journal of Geomechanics*, *14 (2)*, 239-253.

Kohno T., Nakaura T., Shirato M. and Nakatani S. (2009). An evaluation of the reliability of vertically loaded shallow foundations and grouped-pile foundations. Geotechnical Risk and Safety, London.

Kokkali P., Anastasopoulos I., Abdoun T. and Gazetas G. (2014). Static and cyclic rocking on sand: centrifuge versus reduced-scale 1g experiments. *Geotechnique , 64 (11),* 865–880.

Kokkali P., Abdoun T. and Anastasopoulos I. (2015). Centrifuge modeling of rocking foundations on improved soil. *Journal of Geotechnical and Geoenvironmental Engineering, 141 (10),* 04015041.

Kokusho T. (1980). Cyclic triaxial test of dynamic soil properties for wide strain range. *Soils and Foundations, 20*, 45-60.

Kourkoulis R., Anastasopoulos I., Gelagoti F. and Kokkali P. (2012a). Dimensional analysis of SDOF system rocking on inelastic soil. *Journal of Earthquake Engineering, 16,* 995–1022.

Kourkoulis R., Gelagoti F. and Anastasopoulos I. (2012b). Rocking isolation of frames on isolated footings: design in sight sand limitations. *Journal of Earthquake Engineering, 16 (3)*, 374–400.

Kutanis M., Fırat S. and Çelebi E. (2002). Earthquake analysis of building structures with foundation uplift in downtown Adapazarı. *ECAS2002 International Symposium on Structural and Earthquake Engineering*, October 14, 2002, Middle East Technical University, Ankara, Turkey, 103-109.

Kutter B. L., Deng L. and Kunnath S. (2010). Estimation of displacement demand for seismic design of bridges with rocking shallow foundations. *Fifth International Conference on Recent Advances in Geotechnical Earthquake Engineering and Soil Dynamics*, San Diego, California.

Liu W., Hutchinson T. C., Kutter B. L., Gavras A.G. and Hakhamaneshi M. (2015). Effect of earthquake-induced axial load fluctuations on asymmetric frame-wall-rocking foundation. *Earthquake Engineering and Structural Dynamics*, *44,* 1997–2013.

Loli M., Knappett J.M., Brown M.J., Anastasopoulos I. and Gazetas G. (2014). Centrifuge modeling of rocking-ısolated inelastic RC bridge piers. *Earthquake Engineering and Structural Dynamics, 43(15),* 2341-2359.

Loli M., Knappett J., Anastasopoulos I., and Brown M. (2015). Use of ricker motions as an alternative to pushover testing. *International Journal of Physical Modelling in Geotechnics, 15(1),* 44–55.

Mathworks Inc. MATLAB (2008). The Language of Technical Computing, Version 7.7.0 (R2008b). The Mathworks Inc. Nattick, MA.

Massimino M. R. and Maugeri M. (2013). Physical modelling of shaking table tests on dynamic soil-foundation interaction and numerical and analytical simulation. *Soil Dynamics and Earthquake Engineering, 49,* 1–18.

McCallen D. B. and Romstad K. M. (1994). Non-linear model for building–soil systems. *Journal of Engineering Mechanics, 120 (5),* 1129-52.

Mergos P. E. and Kawashima K. (2005). Rocking isolation of typical bridge pier on spread foundation. *Journal of Earthquake Engineering, 9 (2),* 395–414.

Meyerhof G. G. (1963). Some recent research on the bearing capacity of foundations. *Canadian Geotechnical Journal, 1*, 16-26.

Mori K., Murakami K., Sakashita M., Kono S. and Tanaka H. (2008). Seismic performance of multi-story shearwall with an adjacent frame considerıng uplift of foundation. *The 14th World Conference on Earthquake Engineering,* Beijing, China.

Negro P., Paolucci R., Pedretti S. and Faccioli E. (2000). Large scale soil-structure interaction experiments on sand under cyclic loading. *Proc. 12th World Conf. on Earthq. Engineering, 2000*, Auckland, New Zealand, 1191.

Nova R. and Montrasio L. (1991). Settlement of shallow foundations on sand. *Géotechnique, 41(2),* 243–56.

Ntritsos N., Anastasopoulos I. and Gazetas G. (2015). Static and cyclic undrained response of square embedded foundations. *Geotechnique*, *65(10),* 1-19.

Oliveto G., Calio I. and Greco A. (2003). Large displacement behaviour of a structural model with foundation uplift under impulsive and earthquake excitations. *Earthquake Engineering and Structural Dynamics*, *32*, 369–93.

Paolucci R. (1997). Simplified evaluation of earthquake induced permanent displacements of shallow foundations. *Journal of Earthquake Engineering*, *1 (3)*, 563–79.

Paolucci R., Shirato M. and Yilmaz MT. (2008). Seismic behavior of shallow foundations: shaking table experiments vs. numerical modeling. *Earthquake Engineering and Structural Dynamics*, *37(4)*, 577–95.

Paolucci R., Figini R. and Petrini L. (2013). Introducing dynamic nonlinear soil-foundation-structure interaction effects in displacement-based seismic design. *Earthquake Spectra*, *29 (2)*, 475–496.

Pecker A. (1998). Capacity design principles for shallow foundations in seismic areas. *Proceedings 11th European Conference on Earthquake Engineering.* A.A. Balkema Publishing: Rotterdam.

Pecker A. (2003). A seismic foundation design process, lessons learned from two major projects: the Vascode Gama and the Rion Antirion bridges. *ACI International Conference on Seismic Bridge Design and Retrofit. LaJolla,* USA: University of California at San Diego.

Pecker A., Paolucci R., Chatzigogos C., Correia A. A. and Figini R. (2012). The role of non-linear dynamic soil-foundation interaction on the seismic response of structures. *Second International Conference On Performance-Based Design In Earthquake Geotechnical Engineering,* Taormina, Italy.

Pecker A. and Pender MJ. (2000). Earthquake resistant design of foundations: new construction. *In: Proceedings of GeoEngineering 2000 Conf.* Melbourne, Australia, 313–334.

Pender MJ. (2007). Seismic design and performance of surface foundations. *Proceedings of the 4th international conference on earthquake geotechnical engineering,* Thessaloniki, Greece.

Pender MJ., Wotherspoon LM., Ingham JM. and Carr AJ. (2006). Approach to design of shallow foundations for low-rise framed structures. *Proc. of 100th Anniversary Earthquake Conference Commemorating the 1906 San Francisco Earthquake,* EERI.

Perkins S.W. and Madson C.R. (2000). Bearing capacity of shallow foundations on sand: a relative density approach. *Journal of Geotechnical and Geoenvironmental Engineering, 126 (6),* 521-530.

Poulos H. G. and Davis E. H. (1974), Elastic solutions for soil and rock mechanics. Wiley, New York.

Prandtl L. (1921). Uber die Eindringungsfestigkeit (Harte) plasticher Baustoffe und die Festigkeit von Schneiden, *Zeitschrift für Angewandte Mathematik und Mechanik, Basel, Switzerland, l (1),* 15-20.

Psycharis I. N. (1991). Effect of base uplift on dynamic response of SDOF structures. *Journal of Structural Engineering, 117 (3),* 733–54.

Psycharis I. N. (2008). Investigation of the dynamic response of rigid footings on tensionless Winkler foundation, *Soil Dynamics and Earthquake Engineering, 28*, 577-591.

Raychowdhury P. and Hutchinson T. (2009). Performance evaluation of a nonlinear Winkler-based shallow foundation model using centrifuge test results. *Earthquake Engineering and Structural Dynamics, 38 (5),* 679–98.

Raychowdhury P. and Hutchinson T. C. (2011). Performance of seismically loaded shearwalls on nonlinear shallow foundations. *International Journal for Numerical and Analytical methods in Geomechanics, 35,* 846–858.

Reissner H. (1924). Zum Erddruckproblem, *Proceedings, 1st International Congress of Applied Mechanics*, 295- 311.

Roeder W., Eeri M., Banerjee S., Jung D. R., and Smith S. K. (1996). The role of building foundations in seismic retrofit. *Earthquake Spectra, 12 (4),* 925-42.

Rutenberg A., Jennings P. C. and Housner G. W. (1982). The response of veterans building 41 in the San Fernando earthquake. *Earthquake Engineering and Structural Dynamics,10*, 3759-3791.

Schnabel P. B., Lysmer J. and Seed H. B. (1972). SHAKE: a computer program for earthquake response analysis of horizontally layered sites. Report No. EERC72-12, University of California, Berkeley.

Schultz E. and Ing (1961). Distribution of stress beneath a rigid foundation. *Proceedings of the Fifth International Conference on Soil Mechanics and Foundation Engineering*, Dunod, Paris., 1, Division 1-3A.

Shirato M., Kouno T., Asai R., Nakatani S., Fukui J. and Paolucci R. (2008). Large-scale experiments on nonlinear behavior of shallow foundations subjected to strong earthquakes. *Soils and Foundations, 48,* 673-692.

Siddiquee M.S., Tatsuoka F., Tanaka T., Tani K., Yoshida K. and Morimoto T. (2001). Model tests and FEM simulation of some factors affecting the bearing capacity of a footing on sand. *Soils and Foundations, 41 (2),* 53- 76.

Song Y. H. and Lee D. G. (1993). An improved two-spring model for foundation uplift analysis. *Computers and Structures, 46 (5),* 791–805.

Sovinc I. (1969). Displacements and inclinations of resting on a limited elastic layer of uniform thickness. *Proceedings of the 7 th International Conference of Soil Mechanics and Foundations Engineering I,* Ciudad Mexico, 385–389.

Tamura S., Adachi K. and Tokimatsu K. (2011). Centrifuge tests of impulsive vertical acceleration generated by foundation uplift during strong shaking. *Soils and Foundations, 51 (3),* 411-422.

Terzaghi K. (1943). Theoretical Soil Mechanics. J. Wiley, New York.

Terzaghi K. and Peck R. B. (1967). Soil mechanics in engineering practice, John Wiley &Sons, New York.

Uzielli M. and Mayne P. W. (2012). Load-displacement uncertainty of vertically loaded shallow footings on sands and effects on probabilistic settlement estimation. *Georisk: Assessment and Management of Risk for Engineered Systems and Geohazards, 6(1),* 50-69.

Wang X. F. and Gould P. L. (1993). Dynamics of structures with uplift and sliding. *Earthquake Engineering and Structural Dynamics, 22 (12),* 1085–95.

Wolf J. P. (1976). Soil – structure interaction with separation of base mat from soil (Lifting – off). *Nuclear Engineering and Design, 38,* 357–84.

Wolf J. P. and Skrikerud P. E. (1978). Seismic excitation with large overturning moments: Tensile capacity, projecting base mat or lifting–off. *Nuclear Engineering and Design, 50 (2),* 305–81.

Wotherspoon LM., Pender MJ. and Ingham JM. (2004a). Effects of foundation model on the earthquake response of building systems. *Proc. of 3rd ICEGE and 11th ICSDEE, Berkeley,* CA, 766-773.

Wotherspoon L. M., Pender M. J. and Ingham J. M. (2004b). Combined modeling of structural and foundation systems. *Proc. of 13th World Conference on EQ Engineering, Vancouver*, 411-415.

Xu C. and Spyrakos C. C. (1996). Seismic analysis of towers including foundation uplift. *Engineering Structures, 18 (4),* 271–78.

Yamin M. M., Ashteyat A. M., Al-Mohd I. and Mahmoud E. (2016). Numerical study of contact stresses under foundations resting on cohesionless soil: effects of foundation rigidity and applied stress level. *KSCE Journal of Civil Engineering,* DOI 10.1007/s12205-016-1770-0.

Yılmaz M. T. and Bakır B. S. (2009). Capacity of shallow foundations on saturated cohesionless soils under combined loading. *Canadian Geotechnical Journal , 46*, 639-649.

Yim S. C. S. and Chopra A. K. (1984). Dynamics of structures on two-spring foundation allowed to uplift. *Journal of Engineering Mechanics, 110*, 1124.

Zafeirakos A. and Gerolymos N. (2013). On the seismic response of *under*-designed caisson foundations. *Bulletin of Earthquake Engineering, 11*, 1337–1372.

Zamani N. and El Shamy U. (2014). A microscale approach for the seismic response of MDOF structures including soil-foundation-structure interaction. *Journal of Earthquake Engineering, 18 (5),* 785-815.

Zhou F., M. Mori M. and Fukuwa N. (2012). A new uplift foundation analysis model to simulate dynamic nonlinear soil-structure-interaction. *15th World Conference on Earthquake Engineering*, Lisbon, Portugal.

APPENDIX A

The Relation between the Normalized Value of b, c, L, f, I and the Normalized Value of c' for Various Foundations

The shape of rectangular foundation remains stable during uplift (Figure A.1). During the uplift of the shape of rectangular foundation and the shape of square foundation become similar to that of strip foundation.

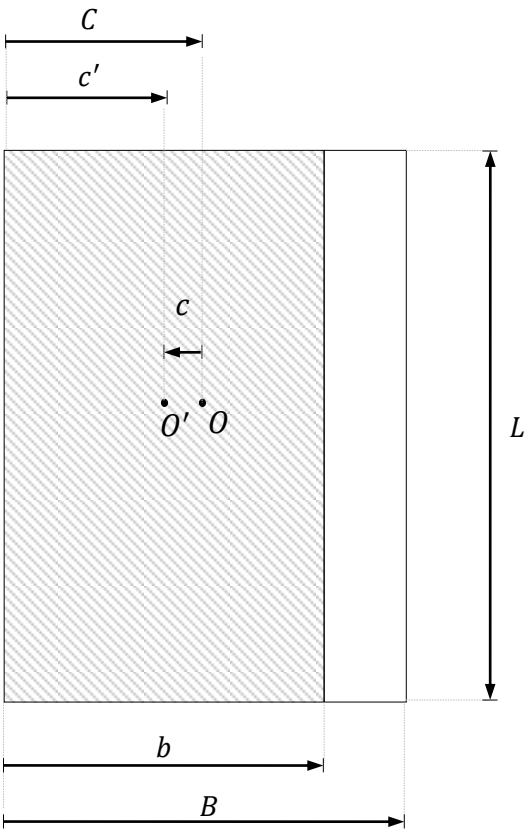

Figure A.1 Reduction in effective foundation width of the rectangular foundation after initiation of uplift

The circular shaped foundation is replaced by an arbitrarily shaped foundation after initiation of uplift (Figure A.2). Approximate methods may be developed to determinate the contact area in the literature. Wolf (1976) proposed that the actual irregular area of contact is replaced by an equivalent circular plate. Consequently, in this research study, the actual irregular area of contact is accurately calculated for the stiffness coefficients of the circular foundation.

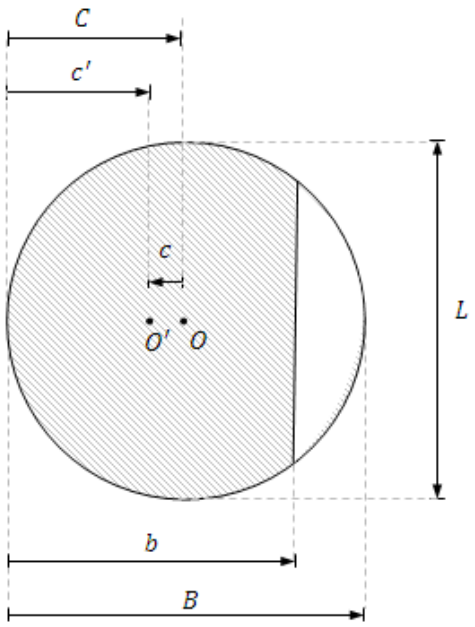

Figure A.2 Reduction in effective foundation width of the circular foundation after initiation of uplift

In the study one way (Figure A.3a) and two-way eccentric loading (Figure A.3b) were applied by using a rotated square foundation (Figure A.4).

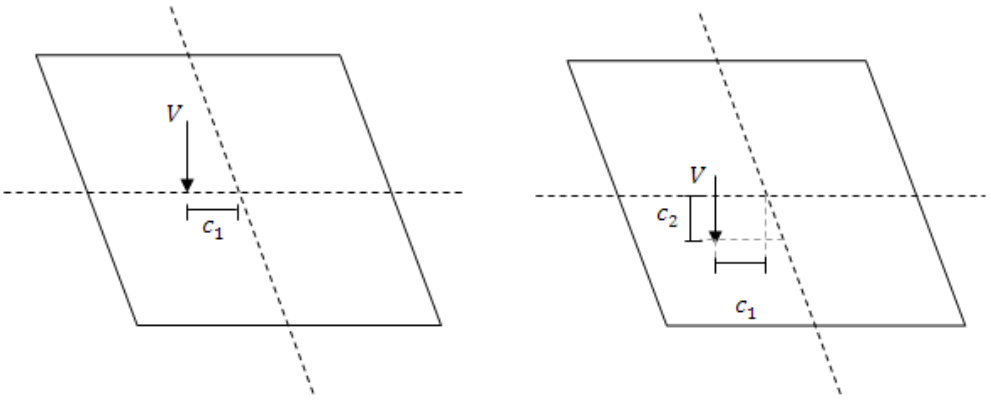

(a) (b)

Figure A.3 Applied loading: (a) one way eccentricity, (b) two-way eccentricity

The shape of a rotated square foundation during uplift changes considerably. In fact, the diagonal square shaped foundation is replaced by an arbitrarily shaped foundation after initiation of uplift (Figure A.4).

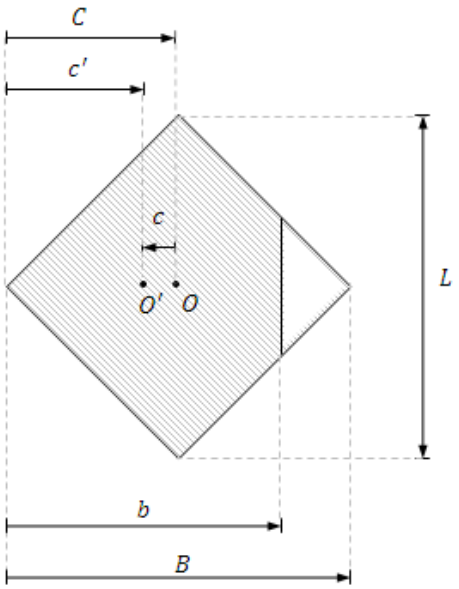

Figure A.4 Reduction in effective foundation width of the diagonal square foundation after initiation of uplift

The relation between c and c' for a foundation is presented in Equation A.1.

$$c = C - c' \qquad (A.1)$$

As an example the analytical relationships between stated parameters are presented for a square foundation:

$$b = 2.c' \qquad (A.2a)$$

$$L = b \qquad (A.2b)$$

$$f = b.L \qquad (A.2c)$$

$$I = \frac{b^3.L}{12} \qquad (A.2d)$$

The relation between the normalized value of b, c, L, f, I (i.e.,b_N, c_N, L_N, f_N, I_N) and the normalized value of c' (i.e., c'_N)for various foundations are presented in Figure A.5 - Figure A.9. c', b, c, L, f and I are normalized with the initial value of that, respectively.

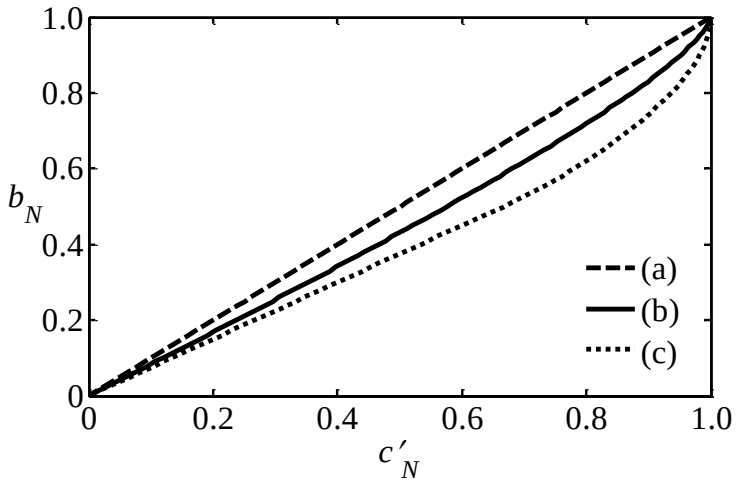

Figure A.5 The relation between b_N and c'_N for (a) rectangular foundations, (b) circular foundations and (c) diagonal square foundations

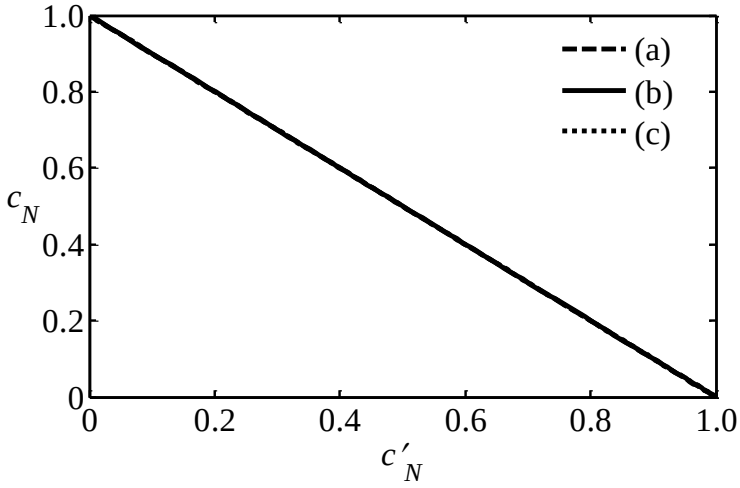

Figure A.6 The relation between c_N and c'_N for (a) rectangular foundations, (b) circular foundations and (c) diagonal square foundations

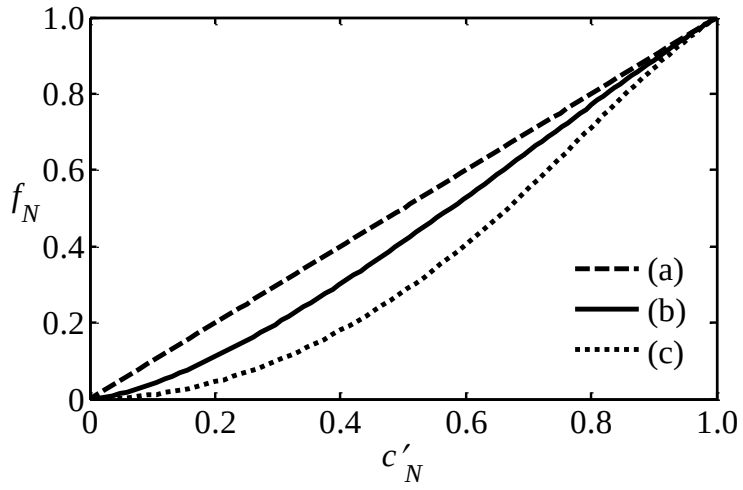

Figure A.7 The relation between f_N and c'_N for (a) rectangular foundations, (b) circular foundations and (c) diagonal square foundations

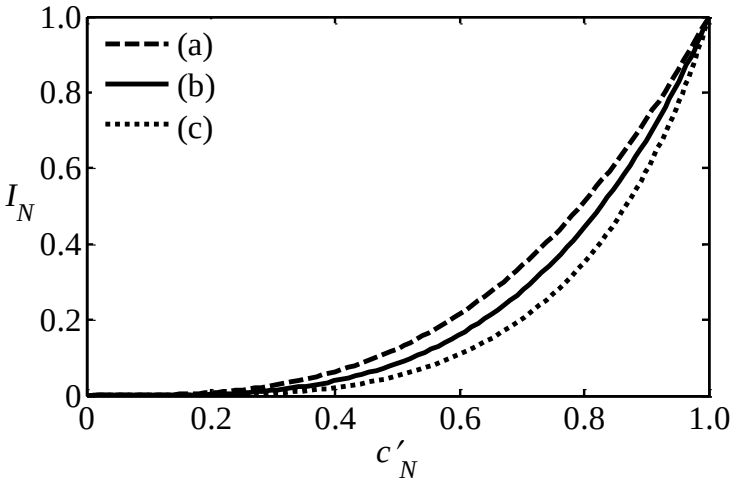

Figure A.8 The relation between I_N and c'_N for (a) rectangular foundations, (b) circular foundations and (c) diagonal square foundations

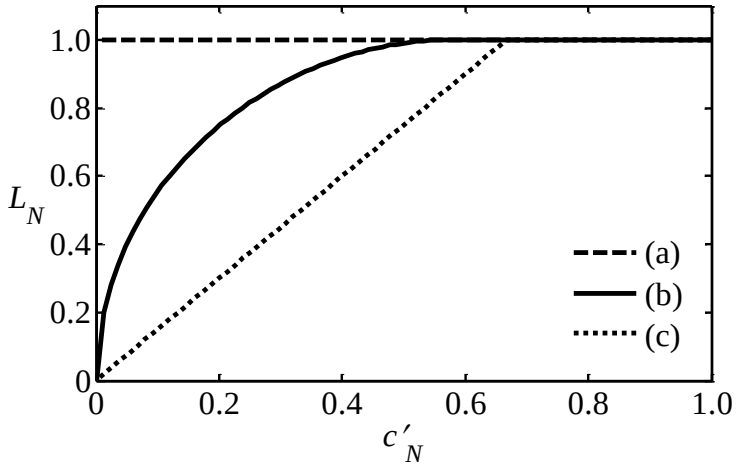

Figure A.9 The relation between L_N and c'_N for (a) rectangular foundations, (b) circular foundations and (c) diagonal square foundations

APPENDIX B

Equations Proposed by Cremer (2001)

Equations proposed by Cremer (2001) to calculate the response parameters of strip foundations.

Cremer (2001) proposed the following relationships;

$$M = K_\theta \theta \qquad M < M_{uplift}\ (before\ uplift) \qquad (B.1)$$

$$M_{uplift} = K_\theta \theta_{uplift} \qquad M = M_{uplift}\ (uplift\ onset) \qquad (B.2)$$

and

$$\frac{M}{M_{uplift}} = 2 - \frac{\theta_{uplift}}{\theta} \qquad M > M_{uplift}\ (during\ uplift) \qquad (B.3)$$

where K_θ is calculated by using Equation 2.7 (a=0).

APPENDIX C

Derivation of α for Foundation on Winkler Springs

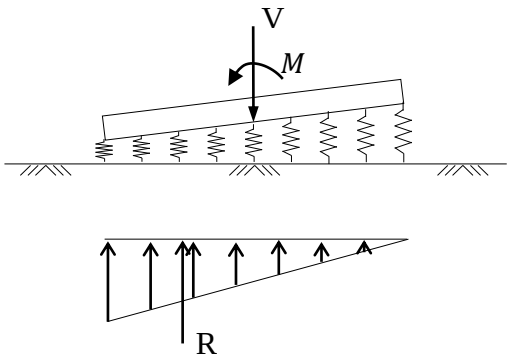

Figure C.1 Typical behavior of foundation on Winkler springs

Derivation of α for foundation on Winkler springs is

$$\sum F_y = 0 \;\rightarrow\; R = V \qquad (C.1)$$

and

$$\sum M = 0 \;\rightarrow\; M_{uplift} = \frac{Rb}{6} = \frac{Vb}{6} \qquad (C.2)$$

Substitution of Equation C.2 in Equation 3.13 yields to

$$\alpha = \frac{1}{3} \qquad (C.3)$$

APPENDIX D

Derivation of α for Foundations with Regular Shapes

For a prismatic section α is calculated using Equation 3.12. From Equation 3.12, it may be observed that the α of a prismatic shaped foundation depends on the term $\partial K_\theta(b,L)/\partial b$. In relation to that $\partial K_\theta(b,L)/\partial b$ of several prismatic foundations are calculated and substituted in to Equation 3.12 to calculate α.

For rectangular foundations on Winkler Springs, $\partial K_\theta(b,L)/\partial b$ is calculated by using Equation 2.9

$$\frac{\partial K_\theta(b,L)}{\partial b} = \frac{3}{b} K_\theta(b,L) \qquad (D.1)$$

Substitutng Equation D.1 in Equation 3.12 results in

$$\alpha = \frac{1}{3} \qquad (D.2)$$

For rectangular foundations on elastic halfspace, $\partial K_\theta(b,L)/\partial b$ is calculated by using the expression giving the rotational stiffness of arbitrarily shaped foundations (Table 2.1)

$$\frac{\partial K_\theta(b,L)}{\partial b} = \frac{2.25}{b} K_\theta(b,L) \qquad (D.3)$$

Substitutng Equation D.3 in Equation 3.12 results in

$$\alpha = \frac{1}{2.25} \qquad (D.4)$$

For circular foundations on elastic halfspace, $\partial K_\theta(b,L)/\partial b$ is calculated by using the expression giving the rotational stiffness of arbitrarily shaped foundations (Table 2.1) or the expression giving the rotational stiffness of circular foundations (Table 2.2)

$$\frac{\partial K_\theta(b,L)}{\partial b} = \frac{3}{b} K_\theta(b,L) \qquad (D.5)$$

Substituting Equation D.5 in Equation 3.12 results in

$$\alpha = \frac{1}{3} \qquad (D.6)$$

For strip foundations on elastic halfspace, $\partial K_\theta(b,L)/\partial b$ is calculated by using the expression giving the rotational stiffness of strip foundations (Table 2.2)

$$\frac{\partial K_\theta(b,L)}{\partial b} = \frac{2}{b} K_\theta(b,L) \qquad (D.7)$$

Substituting Equation D.7 in Equation 3.12 results in

$$\alpha = \frac{1}{2} \qquad (D.8)$$

APPENDIX E

Matlab Code for Calculating the Theoretical Response of Uplifting Shallow Foundations Subjected to Eccentric Loading

```
function [out]=uplift(hs,V,SM,param,Gparam)
Tc=dim(param);
cp=Tc(1,2);
Mult=V*cp;
dM=Mult/SM;
M=0:dM:(Mult-dM);
H=M/hs;
Mupl=SUB1(cp,H,V,SM,Tc,param,Gparam);
MCOUNT=length(M);
  for ICOUNT=1:MCOUNT
if M(ICOUNT)>Mupl
cp=SUB2(cp,H(ICOUNT),V,M(ICOUNT),SM,Tc,param,Gparam);
end
  [alpha(ICOUNT)]=SUB4(cp,H(ICOUNT),V,SM,Tc,param,Gparam);
  hvtheta=SUB3(cp,H(ICOUNT),V,M(ICOUNT),Tc,param,Gparam);
  h(ICOUNT)=hvtheta(1);
  v(ICOUNT)=hvtheta(2);
  theta(ICOUNT)=hvtheta(3);
  end
end

function [x]=dim(param)
  switch param(5)
    case 1
        x=load ('square.txt');
    case 2
        x=load ('rectangularwide.txt');
    case 3
        x=load ('rectangularnarrow.txt');
    case 4
        x=load ('circular.txt');
    case 5
        x=load ('diagonalsquare.txt');
    case 6
        x=load ('strip.txt');
  end
end

function [b,c,L,f,I]=SUB0(cp,Tc)
b=interp1(Tc(:,1),Tc(:,3),cp,'splines');
c=interp1(Tc(:,1),Tc(:,4),cp,'splines');
L=interp1(Tc(:,1),Tc(:,5),cp,'splines');
f=interp1(Tc(:,1),Tc(:,6),cp,'splines');
I=interp1(Tc(:,1),Tc(:,7),cp,'splines');
end
```

```
function [Mupl]=SUB1(cp,H,V,SM,Tc,param,Gparam)
Mult=V*cp;
Mupl=SUB4(cp,H,V,SM,Tc,param,Gparam)*Mult;
end

function [cp]=SUB2(cpold,H,V,M,SM,Tc,param,Gparam)
cp=fzero(@(cpnew)SUB5(cpnew,H,V,M,SM,Tc,param,Gparam),cpold,
         optimset('TolX',1e-12));
end

function [hvtheta]=SUB3(cp,H,V,M,Tc,param,Gparam)
B=Tc(1,1);
[b,c,L,f,I]=SUB0(cp,Tc);
hvtheta=(Kglob(B,b,c,f,I,L,H,V,param,Gparam)\[H;V;M])';
end

function [alpha]=SUB4(cp,H,V,SM,Tc,param,Gparam)
B=Tc(1,1);
[b,c,L,f,I]=SUB0(cp,Tc);
eps=1/(SM*100);
cpforward=cp*(1-eps);
[bf,cf,Lf,ff,If]=SUB0(cpforward,Tc);
alpha=(-(cf-c)/(bf-b))*Kr(B,b,f,I,L,H,V,param,Gparam)
/(((Kr(B,bf,ff,If,Lf,H,V,param,Gparam)-
Kr(B,b,f,I,L,H,V,param,Gparam))/(bf-b))*cp);
end

function [FUN]=SUB5(cp,H,V,M,SM,Tc,param,Gparam)
[b,c,L,f,I]=SUB0(cp,Tc);
HVMp=SUB6(c,H,V,M);
Hp=HVMp(1);
Vp=HVMp(2);
Mp=HVMp(3);
FUN=Mp/Vp-SUB4(cp,H,V,SM,Tc,param,Gparam)*cp;
end

function [HVMp]=SUB6(c,H,V,M)
HVMp=(A(c)'\[H;V;M])';
end

function [x]=A(c)
x=[1,0,0;0,1,c;0,0,1];
end

function [x]=Kglob(B,b,c,f,I,L,H,V,param,Gparam)
x=A(c)'*K(B,b,f,I,L,H,V,param,Gparam)*A(c);
end

function [x]=K(B,b,f,I,L,H,V,param,Gparam)
x=[Kh(B,b,f,L,H,V,param,Gparam),0,0;0,Kv(B,b,f,L,H,V,param,Gparam)
,0;0,0,Kr(B,b,f,I,L,H,V,param,Gparam)];
end
```

```
function [x]=Kh(B,b,f,L,H,V,param,Gparam)
Gb=G(b,f,L,H,V,Gparam);
  switch param(1)
    case 1
        x=Khwinkler(b,L,param);
    case 2
        x=Khrectangular(b,L,Gb,param);
    case 3
        x=Khcircular(b,Gb,param);
    case 4
        x=Khgeneral(b,f,L,Gb,param);
    case 5
        x=Khdepthrect(b,L,Gb,param);
    case 6
        x=Khdeepstrip(B,b,Gb,param);
  end
end

function [x]=Kr(B,b,f,I,L,H,V,param,Gparam)
Gb=G(b,f,L,H,V,Gparam);
  switch param(1)
    case 1
        x=Krwinkler(b,L,param);
    case 2
        x=Krrectangular(b,L,Gb,param);
    case 3
        x=Krcircular(b,Gb,param);
    case 4
        x=Krgeneral(b,I,L,Gb,param);
    case 5
        x=Krdepthrect(b,L,Gb,param);
    case 6
        x=Krdeepstrip(B,b,Gb,param);
  end
end

function [x]=Kv(B,b,f,L,H,V,param,Gparam)
Gb=G(b,f,L,H,V,Gparam);
  switch param(1)
    case 1
        x=Kvwinkler(b,L,param);
    case 2
        x=Kvrectangular(b,L,Gb,param);
    case 3
        x=Kvcircular(b,Gb,param);
    case 4
        x=Kvgeneral(b,f,L,Gb,param);
    case 6
        x=Kvdeepstrip(B,b,Gb,param);
  end
end
```

```
function [x]=Kv0(B,b,f,L,param,Gparam)
Gb=Gparam(1);
  switch param(1)
    case 1
        x=Kvwinkler(b,L,param);
    case 2
        x=Kvrectangular(b,L,Gb,param);
    case 3
        x=Kvcircular(b,Gb,param);
    case 4
        x=Kvgeneral(b,f,L,Gb,param);
    case 5
        x=Kvdepthrect(b,L,Gb,param);
    case 6
        x=Kvdeepstrip(B,b,Gb,param);
  end
end

function [x]=Khwinkler(b,L,param)
k0=param(2);
x=k0*b*L/12;
end

function [x]=Krwinkler(b,L,param)
k0=param(2);
x=k0*b^3*L/12;
end

function [x]=Kvwinkler(b,L,param)
k0=param(2);
x=k0*b*L;
end

function [x]=Khrectangular(b,L,Gb,param)
  if b/L>1
   x=Khxrectangular(b,L,Gb,param);
  else
   x=Khyrectangular(b,L,Gb,param);
  end
end

function [x]=Khxrectangular(b,L,Gb,param)
nu=param(3);
x=Gb*b*(2+2.5*(L/b)^0.85)/(2-nu)-0.1*Gb*b*(1-(L/b))/(0.75-nu);
end

function [x]=Khyrectangular(b,L,Gb,param)
nu=param(3);
x=Gb*L*(2+2.5*(b/L)^0.85)/(2-nu);
end
```

```
function [x]=Krrectangular(b,L,Gb,param)
  if b/L>1
   x=Krxrectangular(b,L,Gb,param);
  else
   x=Kryrectangular(b,L,Gb,param);
  end
end

function [x]=Krxrectangular(b,L,Gb,param)
nu=param(3);
x=(0.465*Gb*(b^4*L)^0.6)/(1-nu);
end

function [x]=Kryrectangular(b,L,Gb,param)
nu=param(3);
x=Gb*b^2*L*(0.372+0.078*b/L)/(1-nu);
end

function [x]=Kvrectangular(b,L,Gb,param)
  if b/L>1
   x=Kvxrectangular(b,L,Gb,param);
  else
   x=Kvyrectangular(b,L,Gb,param);
  end
end

function [x]=Kvxrectangular(b,L,Gb,param)
nu=param(3);
x=Gb*b*(0.73+1.54*(L/b)^0.75)/(1-nu);
end

function [x]=Kvyrectangular(b,L,Gb,param)
nu=param(3);
x=Gb*L*(0.73+1.54*(b/L)^0.75)/(1-nu);
end

function [x]=Khcircular(b,Gb,param)
nu=param(3);
x=4*Gb*b/(2-nu);
end

function [x]=Kvcircular(b,Gb,param)
nu=param(3);
x=2*Gb*b/(1-nu);
end

function [x]=Krcircular(b,Gb,param)
nu=param(3);
x=Gb*b^3/(3-3*nu);
end
```

```
function [x]=Khgeneral(b,f,L,Gb,param)
  if b/L>1
   x=Khxgeneral(b,f,L,Gb,param);
  else
   x=Khygeneral(f,L,Gb,param);
  end
end

function [x]=Khxgeneral(b,f,L,Gb,param)
nu=param(3);
x=Shx(b,f)*Gb*b/(2-nu)-0.105*Gb*b*(1-L/b)/(0.75-nu);
end

function [x]=Shx(b,f)
  if f/(b^2)<0.16
   x=2.24;
  else
   x=4.5*(f/(b^2))^0.38;
  end
end

function [x]=Khygeneral(f,L,Gb,param)
nu=param(3);
x=Shy(f,L)*Gb*L/(2-nu);
end

function [x]=Shy(f,L)
  if f/(L^2)<0.16
   x=2.24;
  else
   x=4.5*(f/(L^2))^0.38;
  end
end

function [x]=Krgeneral(b,I,L,Gb,param)
  if b/L>1
   x=Krxgeneral(I,Gb,param);
  else
   x=Krygeneral(b,I,L,Gb,param);
  end
end

function [x]=Krxgeneral(I,Gb,param)
nu=param(3);
x=3.2*Gb*I^0.75/(1-nu);
end

function [x]=Krygeneral(b,I,L,Gb,param)
nu=param(3);
x=Sr(b,L)*Gb*I^0.75/((1-nu)*(b/L)^0.25);
end
```

```
function [x]=Sr(b,L)
  if b/L<0.4
   x=2.54;
  else
   x=3.2*(b/L)^0.25;
  end
end

function [x]=Kvgeneral(b,f,L,Gb,param)
  if b/L>1
   x=Kvxgeneral(b,f,Gb,param);
  else
   x=Kvygeneral(f,L,Gb,param);
  end
end

function [x]=Kvxgeneral(b,f,Gb,param)
nu=param(3);
x=Svx(b,f)*Gb*b/(1-nu);
end

function [x]=Svx(b,f)
  if f/(b^2)<0.02
   x=0.8;
  else
   x=0.73+1.54*(f/(b^2))^0.75;
  end
end

function [x]=Kvygeneral(f,L,Gb,param)
nu=param(3);
x=Svy(f,L)*Gb*L/(1-nu);
end

function [x]=Svy(f,L)
  if f/(L^2)<0.02
   x=0.8;
  else
   x=0.73+1.54*(f/(L^2))^0.75;
  end
end

function [x]=Khdeepstrip(B,b,Gb,param)
nu=param(3);
a=param(6);
x=2*Gb*(1+2*a*(b/B)/3)/(2-nu);
end

function [x]=Kvdeepstrip(B,b,Gb,param)
nu=param(3);
a=param(6);
x=0.73*Gb*(1+2*a*(b/B))/(1-nu);
end
```

```
function [x]=Krdeepstrip(B,b,Gb,param)
nu=param(3);
a=param(6);
x=pi*Gb*(b^2/4)*(1+a*(b/B)/3)/(2-2*nu);
end

function [x]=Kvdepthrect(b,L,Gb,param)
D=param(4);
mmv=load ('finitelayerKv.txt');
pv=load ('pv.txt');
yv=load ('yv.txt');
[av,cv]=meshgrid(yv,pv);
for i=1:6
    for j=1:48
        zv(i,j)=mmv((i-1)*48+j,3);
    end
end
hbv=D/b;
lbv=b/L;
beta=interp2(av,cv,zv,hbv,lbv,'spline');
x=3*Gb*L/beta;
end


function [x]=Krdepthrect(b,L,Gb,param)
D=param(4);
mmr=load ('finitelayerKr.txt');
pr=load ('pr.txt');
yr=load ('yr.txt');
[ar,cr]=meshgrid(yr,pr);
for i=1:10
    for j=1:49
        zr(i,j)=mmr((i-1)*49+j,3);
    end
end
hbr=D/b;
lbr=b/L;
gama=interp2(ar,cr,zr,hbr,lbr,'spline');
x=3*b^3*Gb/(8*gama);
end

function [G]=G(b,f,L,H,V,Gparam)
G0=Gparam(1);
FS=Vult(b,f,L,H,V,Gparam)/V;
  switch Gparam(6)
    case 1
        G=G0*(1-1/FS);
    case 2
        G=-G0*(1/FS)*(1/log(1-1/FS));
  end
end
```

```
function [Vult]=Vult(b,f,L,H,V,Gparam)
Vult0=qu(b,L,H,V,Gparam)*f;
V0=V*(1+10*eps);
Vult=max(V0,Vult0);
end

function [qu]=qu(b,L,H,V,Gparam)
coh=Gparam(2);
gamma=Gparam(4);
q=Gparam(5);
delqi0=1;
delci0=1;
delgmi0=1;
quold=coh*Nc(Gparam)*delcs(b,L,Gparam)*delci0+q*Nq(Gparam)
      *delqs(b,L,Gparam)*delqi0+(1/2)*gamma*b*Ngm(Gparam)
      *delgms(b,L)*delgmi0;
qu=fzero(@(qu) qu-coh*Nc(Gparam)*delcs(b,L,Gparam)
   *delci(H,V,qu,Gparam)-q*Nq(Gparam)*delqs(b,L,Gparam)
   *delqi(H,V,qu,Gparam)-(1/2)*gamma*b*Ngm(Gparam)*delgms(b,L)
   *delgmi(H,V,qu,Gparam),quold);
end

function [fi]=fi(Gparam)
fii=Gparam(3);
fi=fii*pi/180;
end

function [Nq]=Nq(Gparam)
Nq=exp(pi*tan(fi(Gparam)))*((1+sin(fi(Gparam)))/(1-
sin(fi(Gparam))));
end

function [Nc]=Nc(Gparam)
Nc=(Nq(Gparam)-1)*cot(fi(Gparam));
end

function [Ngm]=Ngm(Gparam)
Ngm=1.5*Nc(Gparam)*(tan(fi(Gparam)))^2;
end

function [delcs]=delcs(b,L,Gparam)
delcs=1+(Nq(Gparam)/Nc(Gparam))*(b/L);
end

function [delqs]=delqs(b,L,Gparam)
delqs=1+(b/L)*tan(fi(Gparam));
end

function [delgms]=delgms(b,L)
delgms=1-0.4*(b/L);
end
```

```
function [delqi]=delqi(H,V,qu,Gparam)
coh=Gparam(2);
alfa=atan(H/V);
delqi=(1-0.5*qu*sin(alfa)/(qu*cos(alfa)+coh*cot(fi(Gparam))))^5;
end

function [delci]=delci(H,V,qu,Gparam)
delci=delqi(H,V,qu,Gparam)-((1-delqi(H,V,qu,Gparam))/(Nq(Gparam)
      -1));
end

function [delgmi]=delgmi(H,V,qu,Gparam)
coh=Gparam(2);
alfa=atan(H/V);
delgmi=(1-0.7*qu*sin(alfa)/(qu*cos(alfa)+coh*cot(fi(Gparam))))^5;
end
```

CURRICULUM VITAE

PERSONAL INFORMATION

Surname, Name: Durucan, Ayşe Ruşen

Nationality: Turkish (TC)

Date and Place of Birth: 10 July 1984, Adıyaman

Marital Status: Married

Phone: +90 537 422 97 99

email: arunsal19@hotmail.com

EDUCATION

Degree	Institution	Year of Graduation
Ph.D.	Middle East Technical University, Engineering Sciences	2016
MS	Middle East Technical University, Engineering Sciences	2010
BS	Fırat University, Civil Engineering	2006

FOREIGN LANGUAGES

English

WORK EXPERIENCE

Year	Place	Enrollment
2007-Present	METU Department of Engineering Sciences	Research Assistant